THE ROLE OF UBIQUITIN C-TERMINAL HYDROLASE L1 IN RENAL FUNCTION AND GLOMERULAR DISEASE

Naomi Boisvert

This thesis is submitted as partial fulfillment of the
Ph.D. program in Cellular and Molecular Medicine

Department of Cellular and Molecular Medicine
Faculty of Medicine
University of Ottawa

AUTHORIZATIONS

Manuscript #1

Read, N.C., A. Gutsol, C.E. Holterman, A. Carter, J. Coulombe, D.A. Gray and C.R.J. Kennedy. 2014. *Ubiquitin C-terminal hydrolase L1* deletion ameliorates glomerular injury in mice with *ACTN4*-associated focal segmental glomerulosclerosis. Biochimica Biophysica et Acta, Molecular Basis of Disease. 1842(7), 1028-1040.

Authorization

ELSEVIER LICENSE
TERMS AND CONDITIONS

Oct 24, 2017

This Agreement between University of Ottawa -- Naomi Read ("You") and Elsevier ("Elsevier") consists of your license details and the terms and conditions provided by Elsevier and Copyright Clearance Center.

License Number	4143740362373
License date	Jul 07, 2017
Licensed Content Publisher	Elsevier
Licensed Content Publication	Biochimica et Biophysica Acta (BBA) - Molecular Basis of Disease
Licensed Content Title	Ubiquitin C-terminal hydrolase L1 deletion ameliorates glomerular injury in mice with ACTN4-associated focal segmental glomerulosclerosis
Licensed Content Author	Naomi C. Read,Alex Gutsol,Chet E. Holterman,Anthony Carter,Josée Coulombe,Douglas A. Gray,Chris R.J. Kennedy
Licensed Content Date	Jul 1, 2014
Licensed Content Volume	1842
Licensed Content Issue	7
Licensed Content Pages	13
Start Page	1028
End Page	1040
Type of Use	reuse in a thesis/dissertation
Portion	full article
Format	both print and electronic
Are you the author of this Elsevier article?	Yes
Will you be translating?	No
Title of your thesis/dissertation	THE ROLE OF UBIQUITIN C-TERMINAL HYDROLASE L1 IN RENAL FUNCTION AND GLOMERULAR DISEASE
Expected completion date	Aug 2017
Estimated size (number of pages)	200
Requestor Location	University of Ottawa 451 Smyth Road Ottawa, ON K1H 8M5 Canada Attn: University of Ottawa
Total	0.00 CAD

Manuscript #2

Boisvert, N., C.E. Holterman, J.F. Thibodeau, R. Nasrallah, E. Kamto, C.H. Comin, L. da F. Costa, A. Carter, R. Hébert, A. Gutsol, G.E. Cron, B. Lacoste, D.A. Gray and C.R. Kennedy. 2017. Hyperfiltration in *Ubiquitin C-Terminal Hydrolase L1*-Deleted Mice. Manuscript in preparation.

Authorization

N/A - This manuscript is currently in preparation.

Manuscript #3

Boisvert, N., C.E. Holterman, A. Gutsol, J. Coulombe, W. Pan, T. Alexander, D.A. Gray and C.R. Kennedy. 2017. *Ubiquitin C-terminal hydrolase L1* deletion is associated with renal α-klotho deficiency and perturbed phosphate homeostasis. American Journal of Physiology-Renal Physiology. Manuscript in revision (#F-00411-2017).

Authorization

N/A - This manuscript is currently in preparation/revision.

LIST OF PUBLICATIONS

Boisvert, N., C.E. Holterman, J.F. Thibodeau, R. Nasrallah, E. Kamto, C.H. Comin, L. da F. Costa, A. Carter, R. Hébert, A. Gutsol, G.E. Cron, B. Lacoste, D.A. Gray and C.R. Kennedy. 2017. Hyperfiltration in *Ubiquitin C-Terminal Hydrolase L1*-Deleted Mice. Manuscript in preparation.

Boisvert, N., C.E. Holterman, A. Gutsol, J. Coulombe, W. Pan, T. Alexander, D.A. Gray and C.R. Kennedy. 2017. *Ubiquitin C-terminal hydrolase L1* deletion is associated with renal α-klotho deficiency and perturbed phosphate homeostasis. American Journal of Physiology-Renal Physiology. Manuscript in revision (#F-00411-2017).

Holterman, C.E., **N.C. Boisvert**, J.F. Thibodeau, E. Kamto, M. Novakovic, K.S. Abd-Elrahman and C.R.J. Kennedy. 2017. Podocyte NADPH Oxidase 5 Promotes Renal Inflammation Regulated by the Toll-Like Receptor Pathway. Manuscript in preparation.

Thibodeau, J.F., C.E. Holterman, Y. He, A. Carter, G. Cron, **N.C. Boisvert**, K.S. Abd-Elrahman, K.J. Hsu, S.S.G. Ferguson and C.R.J. Kennedy. 2016. Vascular smooth muscle-specific EP4 receptor deletion in mice exacerbates angiotensin II-induced renal injury. Antioxidants and Redox Signaling. 25(12), 642-656.

Holterman, C.E., **N.C. Read**, and C.R. Kennedy. 2015. Nox in renal disease. Clinical Science. 128(8), 465-481.

Thibodeau, J.F., C.E. Holterman, D. Burger, **N.C. Read**, T.L. Reudelhuber, and C.R. Kennedy. 2014. A novel model of advanced diabetic kidney disease in mice. PLoS ONE. 9(12), e113459.

Read, N.C., A. Gutsol, C.E. Holterman, A. Carter, J. Coulombe, D.A. Gray and C.R.J. Kennedy. 2014. *Ubiquitin C-terminal hydrolase L1* deletion ameliorates glomerular injury in mice with *ACTN4*-associated focal segmental glomerulosclerosis. Biochimica Biophysica et Acta, Molecular Basis of Disease. 1842(7), 1028-1040.

Burger, D., D.G. Kwart, A. Montezano, **N.C. Read**, C.R.J. Kennedy, C.S. Thompson, and R.M. Touyz. 2012. Microparticles induce Cell Cycle Arrest through Redox-sensitive Processes in Endothelial Cells: Implications in Vascular Senescence. Journal of the American Heart Association. 1, e001842.

LIST OF ABSTRACTS

Boisvert, N.C., C.E. Holterman, M. Novakovic and C.R. Kennedy. TRPC5 is required for NADPH oxidase 5 activity in podocytes. Department of Medicine Research Day, Ottawa Hospital Research Institute / University of Ottawa, Ottawa, ON, June 2017. Poster presentation (abstract #13A).

Boisvert, N.C., C.E. Holterman, M. Novakovic and C.R. Kennedy. TRPC5 is required for NADPH oxidase 5 activity in podocytes. Gordon Research Conferences / Gordon Research Seminar – NADPH oxidases, Waterville Valley, NH, June 2016. Poster presentation / Oral presentation.

Holterman, C.E., **N.C. Boisvert**, J.F. Thibodeau, M. Novakovic. and C.R. Kennedy. Toll-like Receptors and NADPH Oxidase 5 Activity; Oxidative Stress Takes a Toll on Renal Function. Gordon Research Conferences – NADPH oxidases, Waterville Valley, NH, June 2016. Oral presentation.

Read, N.C., C.E. Holterman, D.A. Gray and C.R. Kennedy. Podocyte Oxidative Stress Coupled With *Ubiquitin C-Terminal Hydrolase L1* Deletion Exacerbates Renal Damage. American Society of Nephrology (ASN) – Kidney Week, San Diego, CA, November 2015. Poster presentation (abstract #4813).

Read, N.C., J. Coulombe, A. Gutsol, A. Carter, D.A. Gray and C.R.J. Kennedy. *Ubiquitin C-terminal hydrolase L1* deletion ameliorates glomerular injury in mice with *ACTN4*-associated focal segmental glomerulosclerosis. Ottawa Hospital Research Institute - Research Day 2013, Ottawa, ON, November 2013. Poster presentation (abstract #39).

Read, N.C., J. Coulombe, D.A. Gray and C.R.J. Kennedy. The role of ubiquitin C terminal hydrolase L1 (UCH-L1) in *ACTN4*-associated focal segmental glomerulosclerosis. Ottawa Hospital Research Institute - Research Day 2012, Ottawa, ON, November 2012. Poster presentation (abstract #40).

Read, N.C., J. Coulombe, D.A Gray and C.R.J. Kennedy. The role of ubiquitin C-terminal hydrolase L1 (UCH-L1) in *ACTN4*-associated focal segmental glomerulosclerosis (FSGS). American Society of Nephrology (ASN), San Diego, CA, October-November 2012. Oral presentation (abstract #21735).

Read, N.C., J. Coulombe, D.A. Gray and C.R.J. Kennedy. A detrimental role for ubiquitin C-terminal hydrolase L1 (UCH-L1) in *ACTN4*-associated FSGS. American Society of Nephrology (ASN), Philadelphia, PA, November 2011. Poster presentation (abstract #1212).

LIST OF SCHOLARSHIPS AND AWARDS

2017 **Basic Research Poster Award**
Department of Cellular and Molecular Medicine Research Day
University of Ottawa, Ottawa, Ontario, Canada
Description: Awarded for the best poster presentation at the Department of Medicine's Research Day

2016 **Gordon Research Seminar Travel Award**
NOX Family, NADPH Oxidases
Waterville Valley, New Hampshire, United States
Award Value: $153.86 USD
Description: Travel stipend awarded to trainees selected for an oral presentation at the Gordon Research Seminar for NOX Family, NADPH Oxidases

2015 **Kidney STARS (Students and Residents) Travel Award**
American Society of Nephrology – Kidney Week Conference
San Diego, California, United States
Award Value: $800 USD
Description: Travel stipend awarded to top trainees in attendance at the largest international kidney conference. This also included an opportunity for private mentorship (during the conference) by an American Society of Nephrology faculty member.

2014-2015 **Queen Elizabeth II Graduate Scholarship in Science and Technology**
University of Ottawa, Ottawa, Ontario, Canada
Award Value: $15,000
Description: Stipend award "to encourage and support the best students involved in science and technology research."

2014-2015 **Excellence Scholarship**
University of Ottawa, Ottawa, Ontario, Canada
Award Value: $9,000
Description: Awarded by the University of Ottawa to student recipients of major external awards

2013 **Italian Night Scholarship of the Kidney Foundation of Canada**
Italian Night, Ottawa, Ontario, Canada
Award Value: $3,000
Description: Awarded to trainees at the Kidney Research Centre, Ottawa Hospital Research Institute, for their outstanding research contributions

2012 **Seminar Award - Best Research Achievement by a graduate M.Sc. Student in Spring-Summer 2012**
Department of Cellular and Molecular Medicine, University of Ottawa
Ottawa, Ontario, Canada
Description: Awarded for best oral presentation in the M.Sc. seminar course CMM8324S at the University of Ottawa

2012-2016 **Admission Scholarship (PhD Level)**
University of Ottawa, Ottawa, Ontario, Canada
Award Value: $36,000
Description: Awarded by the University of Ottawa to students that have maintained 8.0/10 GPA at the M.Sc. level

2012 **Dean's Scholarship**
University of Ottawa, Ottawa, Ontario, Canada
Award Value: $1,500
Description: Awarded by the University of Ottawa to graduate students that have transferred from the M.Sc. to the PhD program in a timely manner

2011-2012 **Admission Scholarship (M.Sc. Level)**
University of Ottawa, Ottawa, Ontario, Canada
Award Value: $10,000
Description: Awarded by the University of Ottawa to students that have maintained 8.0/10 GPA at the B.Sc. level

ABSTRACT

Ubiquitin C-terminal hydrolase L1 is a deubiquitinating enzyme that salvages ubiquitin from substrates and maintains intracellular ubiquitin pools. While the role of ubiquitin C-terminal hydrolase L1 is well characterized in neurons, there is an increasing scope of evidence to suggest that ubiquitin C-terminal hydrolase L1 also plays a role in renal function and glomerular disease, however, its specific role in these settings remains incompletely elucidated. In the present thesis we explored the role of ubiquitin C-terminal hydrolase L1 in a mouse model of glomerular disease, *ACTN4*-associated focal segmental glomerulosclerosis and the role of ubiquitin C-terminal hydrolase L1 in renal function. Deletion of *ubiquitin C-terminal hydrolase L1* in a mouse model of *ACTN4*-associated focal segmental glomerulosclerosis significantly improved indices of podocyte injury, a likely result of ubiquitin pool attenuation and sustained α-actinin-4 levels. However, global ablation of *ubiquitin C-terminal hydrolase L1* in mice led to altered renal hemodynamics, namely glomerular hyperfiltration, most likely attributed to nerve dysfunction and loss of arterial resistance. Finally, mice lacking *ubiquitin C-terminal hydrolase L1* exhibited perturbations in phosphate homeostasis as these showed evidence of hyperphosphatemia and phosphaturia, indicating altered renal phosphate balance. Altogether, these data show that while ubiquitin C-terminal hydrolase L1 plays a maladaptive role in glomerular disease, it also functions as a crucial regulator of renal hemodynamics and renal phosphate handling, suggesting that it may have distinct functions in diseased and non-diseased kidneys.

TABLE OF CONTENTS

LIST OF TABLES

LIST OF FIGURES

LIST OF ABBREVIATIONS

1,25-$(OH)_2$-D_3	Calcitriol
ABS	Actin-binding site
ACE/ACE1	Angiotensin-converting enzyme 1
ACE2	Angiotensin-converting enzyme 2
ACR	Albumin/creatinine ratios
ACTN4	α-actinin-4 (gene)
Ang II	Angiotensin II
AT1R	Angiotensin type 1 receptor
AT2R	Angiotensin type 2 receptor
AUC	Area under the curve
BBMVs	Brush border membrane vesicles
BBM(s)	Brush border membrane(s)
BSA	Bovine serum albumin
CD2AP	CD2-associated protein
CD31	Cluster of differentiation 31
CHD	Calponin-homology domain
COX-2	Cyclooxygenase-2
Cy3	Cyanine 3
CYP24A1	Cytochrome P450 family 24 subfamily A member 1
CYP27B1	Cytochrome P450 family 27 subfamily B member 1
DCE-MRI	Dynamic contrast-enhanced magnetic resonance imaging
ENaC	Epithelial sodium channel
eNOS	Endothelial nitric oxide synthase
FGF23	Fibroblast growth factor 23
FGFR1	Fibroblast growth factor receptor 1
FGFR4	Fibroblast growth factor receptor 4
FITC	Fluorescein isothiocyanate
FP	Foot process
FSGS	Focal segmental glomerulosclerosis

Gad	Gracile axonal dystrophy
GAPDH	Glyceraldehyde 3-phosphate dehydrogenase
GBM	Glomerular basement membrane
GFB	Glomerular filtration barrier
GFR	Glomerular filtration rate
HA	Hemagglutinin
iNOS	Inducible nitric oxide synthase
IP3	Inositol trisphosphate
JGA	Juxtaglomerular apparatus
Kf	Glomerular capillary filtration coefficient
L-NAME	*N*ω-Nitro-L-arginine methyl ester
LPS	Lipopolysaccharides
MasR	Mas receptor
mono-Ub	Mono-ubiquitin
NCC	Sodium/chloride cotransporter
NE	Norepinephrine
NKCC2	Na-K-Cl cotransporter
nNOS	Neuronal nitric oxide synthase
NO	Nitric oxide
nonTG	Non-transgenic
Npt(s)	Sodium-phosphate cotransporter(s)
Npt2a	Sodium-phosphate cotransporter 2a
Npt2b	Sodium-phosphate cotransporter 2b
Npt2c	Sodium-phosphate cotransporter 2c
PAS	Periodic acid-Schiff
PECs	Parietal epithelial cells
PG	Prostaglandin
Phe	Phenylephrine
PHN	Passive Heyman's nephritis
Pit2	Phosphate transporter 2
PKA	Protein kinase A

PKC	Protein kinase C
PLA	Phospholipase A
PLC	Phospholipase C
Poly-Ub	Poly-ubiquitin
PTH	Parathyroid hormone
RAS	Renin angiotensin system
RBF	Renal blood flow
SBP	Systolic blood pressure
SD	Slit diaphragm
SGLT2	Sodium/glucose cotransporter 2
SLC34A1	Solute carrier family 34 member 1
SLC34A2	Solute carrier family 34 member 2
SLC34A3	Solute carrier family 34 member 3
TGF	Tubuloglomerular feedback
TI	Triton-insoluble
TRICKS	Time resolved imaging of contrast kinetics
TRPV5	Transient receptor potential cation channel subfamily V member 5
TRPV6	Transient receptor potential cation channel subfamily V member 6
TS	Triton-soluble
TxA2	Thromboxane A2
Ub	Ubiquitin
UCH	Ubiquitin C-terminal hydrolase
UCHL1	Ubiquitin C-terminal hydrolase L1
UPS	Ubiquitin-proteasome system
VAMP2	Vesicle-associated membrane protein 2
VDR	Vitamin D receptor
WT	Wild type
WT1	Wilm's tumour 1

ACKNOWLEDGEMENTS

First and foremost, I would like to thank my supervisor, Dr. Chris Kennedy, for his ongoing support throughout the last six and a half years of my graduate studies. His guidance has been invaluable not only in teaching me to become a better scientist, but also in helping me to grow into a critical-thinking researcher. I am forever grateful for all of the opportunities he has provided to me, including presenting my research at various conferences and allowing me to take more leadership in some of the laboratory projects. I would also like to sincerely thank my co-supervisor, Dr. Douglas Gray, for providing me the opportunity to conduct my graduate research and for his guidance throughout.

My thanks are owed to current and past members of the Kennedy laboratory, especially Chet Holterman, Jean-François Thibodeau, Lihua (Julie) Zhu and Anthony Carter. Their support with my experiments and their insightful suggestions undoubtedly allowed me to persevere in my research. My gratitude is also owed to several undergraduate students who have helped me along the way, including Justin Morin, Milica Novakovic, Andrea Liu and Eldjonai Kamto. Thanks to you all for being great lab mates. Moreover, I am grateful to some of the members of the Gray laboratory, especially Josée Coulombe and Mei Zhang for their help and guidance. There are also numerous individuals at the Kidney Research Centre who have provided me with advice and/or a helping hand and have been instrumental in helping me perform more stringent work. For this I am thankful.

I am grateful to my advisory committee, Luc Sabourin, Todd Fairhead and Dylan Burger for their input and suggestions to help me better my research.

I am grateful to the staff at the Animal Care and Veterinary Services for their assistance in maintaining my mice colonies and conducting mice procedures, especially Eileen Franklin, Kim Yates and Melissa Washington.

A special thanks goes to my parents, Lynn Lavictoire and William Read, for their support throughout my studies. Thank you for teaching me to persevere and to constantly aspire to achieve more. This has no doubt contributed to my successes throughout my graduate studies. I would also like to thank my brother, Zachary Read, for his emotional support and often much needed comic relief.

Finally, I would like to thank my husband, Eric Boisvert, for his continued love, support and encouragement throughout my graduate journey. Even when I preferred not to discuss my research or when the research wasn't quite going as well as I expected, his encouragements nevertheless gave me strength to persevere and achieve my goals.

GENERAL INTRODUCTION

UBIQUITIN C-TERMINAL HYDROLASE L1

Molecular Roles of Ubiquitin C-Terminal Hydrolase L1

Ubiquitin C-terminal hydrolase L1 (UCHL1), formerly protein gene product 9.5 (PGP 9.5), belongs to the ubiquitin C-terminal hydrolase (UCH) class of deubiquitinating enzymes. The UCH subgroup comprises three other members including UCHL3, UCHL5 (UCH37) and BAP1 (Bishop et al., 2016, Day et al., 2010). As a deubiquitinating enzyme, UCHL1 hydrolyses C-terminal esters and N-terminal amides of ubiquitin (Ub) that are tagged to proteins. The length of UCHL1's crossover loop limits its hydrolysis activity to mono-ubiquitinated substrates and as such, UCHL1 is not involved in disassembling poly-ubiquitin (poly-Ub) chains tagged to proteins (Zhou et al., 2012). This crossover loop contains a cysteine 90, aspartate 176 and histidine 161 that bridge access to the catalytic site. These residues are conserved in all UCH family members, however, the length of the crossover loops differ. As a result of its shorter crossover loop, UCHL1 demonstrates weak hydrolase activity, limiting it to mono-ubiquitinated substrates (Zhou et al., 2012). A crucial role for UCHL1 lies in its ability to bind to and stabilize mono-ubiquitin (mono-Ub) thereby maintaining Ub pools in the cell. UCHL3 is the most closely related paralog to UCHL1, sharing 52% identity to UCHL1 (Wilkinson et al., 1989). Similar to UCHL1, it is involved in hydrolysing small adducts of Ub tagged to substrates, but may also be involved in processing larger Ub conjugates as a result of its larger crossover loop (Grou et al., 2015, Larsen et al., 1998). UCHL3 is distributed in

lung, red cells and significant levels are also found in the brain (Wilkinson et al., 1989, Wilkinson et al., 1992). UCHL5 and BAP1, on the other hand, each possess a larger crossover loop that enables these to hydrolyse poly-Ub from substrates, thereby negatively regulating proteasomal degradation (Zhou et al., 2012). UCHL5 plays a role in recycling Ub from proteasomal degradation through direct interaction with the Ub-proteasome (Burgie et al., 2012, Yao et al., 2006). BAP1 plays a role in histone ubiquitination and transcriptional regulation (Fukuda et al., 2016, Yu et al., 2010). As such, UCHL1 is unique among its family members in its ability to maintain Ub pools.

Studies in *Uchl1*-deficient mice have demonstrated that loss of UCHL1 expression led to reduced Ub in the cerebellum (Osaka et al., 2003). Additionally, a D30K UCHL1 mutation (that results in lower Ub-binding affinity) reduced Ub pools in SH-SY5Y neuronal cells. Ablation of UCHL1's hydrolase domain through a C90S mutation (while the Ub-binding affinity remained intact) led to sustained Ub levels, supporting the conclusion that UCHL1 binds to and maintains Ub pools both *in vivo* and *in vitro* (Osaka et al., 2003). UCHL1 is also involved in processing polymeric Ub (Larsen et al., 1998).

UCHL1 Distribution in Neurons

UCHL1 expression predominates in the brain where it comprises a marked 1-5% of total neuronal protein. UCHL1 is detected in mouse neural epithelia as early as embryonic day 8.5-9. Its expression remains ubiquitous in terminally differentiated neurons throughout the brain and in both motor and sensory neurons of adult mice. UCHL1 distribution extends from the neuronal cytoplasm to the finest axonal branches that innervate a

respective tissue. Additionally, Wilson et *al* observed that UCHL1 is also expressed in the nuclei of a small percentage of neurons (Wilson et al., 1988).

Uchl1-Deficient Models

Studies in the gracile axonal dystrophy (gad) mouse have provided the greatest insight to UCHL1's role in neurons. The gad mouse was discovered by chance in an inbred strain of lab mice that began to demonstrate sensory ataxia at 12 weeks of age, followed by motor ataxia at 16 weeks of age. These mice developed significant neurodegeneration, which manifested first as hind limb paralysis, eventually spreading to the forelimbs. The mice did not survive past 6 months of age (Mukoyama et al., 1989). The phenotype was later attributed to an in-frame deletion of exons 7 and 8 of the *Uchl1* gene, corresponding to amino acid residues 154 to 196, including the catalytic histidine at position 161 (Saigoh et al., 1999). While the truncated version of UCHL1 was transcribed, no UCHL1 protein was detected, suggesting total ablation of UCHL1 in these mice (Saigoh et al., 1999).

Post-mortem histological analysis of gad mice revealed an axonal "dying back" type of degeneration, similar to Wallerian degeneration (Oda et al., 1992). Specifically, spheroidal inclusion bodies were detectable in axons emanating from the dorsal root ganglions of the gracile tract, which comprises the longest axons of the central nervous system (Ichihara et al., 1995, Mukoyama et al., 1989, Yamazaki et al., 1988). Other primary sensory neurons were also affected, including second order neurons from the dorsal nucleus, dorsal spino-cerebellar tracts and trigeminal tracts, afferent neurons from muscle spindles and efferent motor neurons (Kikuchi et al., 1990, Oda et al., 1992).

Within these neurons, β- and γ-synuclein, β-amyloid and Ub-positive aggregates were observed in spheroid deposits (Osaka et al., 2003, Wang et al., 2004). Together, these data point to a crucial role for UCHL1 in axonal transport, as spheroids are generally indicative of impaired axonal transport, leading to the accumulation of proteins involved in neuronal firing upstream of axon termini and subsequent dysregulation of neuroeffector communication (Coleman, 2005). In the nm3419 mouse, a premature stop codon was introduced, resulting in the deletion of the seventh exon of the *Uchl1* gene and no detectable UCHL1 protein expression. Similar to gad mice, nm3419 mice displayed neurodegeneration, motor defects, attenuated Ub levels in brain extracts and ER stress in corticospinal motor neurons (Jara et al., 2015, Walters et al., 2008). Chen *et al* also found a similar phenotype in another *Uchl1*-/- mouse model that lacks exons 6-8 (and the first 6bp of exon 9) of the *Uchl1* gene. In the absence of UCHL1, synaptic transmission at the neuromuscular junction was impaired and muscle denervation was evident. Moreover, tubulovesicular structures were evident in presynaptic nerve termini (Chen et al., 2010). More recently, the Gray lab has developed *Uchl1*-/- mice where a 16kbp fragment of exon 4 was replaced by a selectable marker pgk-neo-pgk (phosphoglycerate kinase promoter/neomycin phosphotransferase/phosphoglycerate kinase 3′ untranslated region), leading to neurodegeneration, similar to gad mice. *Uchl1* deletion also led to axonal swellings in the striatum, perturbations in Ub pools and a significant reduction in glutathione levels. Studies of the *Uchl1* null enteric nervous system showed significant morphological changes associated with increased gastrointestinal transit time, rendering *Uchl1* null mice a useful model of gut aging. Moreover, their data suggest that reduced

glutathione levels may increase susceptibility of *Uchl1*-/- mice to oxidative stress (Coulombe et al., 2014).

UCHL1 in Non-Neuronal Cells

UCHL1 expression is low in somatic tissues, with the exception of testes and ovaries. In the human testis, UCHL1 expression is prominent in spermatogonia and Leydig cells where its function is still unclear. In ovaries, UCHL1 is thought to play a role in oocyte maturation and the prevention of polyspermy. Gad mice display a 10-fold increase in polyspermy at fertilization (Ellederova et al., 2004, Sekiguchi et al., 2006). An increasing body of evidence has demonstrated abnormal UCHL1 expression in cells undergoing stress (Wilson et al., 1988). For instance, UCHL1 is expressed in cancer cells originating from tissues where UCHL1 is normally absent (Jang et al., 2011, Kim et al., 2009, Miyoshi et al., 2006, Tezel et al., 2000, Yamazaki et al., 2002).

In diseased tissues there is also a strong correlation between UCHL1 induction and Ub pools. Recent findings describe significant UCHL1 expression in diseased non-neuronal kidney cells, specifically in podocytes, suggesting a role for UCHL1 in glomerular disease (1). Additionally, Bradbury *et al* demonstrated significant UCHL1 protein levels in the healthy human kidney (after the brain and testis) but the contribution of neuronal UCHL1 to this has not been investigated (Bradbury et al., 1985). Renal innervation is required to maintain glomerular hemodynamics and renal function and neuronal UCHL1 may therefore play a role to these ends (2). These points will be addressed in detail in projects (1) and (2) outlined below.

THE ROLE OF UCHL1 IN GLOMERULAR DISEASE (1)

The Glomerulus

The glomerulus is the principal filtration unit of the kidney that provides the foremost barrier to filtration in the nephron. Blood enters into the glomerulus through the afferent arteriole, circulates through a network of capillary loops where filtration occurs, and finally, exits the glomerulus by the efferent arteriole before continuing downstream to the peritubular capillaries where tubular secretion and reabsorption take place. The glomerular capillaries form a network of capillary loops held together by mesangial cells. The glomerular capillaries are lined with a layer of fenestrated endothelial cells, a glomerular basement membrane (GBM) and podocytes (and their foot processes (FP)), together forming the tripartite glomerular filtration barrier (GFB). This specialized filtration barrier blocks the passage of large macromolecules and plasma proteins while permitting water and small solutes to be filtered into the urinary filtrate. The urinary filtrate is then collected into Bowman's space, which is surrounded by a Bowman's capsule lined by parietal epithelial cells (PECs), and leads downstream into the proximal tubule and through the remainder of the nephron (Figure 1) (Kurts et al., 2013).

The Podocyte

Podocytes (also known as visceral glomerular epithelial cells) are terminally differentiated cells that lie on the extravascular side of the glomerular capillary. Podocytes are characterized by a large cell body that gives rise to major processes that

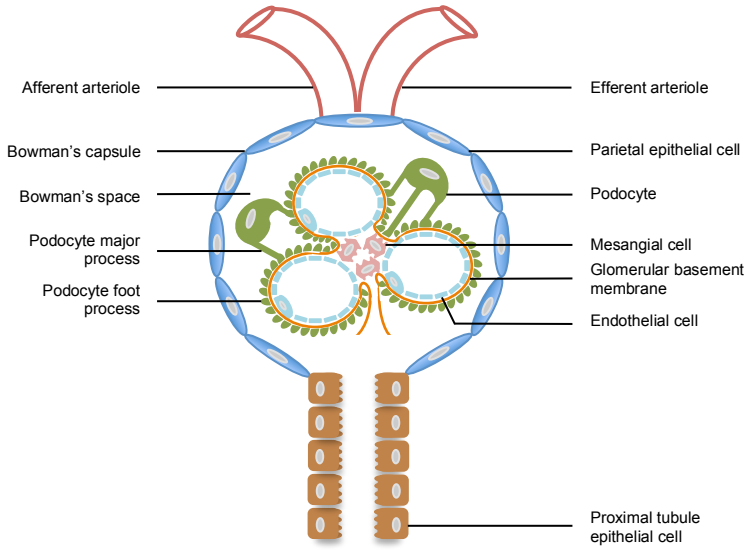

Figure 1. The glomerulus. Blood enters the glomerulus through the afferent arteriole where it passes through a network of capillary loops maintained together by mesangial cells. The glomerular capillaries are lined with a layer of fenestrated endothelial cells, a glomerular basement membrane and podocytes (and their foot processes). Together these form the glomerular filtration barrier. The filtered load passes through the glomerular filtration barrier before entering the Bowman's space, which is surrounded by a layer of parietal epithelial cells (Bowman's capsule), and continues downstream into the proximal tubule (lined by proximal tubule epithelial cells) and through the remainder of the nephron.

further extend into primary FP that cover the GBM. This highly specialized morphology is crucial, as podocytes must constantly counteract the distending forces of the glomerular capillary (Greka et al., 2012, Pavenstadt et al., 2003). Furthermore, podocyte FPs interdigitate and join laterally to FPs of adjacent podocytes forming uniform slits between them. These slits are interconnected by an extracellular structure known as the slit diaphragm (SD), which provides a final barrier to filtration. The SD provides an isoporous filter to control the size and selectivity of molecules (30-40μm) passing though the filtration barrier (Furukawa et al., 1991, Rodewald et al., 1974).

The Podocyte Cytoskeleton and the Slit Diaphragm

The podocyte cytoskeleton plays a crucial role in maintaining podocyte integrity. The podocyte cell body and its major processes are mainly composed of intermediate filaments and microtubules. Podocyte FPs, on the other hand, comprise a large network of contractile F-actin microfilaments that bind to filaments in the major processes and emanate into the FP. The F-actin cytoskeleton is organized in bundles by bivalent actin cross-linking proteins such as dystrophin or α-actinin-4. The specific assembly of F-actin filaments extending to the base of podocyte FPs permits binding of F-actin to integrins (predominantly α3β1 integrin) and α- and β-dystroglycans, those in turn bind and affix the FPs to the GBM. On the lateral side of the podocyte FP, F-actin also binds to several adapter proteins that extend into and help to form the SD (Cortes et al., 2000, Drenckhahn et al., 1988, Kobayashi et al., 1998, St John et al., 2001). Not only does the SD provide structural integrity and a barrier for filtration, it also comprises a signaling network of proteins in adjacent podocyte FPs. The SD proteins include zonula occludens-1, nephrin, CD2-associated protein (CD2AP), P-cadherin, synaptopodin and podocin among others. Maintenance of the podocyte cytoskeleton and by extension the SD is crucial to maintain proper function of the GFB (Pavenstadt et al., 2003).

Podocyte Injury

Podocyte injury is the hallmark of several glomerular diseases including minimal change disease, focal segmental glomerulosclerosis (FSGS), membranous glomerulopathy, diabetic nephropathy and lupus nephritis. Podocyte injury may stem from various insults, internal or external, ultimately leading to variations including (but not limited to)

alterations of SD architecture, interference with the GBM, changes to the negative surface charge of podocytes, variations in Ca^{2+} homeostasis and disruptions of the actin cytoskeleton. Podocytes in turn react according to a specific pattern, by retracting their FPs into their cell bodies, forming a flattened epithelium. As a result, the integrity of the GFB becomes compromised, allowing larger plasma proteins and macromolecules to be filtered through into the urinary filtrate and into the urine, a condition known as proteinuria. Podocytes may also undergo hypertrophy and detach from the GBM leading to denuding of the glomerular capillary and glomerulosclerosis (Greka et al., 2012). Several human genetic mutations to podocyte-specific proteins can lead to a similar injury pattern, and have provided insight to the understanding of podocyte injury. Mutations in the nephrin and podocin genes, for instance, disrupt the SD, causing early onset proteinuria, glomerular lesions and FSGS in humans (Boute et al., 2000, Kestila et al., 1998). Moreover, mutations to several podocyte-specific gene products including CD2AP, inverted formin-2, transient receptor potential cation channel subfamily C member 6, synaptopodin and α-actinin-4 result in FSGS, a condition that manifests as adult-onset proteinuria and progressive glomerular scarring (Brown et al., 2010, Dai et al., 2010, Kaplan et al., 2000, Kim et al., 2003, Winn et al., 2005).

α-Actinin-4

α-Actinin-4 belongs to the family of α-actinins, a family comprised of four isoforms (α-actinins-1-4, encoded by the *ACTN1-4* genes, respectively). α-Actinins cross-link F-actin and bridge it to the plasma membrane (Abe et al., 1973, Dixson et al., 2003, Otey et al., 2004). In humans, α-actinin-4 is the only α-actinin isoform expressed in the kidney

(Kaplan et al., 2000). In the mouse kidney, α-actinin-1 and α-actinin-4 are expressed. Their roles are however not functionally redundant as global deletion of *ACTN4* leads to severe glomerular injury in mice (Kos et al., 2003). α-Actinin-1 is a non-muscle α-actinin that is thought to play a role in focal adhesions, such as anchoring F-actin to proteins including talin, vinculin and β-integrins (Chen et al., 1982, Honda et al., 1998, Langanger et al., 1984, Lazarides et al., 1975, Meigs et al., 1986). Conversely, α-actinin-2 is expressed in cardiac and skeletal muscle, whereas α-actinin-3 expression is limited to skeletal muscle (Beggs et al., 1992). α-Actinin-2 and α-actinin-3 are both Ca^{2+}-insensitive α-actinins that cross-link F-actin in Z-discs of striated muscle cells (Endo et al., 1984).

α-Actinin-4 is a head-to-tail homodimer that cross-links and bundles F-actin. α-Actinin-4 houses three actin-binding sites (ABS), ABS1, ABS2 and ABS3 and a phosphatidyl inositide (PI)-binding site within two calponin-homology domains (CHD), CHD1 and CHD2 at its N-terminus. The CHD are followed by four spectrin-like repeats, R1-R4 and two EF-hand calcium regulation domains, EF1 and EF2 at the C-terminus (Djinovic-Carugo et al., 1999, Pelletier et al., 2003). Normally, α-actinin-4 adopts a closed conformation between CHD1 and CHD2, which exposes ABS2 and ABS3 to F-actin binding, whereas ABS1 remains buried and inaccessible to F-actin. α-Actinin-4's function to bind to F-actin allows stress fibre formation and F-actin anchoring (via α-actinin-4) to the cell's focal adhesions. Disruption of α-actinin-4 results in breakage of these links and loss of actin stress fibres (Rajfur et al., 2002). Thus, α-actinin-4 has an important role in regulating cell motility, endocytosis and adhesion, as α-actinin-4 deficiency impairs these processes (Rajfur et al., 2002, Weins et al., 2007).

Mutations in the *ACTN4* gene are associated with a familial autosomal dominant form of FSGS (Dai et al., 2009, Winn et al., 1999). Although α-actinin-4 is widely expressed, the effects of mutations in the *ACTN4* gene are exclusively apparent in the podocyte. Homozygous mice deficient for α-actinin-4 exhibit progressive podocyte FP effacement and severe glomerular disease with FSGS-like lesions by 10 weeks of age, leading to death by several months of age (Kos et al., 2003). Conditionally immortalized *ACTN4*-/- podocytes express podocyte markers similar to controls; however, adhesion to components of the GBM is significantly impaired, providing the most likely explanation for podocyte loss and subsequent glomerular injury in *ACTN4*-/- mice (Dandapani et al., 2007). Furthermore, missense mutations (i.e. W59R, K228E, T232I, K255E, T259I, S262P, Q348R, V801M and R837Q) of the *ACTN4* gene result in FSGS in both humans and similarly in mice (Kaplan et al., 2000, Mathis et al., 1998, Michaud et al., 2003, Weins et al., 2005). These missense mutations are associated with a gain of function, increasing α-actinin-4's binding affinity for F-actin. Further work has demonstrated that the missense mutations cause a conformational change to α-actinin-4's protein structure, exposing the third actin-binding site (ABS1) that is normally buried and inaccessible to F-actin, thereby allowing α-actinin-4 to bind to F-actin with all three of its ABS (Kaplan et al., 2000, Weins et al., 2007). As a result, mutant α-actinin-4/F-actin aggregates begin to form, leading to the redistribution of α-actinin-4 from the podocyte cell periphery to the cell body (Figure 2) (Michaud et al., 2006, Weins et al., 2005). The Kennedy lab has previously developed mice with podocyte-specific K256E-α-actinin-4 transgene expression (where K256E is the mouse ortholog to the human K255E mutation). Indeed,

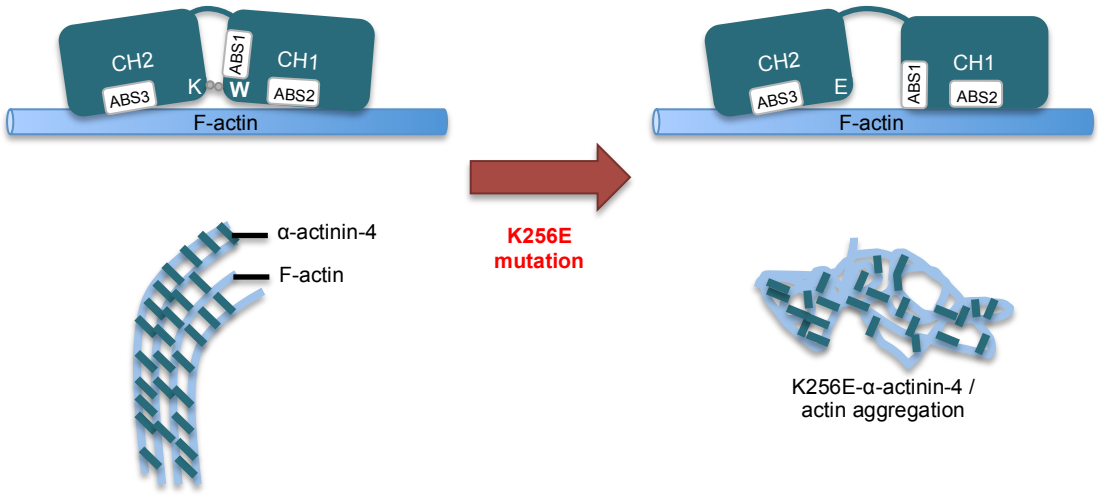

Figure 2. K256E-α-actinin-4 mutation. α-Actinin-4 normally adopts a closed conformation between CH1 and CH2 allowing it to form actin bundles. The K256E mutation disrupts the wild type lysine-tryptophan hinge, causing a change in conformation that exposes a third actin-binding site, ABS1. K256E-α-actinin-4 binds to F-actin with all three of its ABS, forming K256E α-actinin-4/F-actin aggregates. Adapted from Weins *et al.*, 2007.

similar to the pathophysiology of FSGS in humans, a proportion of these mice develop proteinuria and glomerular disease with FSGS lesions (Michaud et al., 2003). The expression of K256E-α-actinin-4 in conditionally immortalized mouse podocytes impairs spreading, motility and peripheral projection formation, providing evidence on how cytoskeletal defects due to the disruption of α-actinin-4 can lead to podocyte damage and FP effacement *in vivo* (Michaud et al., 2006). Interestingly, the estimated half-life of the mutant α-actinin-4 protein is shortened compared to the wild type. To this end, it has been shown that the mutant α-actinin-4 is degraded via the Ub-proteasome system (UPS) (Cybulsky et al., 2009, Yao et al., 2004). However, these aggregates may eventually exhaust the UPS, as mutant α-actinin-4/F-actin aggregates continue to accumulate, presumably "choking" or impairing the Ub-proteasome (Cybulsky et al., 2009).

UCHL1 in the Kidney

While UCHL1 expression is largely neuronal, there is an increasing amount of data to support that UCHL1 is also expressed in healthy and diseased kidneys, specifically in diseased glomeruli. In the kidney, UCHL1 localization differs according to the species in question. Wilson *et al* led one of the first reports describing UCHL1 in the rat distal tubule and PECs surrounding the Bowman's capsule (Wilson et al., 1988). Shirato *et al* corroborated these findings by demonstrating strong UCHL1 expression in PECs of the adult rat kidney. Additionally, during rat nephrogenesis, UCHL1 was expressed in PECs and to a lesser extent, in presumptive podocytes of the S-shaped body, suggesting a role for UCHL1 in PEC and podocyte development. UCHL1 expression was also depicted in cellular crescents and cells adhered to the glomerular tuft in rat glomerular disease models such as Masudi-nephritis and puromycin aminonucleoside nephrosis, providing the first evidence that UCHL1 is associated with glomerular disease (Shirato et al., 2000). In healthy human renal biopsies, UCHL1 is expressed in the macula densa, PECs and proximal tubules (Diomedi-Camassei et al., 2005, Meyer-Schwesinger et al., 2009).

In vitro, UCHL1 levels are detectable in undifferentiated conditionally immortalized mouse podocytes. Upon differentiation, UCHL1 levels decline, similar to the developmental pattern observed in rat podocytes *in vivo*. Loss of UCHL1 in differentiated podocytes correlates with increased expression of podocyte-specific markers such as α-actinin-4, nephrin and synaptopodin. Similarly, UCHL1 inhibition promotes membrane protrusion formation accompanied by podocyte FP-associated protein redistribution to the plasma membrane, in a time and dose-dependent manner (Meyer-Schwesinger et al.,

2009). Consistent with these findings, Diomedi-Camassei *et al* showed UCHL1 immunopositivity in metabolically active cells of human renal conditions such as tubular hypertrophy, cellular regeneration and crescent formation. Importantly, UCHL1 levels strongly correlated with Ub levels in these locales (Diomedi-Camassei et al., 2005).

UCHL1 in Diseased Podocytes

Terminally-differentiated podocytes lack UCHL1 expression *in vivo* and *in vitro*. Upon disease induction, specifically in glomerular disease, UCHL1 upregulation is evident in podocytes, as demonstrated in rats and humans (Meyer-Schwesinger et al., 2009, Shirato et al., 2000). The first studies utilized colloidal gold labelling to show UCHL1 upregulation in podocytes of humans biopsies with IgA nephropathy and lupus nephritis. Similarly, Meyer-Schwesinger *et al* demonstrated podocyte UCHL1 induction (along with elevated Ub levels) in numerous human proteinuric glomerular diseases, where Alport's syndrome, membranous glomerulonephritis, idiopathic FSGS, SLE class V, TBM disease (among other glomerular diseases) showed the strongest UCHL1 immunopositivity (Meyer-Schwesinger et al., 2009). Together these data suggest a role for UCHL1 in metabolically active podocytes subjected to diseased conditions.

Studies investigating UCHL1 inhibition in glomerular disease further suggest that UCHL1 plays a detrimental role in the pathogenesis of glomerular lesions. In Passive Heyman's nephritis (PHN), a rat model of membranous nephropathy, podocyte UCHL1 is upregulated, coincident with an increase in poly-ubiquitinated proteins in glomerular lysates. The chymotrypsin-like activity of the Ub-proteasome was increased 4 days post-

disease induction followed by a significant decline in activity 6-365 days post-disease induction. These phenotypic changes were associated with podocyte FP effacement and albuminuria. UCHL1 inhibition with the pharmacological inhibitor LDN57444 restored Ub-proteasome activity and ameliorated albuminuria and podocyte FP effacement (Meyer-Schwesinger et al., 2011). In diseased conditions, UCHL1 may therefore play a maladaptive role in podocytes by promoting increased Ub pools to facilitate the degradation of cytotoxic proteins via the UPS. However, these may eventually overwhelm the UPS, leading to the accumulation of damaged proteins, podocyte damage, albuminuria and glomerular disease. UCHL1 inhibition may therefore restore UPS activity in podocytes via lowering of Ub pools. Together these data support the notion that UCHL1 induction in glomerular disease is maladaptive.

Rationale (1)

Work from the Kennedy lab shows that the FSGS-associated mutant K256E-α-actinin-4 predominates in the podocyte cell centre where it forms aggregates that are targeted for Ub-mediated proteosomal degradation (Cybulsky et al., 2009, Michaud et al., 2006). Similarly, podocyte UCHL1 induction is associated with the sequestration of wild type α-actinin-4 from the plasma membrane to the cell centre. Meyer-Schwesinger *et al* also demonstrated that UCHL1 is upregulated in podocytes of patients with FSGS and this induction was accompanied by a concomitant increase in podocyte Ub pools (Meyer-Schwesinger et al., 2009). As such, we postulate that UCHL1 may be upregulated in podocytes expressing the FSGS-associated K256E-α-actinin-4. UCHL1 induction in this context may be an adaptive mechanism, serving to promote Ub pools for UPS-mediated

degradation of K256E-α-actinin-4/F-actin aggregates. Furthermore, UCHL1 inhibition in PHN rats significantly reduced poly-ubiquitinated proteins and restored Ub-proteasome activity compared to rat PHN controls (Meyer-Schwesinger et al., 2011). As such, these data imply that UCHL1 induction promotes maintenance of Ub pools, poly-ubiquitination of proteins and aggregate formation that may in turn impair the Ub-proteasome, as UCHL1 inhibition significantly improved Ub-proteasome activity, podocyte FP effacement and the degree of albuminuria in this model. Similarly, we propose that UCHL1 also plays a maladaptive role in *ACTN4*-associated FSGS wherein UCHL1 exacerbates the formation of K256E-α-actinin-4/F-actin aggregates that impair the UPS, thereby leading to albuminuria, podocyte injury and glomerulosclerosis (Figure 3). Based on these findings we hypothesize the following:

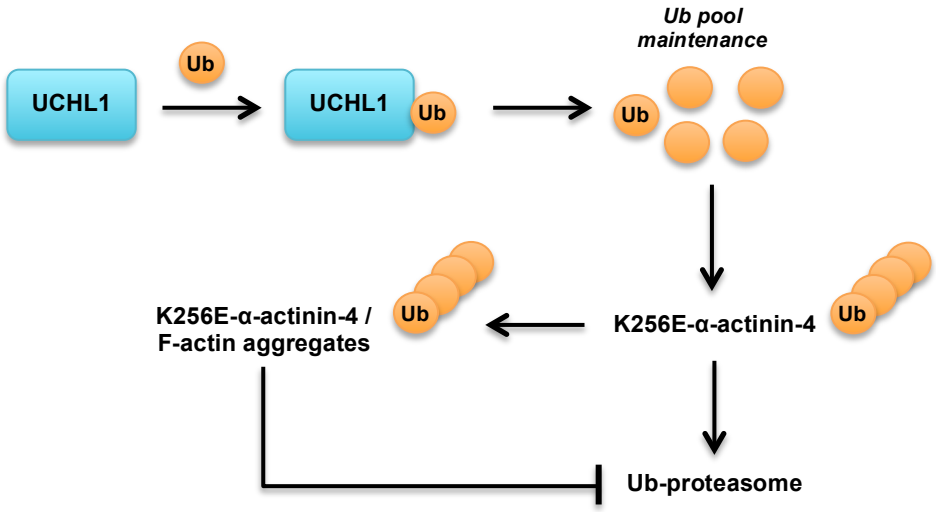

Figure 3. Proposed mechanism: The role of UCHL1 in *ACTN4*-associated FSGS. UCHL1 upregulation serves to promote ubiquitin (Ub) pools for the degradation of cytotoxic proteins, including K256E-α-actinin-4, via the Ub-proteasome. Over time, however, K256E-α-actinin-4 poly-ubiquitinated aggregates accumulate thereby impairing the Ub-proteasome.

Hypothesis (1)

Podocyte UCHL1 is upregulated in mice overexpressing podocyte-specific K256E-α-actinin-4 (K256E-*ACTN4*$^{pod+}$) where it promotes Ub pools for the degradation of K256E-α-actinin-4/F-actin aggregates. However, these may eventually overwhelm the UPS, leading to podocyte injury and glomerular scarring. *Uchl1* deletion in K256E-*ACTN4*$^{pod+}$ mice should therefore ameliorate indices of podocyte and glomerular injury.

THE ROLE OF UCHL1 IN RENAL HEMODYNAMICS (2)

Renal Blood Flow

Renal blood flow (RBF) accounts for 20-22% of the cardiac output, translating to 1100ml/min in a 70kg man. Blood enters through the renal artery located at the hilum of the kidney and passes through a network of renal arteries that include the interlobar arteries, arcuate arteries and interlobular arteries, before passing through the afferent arterioles, glomerular capillaries, efferent arterioles, and finally, the peritubular capillaries. The high hydrostatic forces of the glomerular capillaries promotes glomerular filtration, whereas downstream of these, low hydrostatic forces in the peritubular capillaries promote tubular reabsorption. The highest vascular resistances occur in the interlobular arteries, afferent arterioles and notably, in the glomerular capillaries. The peritubular capillaries then connect to the venous system through the interlobular veins, after which the blood passes through the arcuate veins, interlobar veins and finally, into the renal vein, which exits the kidney at the hilum, parallel to the renal artery and ureter (Guyton et al., 2006).

Glomerular Filtration Rate

Glomerular filtration rate (GFR) is defined as the product of the net filtration pressure and the glomerular capillary filtration coefficient (Kf). The net filtration pressure includes the glomerular capillary hydrostatic pressure (P_G; 60mm Hg; promotes filtration), the glomerular capillary colloid osmotic pressure (π_G; 32mm Hg; opposes filtration), the hydrostatic pressure in the Bowman's capsule (P_B; 18mm Hg; opposes filtration) and the colloid osmotic pressure from proteins in the Bowman's capsule (π_G; 0mm Hg; promotes filtration). Kf is dependent on the hydraulic conductivity across the glomerular capillary and the glomerular capillary surface area. GFR is expressed mathematically as GFR = Kf x (P_G - π_G - P_B + π_B). Under healthy conditions, the net filtration pressure across the glomerular capillary is 10mm Hg. Thus, the major determinant of GFR is P_G across the glomerular capillary. P_G can be adjusted by altering afferent and efferent arteriole

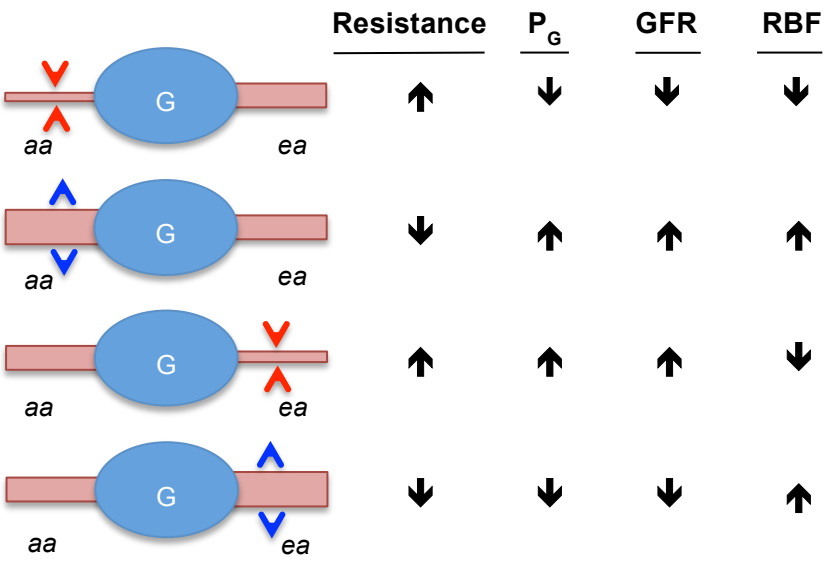

Figure 4. Glomerular hemodynamics. Increased/decreased resistance of the afferent or efferent arterioles (denoted aa and ea, respectively) will have differential effects on glomerular capillary hydrostatic pressure (P_G), glomerular filtration rate (GFR) and renal blood flow (RBF), as outlined above. G denotes the glomerulus.

resistance. Increasing afferent arteriole resistance decreases P_G and reduces GFR while reducing afferent arteriole resistance increases P_G and elevates GFR. Conversely, increasing efferent arteriole resistance increases P_G and elevates GFR, while decreasing efferent arteriole resistance decreases P_G and reduces GFR (Figure 4). Moderate efferent arteriole constriction will raise GFR, however, upon severe efferent arteriole constriction, there is a gradual increase in plasma protein levels that increases π_G, opposing filtration and reducing GFR. Of note, increased arterial pressure can increase GFR by raising P_G, however, autoregulation generally counteracts these effects (Guyton et al., 2006).

Autoregulation

The ability of the kidneys to autoregulate RBF and GFR allow it to keep these parameters constant despite fluctuations in arterial pressure. The kidney achieves this through two different mechanisms. The first, the myogenic mechanism, is activated upon increases in vessel wall tension. This initiates vascular smooth muscle cell contraction of the pre-glomerular arterioles, mainly the afferent arterioles, to help prevent overdistension of vessel walls. As a result, afferent arteriole constriction reduces P_G, thereby decreasing GFR. RBF is reduced in this setting. The second, tubuloglomerular feedback (TGF), maintains GFR by regulating increases in extracellular volume, specifically through the detection of chloride ions at the macula densa. TGF is activated following increases in arterial pressure that cannot be completely compensated for by the myogenic mechanism (Burke et al., 2014). The TGF mechanism depends on a special arrangement of cells at the vascular pole of the glomerulus: the macula densa cells and the juxtaglomerular cells. Macula densa cells are a group of highly specialized epithelial cells located at the end of

the thick ascending limb/beginning of the distal tubule. These detect changes in chloride ions and initiate subsequent signaling cascades. The juxtaglomerular cells of the afferent and efferent arterioles come into contact with the macula densa cells and together form the juxtaglomerular apparatus (JGA). The juxtaglomerular cells are granular in appearance due the presence of renin secretory granules. Finally, the extra-glomerular mesangial cells maintain this structure (Peti-Peterdi et al., 2010). GFR elevations are associated with increased tubular flow rate and, by pressure natriuresis, the likelihood of sodium and chloride reabsorption in the proximal tubule is decreased (Roman et al., 1988, Williams et al., 2007). Macula densa cells subsequently sense the increased distal chloride delivery through the Na-K-Cl cotransporter 2 (NKCC2) and initiate signaling cascades that lead to adenosine/ATP release and afferent arteriole constriction (Oppermann et al., 2006, Oppermann et al., 2007, Schlatter et al., 1989). This is a negative feedback mechanism that normalizes GFR (Burke et al., 2014).

In contrast, GFR reductions attenuate the TGF mechanism. A drop in GFR is associated with a reduced tubular flow rate and increased sodium and chloride reabsorption in the tubules. This in turn reduces chloride delivery at the macula densa, which responds by initiating afferent arteriole dilation and efferent arteriole constriction. Together, these normalize RBF and GFR. Afferent arteriole dilation is achieved by attenuating adenosine/ATP release and by stimulating nitric oxide (NO) release through macula densa-derived neuronal nitric oxide synthase (nNOS). Efferent arteriole constriction is dependent on renin release by the juxtaglomerular cells, which serves to promote

angiotensin II (Ang II) formation and efferent arteriole vasoconstriction through the angiotensin type 1 receptor (AT1R) (Burke et al., 2014, Peti-Peterdi et al., 2010).

The Renin Angiotensin System

Renin release from the juxtaglomerular cells is the first and the rate-limiting enzyme of the renin angiotensin system (RAS) pathway. Renin secretion is controlled by several mechanisms including renal sympathetic nerve stimulation of the JGA, low perfusion pressure and low salt delivery at the macula densa. Briefly, renin enters the circulation where it converts angiotensinogen (produced by the liver) to angiotensin I (Ang I), where Ang I is converted to Ang II by the angiotensin-converting enzyme 1 (ACE1) in the lungs (Figure 5). Ang II exerts a potent vasoconstrictive effect on the peripheral vasculature thereby increasing arterial pressure and sodium retention. It also increases cardiac output. In the kidney, Ang II may predominantly constrict the efferent arteriole as AT1R expression is greater compared to the afferent arteriole, thereby normalizing renal perfusion by increasing GFR. However, some studies show that Ang II equally constricts both afferent and efferent arterioles (Carmines et al., 1986, Schweda et al., 2007).

Ang II's effects through the AT1R are well defined. The AT1R is a Gq-coupled receptor that promotes phospholipase C (PLC) activation and inositol trisphosphate (IP3) production, the release of intracellular calcium stores and protein kinase C (PKC) activation. Ang II's effects through the AT2R are less known, but it appears that AT2R-mediated signaling has vasodilatory effects, promoting renal NO formation, bradykinin and eicosanoid synthesis (Siragy et al., 1997, Siragy et al., 1999, Siragy et al., 2000).

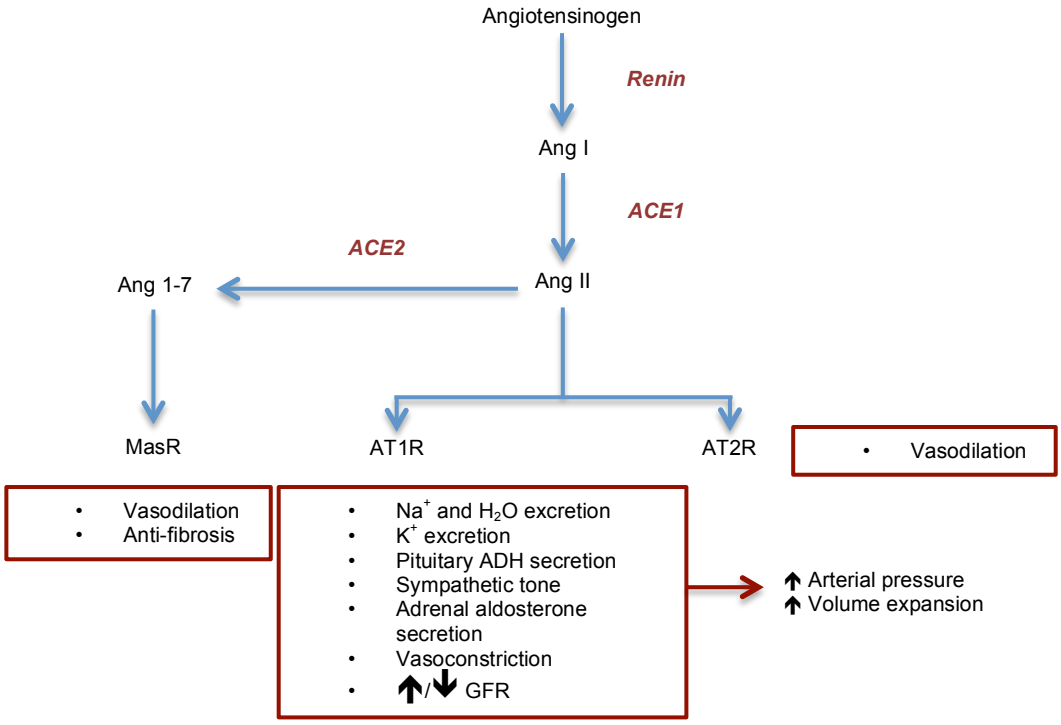

Figure 5. The renin angiotensin system. Angiotensinogen (produced by the liver) is converted by renin (secreted by renal juxtaglomerular cells) to angiotensin I (Ang I), which is then converted to angiotensin II (Ang II) by the angiotensin-converting enzyme 1 (ACE1; in the lungs). Ang II acts through the angiotensin type 1 receptor (AT1R) to promote vasoconstriction, increased arterial pressure and volume expansion. Ang II's effects through the AT2R are vasodilatory. The angiotensin-converting enzyme 2 (ACE2) can also convert Ang II to Ang 1-7, which acts through the Mas receptor (MasR) to promote vasodilation and anti-fibrotic effects.

Cyclooxygenase-2

Renin release is influenced by cyclooxygenase-2 (COX-2)-derived prostaglandins (PG). Briefly, the COX-2 enzyme converts arachidonic acid to PGH2, which is metabolized to biologically active prostanoids, PGE2, PGI2, PGD2, PGF2 and thromboxane A2 (TxA2), which act on their respective receptor(s) to exert distinct signal transductions. Among these, the effects of PGE2 (through the EP receptors 1-4) in renal pathophysiology are best understood (Figure 6) (Hao et al., 2008). COX-2-derived PGE2 from macula densa cells acts primarily through EP4 Gs-coupled receptors on the juxtaglomerular cells to

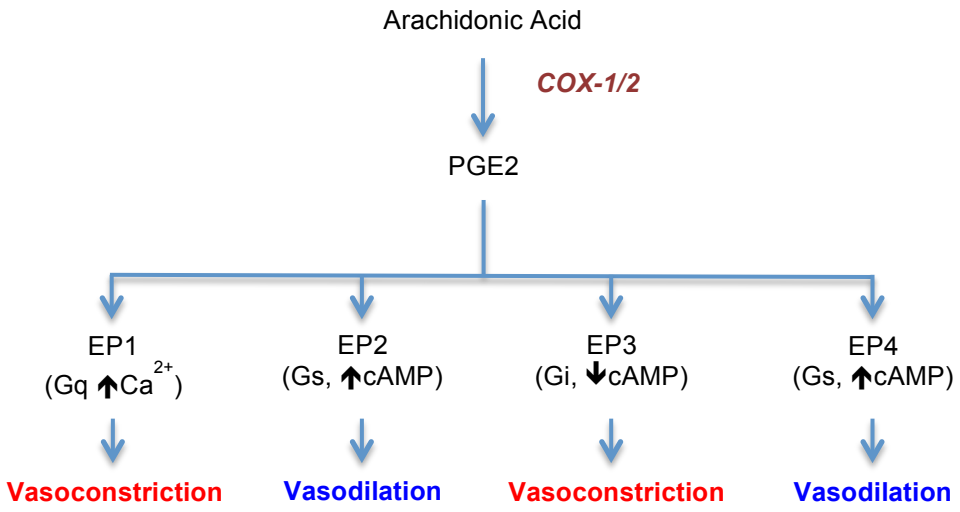

Figure 6. Cyclooxygenase/prostaglandin-mediated stimulation of EP receptors. Arachidonic acid derived from membrane phospholipids is converted to prostaglandin E2 (PGE2) by cyclooxygenases-1 and -2 (COX-1/2). PGE2 in turn stimulates the G-coupled EP receptors 1-4 to increase/decrease cyclic AMP or increase intracellular calcium, thereby promoting vasoconstriction or vasodilation.

increase cAMP and stimulate renin secretion (Wang et al., 1999). COX-2-deficient mice show reduced renin expression associated with attenuated plasma renin activity (Kim et al., 2007). Macula densa COX-2 is constitutively expressed, however, under low dietary salt conditions, high renin, diuretics or ACE inhibition, COX-2 is induced (Cheng et al., 2001, Kim et al., 2007, Mann et al., 2001, Reinalter et al., 2002, Yang et al., 1998). Renin induction by PGE2 is undoubtedly an important mechanism to help regulate GFR following volume depletion. Moreover, COX-2 also regulates GFR independently of its ability to promote renin secretion. COX-2 inhibition following high protein loading-induced hyperfiltration reduced GFR but had no effect on renin levels, indicating the involvement of an alternate mechanism. COX-2 via PGE2 primarily mediates a vasodilatory effect in the renal vasculature, and these studies determined that this includes the afferent arteriole (through EP2 and EP4 receptors) (Yao et al., 2006). COX-2

is also a target of negative feedback by the RAS. Ang II inhibits COX-2 through AT1R signaling (Cheng et al., 1999, Zhang et al., 2006). However, upon AT1R inhibition, Ang II-associated AT2R-derived signaling induces COX-2 (Zhang et al., 2006).

Nitric Oxide

In addition to PGE2 release by the macula densa cells, nNOS-derived NO is released as a counteregulatory mechanism to autoregulation. NO also counterbalances Ang II-associated vasoconstriction of the afferent and efferent arterioles (Manning et al., 1993, Patzak et al., 2001). In the kidney, NO is a potent vasodilator derived from nNOS in the macula densa or endothelial nitric oxide synthase (eNOS) in the renal endothelium (Majid et al., 2001). Non-selective NOS inhibition with *N*ω-Nitro-L-arginine methyl ester (L-NAME) significantly elevated renal vascular resistance (Alberola et al., 1994, Baumann et al., 1992, Berthold et al., 1999). In macula densa preparations perfused with a high salt solution, L-NAME significantly increased afferent arteriole constriction, suggesting that NO attenuates afferent arteriole resistance upon TGF activation (Ren et al., 2001). Selective nNOS inhibition promoted hypertension and a transient sensitization of TGF, highlighting a role for NO in regulating afferent arteriolar tone (Ollerstam et al., 1997). Acute nNOS inhibition in rats led to a significant reduction in GFR, without affecting RBF, renal vascular resistance or blood pressure (Sigmon et al., 2000).

The notion that Ang II constricts both the afferent and efferent arterioles is controversial. AT1Rs are expressed on both arterioles and multiple studies have shown proportional constriction of both arterioles. However, as NO primarily dilates the afferent arteriole,

this may offset Ang II-mediated constriction, allowing for Ang II-mediated constriction of the efferent arteriole to predominate (Ichihara et al., 1998, Patzak et al., 2005).

Renal Sympathetic Nerve Activity

Renal sympathetic activity directly regulates GFR and RBF by promoting constriction of the renal vasculature, decreasing both GFR and RBF. Sympathetic nerves richly innervate the renal vasculature. These also come into contact with the juxtaglomerular granular cells and the renal tubules. Efferent renal preganglionic fibres arise from the intermediolateral column of the spinal cord (T9-T13), descending the spinal segments before exiting the spinal cord at T11-L3. These preganglionic fibres then interconnect to the paravertebral, splanchnic, celiac and superior mesenteric ganglia and the prevertebral ganglia where these contact postganglionic neurons that emanate to the kidney (Barajas et al., 1984, Barajas et al., 1992). The nerves enter the kidney via the renal artery and further divide into bundles that run parallel to renal vessels. A single network of fibres is readily identifiable at the afferent and efferent arterioles (with predominance at the afferent arteriole), juxtaglomerular cells and the tubules (proximal, thick ascending limb of the loop of Henle, distal tubule and the collecting duct) (Barajas et al., 1984). Neural stimulation promotes renin secretion at the JGA while in the renal tubules, neural stimulation promotes sodium reabsorption. In the kidney, norepinephrine (NE) is the most abundant neurotransmitter released at the neuroeffector junctions and its actions are mediated through the α1- (α_{1A}-, α_{1B}- and α_{1D}-), α2- (α_{2A}-, α_{2B}- and α_{2C}-) and β- (β1-, β2- and β3-) G-coupled adrenoceptors (Figure 7). Activation of these receptors leads to PLC and phospholipase A (PLA) activation, and subsequent opening of calcium channels,

combined with the release of intracellular calcium stores, ultimately promoting vascular smooth muscle cell contraction (Barajas et al., 1984, Johns et al., 2011).

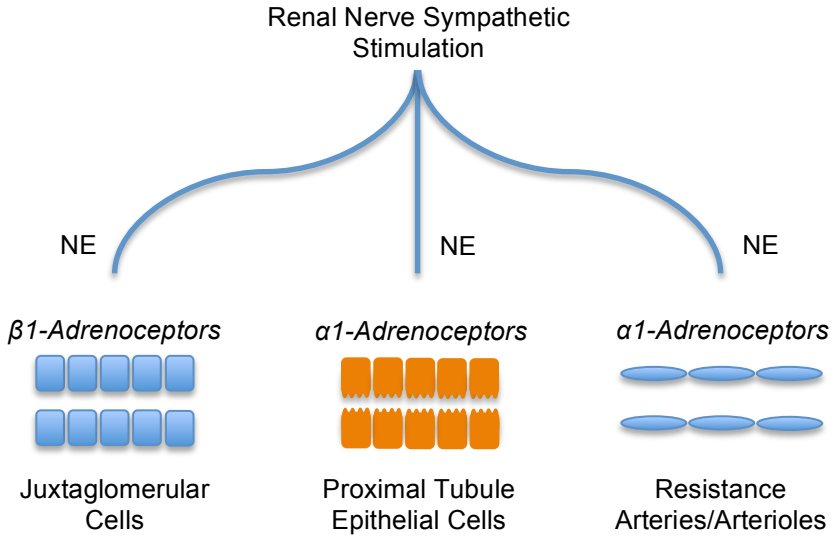

Figure 7. Renal efferent innervation. Renal efferent nerve termini are located on juxtaglomerular cells, proximal tubule cells and vascular smooth muscle cells of resistance arteries and arterioles. Norepinephrine (NE) is the main neurotransmitter released at the renal neuroeffector junctions, acting through α1- or β1-adrenoceptors to mediate downstream signal transductions. Adapted from Johns *et al*., 2011.

Renal afferent nerves have been characterized according to substance-P or calcitonin gene-related peptide immunopositivity. These are also the main putative renal afferent nerve neurotransmitters (Barajas et al., 1992, Franco-Cereceda et al., 1987). Substance-P-positive nerves are located along the wall of the proximal ureter, the renal pelvis and the interlobar branches of the renal artery where they are thought to mediate chemoreceptor function (Barajas et al., 1992). Calcitonin gene-related peptide-positive nerves are located around major renal arteries and veins, and the glomeruli and their associated vessels, where they are thought to promote baroreceptor activation following changes to vessel and interstitial pressures (Franco-Cereceda et al., 1987). In various species, including

rats, renal afferent nerves emanate to the spinal cord, enter the dorsal root ganglion (T6-L2) and terminate within lamina I-III of the ipsilateral spinal cord where these synapse to nerves that relay to the brain (Ciriello et al., 1983). Renal afferent nerve stimulation mediates baroreflexes, vascular tone and the production of anti-diuretic hormone (Caverson et al., 1987, Ciriello et al., 1986, Housley et al., 1987, Simon et al., 1989).

Renal sympathetic nerve stimulation plays an important role in renal hemodynamics. Stimulation of the renal nerve promotes vasoconstriction, associated with a 15-20% decrease in RBF and an increase in renin secretion and sodium reabsorption (Handa et al., 1985, Hesse et al., 1984, Johns et al., 1976). In this setting, GFR is unaltered due to activation of Ang II-mediated vasoconstriction of the efferent arteriole. However, upon ACE1 inhibition with captopril, renal nerve stimulation significantly reduced GFR in rats (Handa et al., 1985). Conversely, the effects of renal denervation on RBF and GFR are uncertain and may vary according to the animal's state of consciousness. Studies in anesthetised rats and rabbits have shown that renal nerve ablation caused little change on renal hemodynamics (Johns et al., 2011, Kompanowska-Jezierska et al., 2001, Salman et al., 2010). In conscious rats, however, renal denervation increased RBF while these were performing their daily activities such as feeding and grooming (Yoshimoto et al., 2004). Furthermore, in a cohort of patients subjected to bilateral renal denervation, where NE spillover decreased by 50%, GFR trended higher (Krum et al., 2009). In mice, renal denervation alone had no impact on GFR. However, denervated mice subjected to lipopolysaccharides (LPS)-induced renal injury showed a significant protection against

LPS-mediated decreases in RBF and GFR (Wang et al., 2002). Therefore, the degree of renal sympathetic tone can positively and negatively regulate renal hemodynamics.

UCHL1 in Renal Nerves

While UCHL1 has been widely studied in neurons, its function in the renal nerves is not known. UCHL1 is likely required for axonal transport and Ub maintenance in this compartment. As previously mentioned, UCHL1 protein levels are significant in human kidney homogenates after the brain and testes and this is most likely not exclusively attributed to UCHL1 expression in the macula densa, but also due to UCHL1 expression in renal axons surrounding the renal vasculature (Bradbury et al., 1985). Several studies have focused on UCHL1 localization in the nephrons of healthy rats, mice and humans, however, the presence and function of UCHL1 in the renal nerves remains unclear. Limited evidence shows neuronal UCHL1 expression in the kidney, although Shirato *et al* noted UCHL1 expression in axons located at the vascular pole of healthy rat glomeruli, suggesting a role for UCHL1 in glomerular hemodynamics (Shirato et al., 2000).

Rationale (2)

The kidney is richly endowed with renal vessels that require regulation by renal sympathetic nerves. Indeed, renal sympathetic stimulation is required to promote renin release, sodium reabsorption and renal vascular resistance (Barajas et al., 1984, Johns et al., 2011). As UCHL1 is involved in axonal trafficking and Ub maintenance, loss of *Uchl1* may therefore impair neurotransmission at the neuroeffector junctions of the kidney (Osaka et al., 2003, Wang et al., 2004). Interestingly, *Uchl1*-deleted mice undergo

neurodegeneration of the dorsal root ganglion of the gracile tract, a region that comprises renal afferent nerves (Ciriello et al., 1983, Ichihara et al., 1995, Mukoyama et al., 1989, Yamazaki et al., 1988). Moreover, as neurodegeneration progresses in *Uchl1*-deleted mice, efferent nerve function also becomes impaired, as manifested by motor ataxia, and as such, renal efferent nerves may also be affected (Mukoyama et al., 1989). We therefore speculate that UCHL1 may play an important role in regulating neural control of renal hemodynamics, including RBF and GFR (Figure 8).

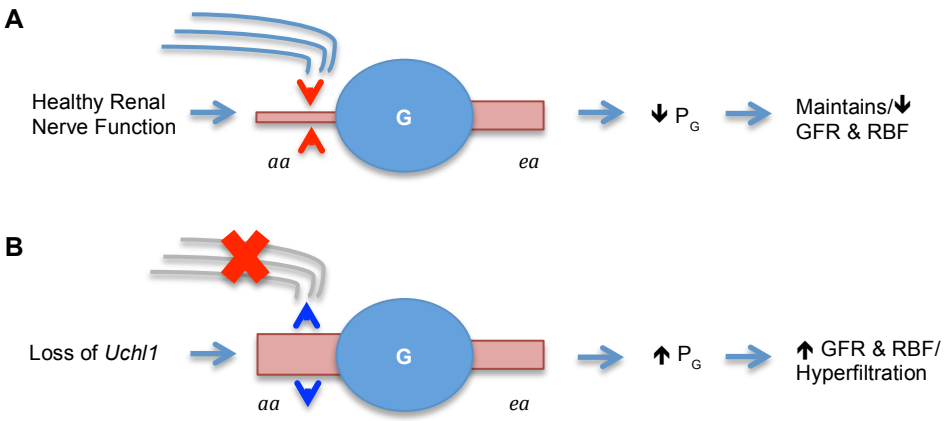

Figure 8. Proposed mechanism: How loss of *Uchl1* alters renal hemodynamics. **A.** Neuronal stimulation promotes vasoconstriction of the afferent arteriole (aa), decreasing glomerular capillary hydrostatic pressure (P_G), glomerular filtration rate (GFR) and renal blood flow (RBF). **B.** Loss of *Uchl1* results in dysfunctional/ reduced neurotransmission at the aa subsequently leading to loss of vascular resistance. As such, P_G and GFR increase, resulting in hyperfiltration. RBF is also increased. Ea denotes the efferent arteriole. G denotes the glomerulus.

Hypothesis (2)

UCHL1 is required for renal nerve maintenance and function. Loss of *Uchl1* in mice will promote dysregulated/reduced renal sympathetic tone thereby impairing renal vascular resistance. We hypothesize that *Uchl1* deletion in mice leads to increased RBF and GFR as a result of decreased renal sympathetic tone.

CHAPTER 1

Ubiquitin C-terminal hydrolase L1 deletion ameliorates glomerular injury in mice with *ACTN4*-associated focal segmental glomerulosclerosis

General Description

FSGS is one of the leading causes of glomerular disease that affects both children and adults. It is characterized by the progressive scarring of the glomeruli, leading to podocyte injury and albuminuria. Podocyte UCHL1 is upregulated in the glomeruli of patients affected by FSGS indicating that UCHL1 may play a role in the pathogenesis of glomerular lesions. UCHL1 is required for Ub maintenance and loss of *Uchl1* is associated with significant Ub pool depletion *in vivo* and *in vitro*. UCHL1 induction may therefore play a maladaptive role in FSGS by overfueling the Ub-proteasome. In the present study we sought to determine whether UCHL1 was upregulated in a mouse model of *ACTN4*-associated FSGS, specifically in mice that overexpress mutant K256E-α-actinin-4 selectively in podocytes. We hypothesized that *Uchl1* deletion in mice overexpressing podocyte-specific K256E-α-actinin-4 would ameliorate indices of podocyte injury, such as albuminuria and glomerular scarring.

Ubiquitin C-terminal hydrolase L1 deletion ameliorates glomerular injury in mice with *ACTN4*-associated focal segmental glomerulosclerosis

Naomi C. Read[a,b,c], Alex Gutsol[a,b], Chet E. Holterman [a,b], Anthony Carter[a,b], Josée Coulombe[b], Douglas A. Gray[b,d] and Chris R.J. Kennedy[a,b,c]

[a]Kidney Research Centre, [b]Ottawa Hospital Research Institute, The Ottawa Hospital, Ottawa, Ontario, Canada
[c]Department of Cellular and Molecular Medicine, Faculty of Medicine, University of Ottawa, Ottawa, Ontario, Canada
[d]Department of Biochemistry, Microbiology and Immunology, Faculty of Medicine, University of Ottawa, Ottawa, Ontario, Canada.

Corresponding Author:
Dr. Chris R.J. Kennedy
Kidney Research Centre, Ottawa Hospital Research Institute, The Ottawa Hospital
Department of Cellular and Molecular Medicine, Faculty of Medicine, University of Ottawa
451 Smyth Rd, Roger-Guindon Hall, room 2515
Ottawa, Ontario, Canada, K1H 8M5
Phone: 1-613-562-5800, extension 8529
Fax: 1-613-562-5487
E-mail: ckennedy@uottawa.ca

This work is supported by the Kidney Foundation of Canada.

Running Headline: *UCHL1* deletion in *ACTN4*-associated FSGS

Word Count: 5263

Author Contributions

Naomi C. Read	▪ Planned and performed the bulk of the experiments (excluding those specified below) ▪ Wrote the manuscript
Alex Gutsol	▪ Performed the UCHL1/α-actinin-4 immunofluorescence, UCHL1 immunohistochemistry and renal TUNEL assay
Chet E. Holterman	▪ Conducted the UCHL1 western blot in COS7 cells overexpressing K256E-α-actinin-4
Anthony A. Carter	▪ Designed and maintained mice colonies
Josée Coulombe	▪ Provided assistance with manuscript revisions
Douglas A. Gray	▪ Co-supervised the project ▪ Assisted with manuscript revisions
Chris R.J. Kennedy	▪ Supervised the project ▪ Assisted with manuscript revisions

ABSTRACT

Renal ubiquitin C-terminal hydrolase L1 (UCHL1) is upregulated in a subset of human glomerulopathies, including focal segmental glomerulosclerosis (FSGS), where it may serve to promote ubiquitin pools for degradation of cytotoxic proteins. In the present study, we tested whether UCHL1 is expressed in podocytes of a mouse model of *ACTN4*-associated FSGS. Podocyte UCHL1 protein was detected in glomeruli of K256E-*ACTN4*$^{pod+}$ / *UCHL1*+/+ mice. *UCHL1*+/- mice were intercrossed with K256E-*ACTN4*$^{pod+}$ mice and monitored for features of glomerular disease. 10-week-old K256E-*ACTN4*$^{pod+}$ / *UCHL1*-/- mice exhibited significantly ameliorated albuminuria, glomerulosclerosis, tubular pathology and blood pressure. Interestingly, while *UCHL1* deletion diminished both tubular and glomerular apoptosis, WT1-positive nuclei were unchanged. Finally, UCHL1 levels correlated positively with poly-ubiquitinated proteins but negatively with K256E-α-actinin-4 levels, implying reduced K256E-α-actinin-4 proteolysis in the absence of UCHL1. Our data suggest that UCHL1 upregulation in *ACTN4*-associated FSGS fuels the proteasome and that *UCHL1* deletion may impair proteolysis and thereby preserve K256E/wt-α-actinin-4 heterodimers, maintaining podocyte cytoskeletal integrity and protecting the glomerular filtration barrier.

Keywords

UCHL1, α-actinin-4, K256E, ubiquitin, glomerular disease, podocyte

1. INTRODUCTION

α-Actinin-4 cross-links and bundles F-actin [1, 2] regulating key cytoskeletal dependent processes [3, 4]. Mutations in the *ACTN4* gene are associated with a familial autosomal dominant form of focal segmental glomerulosclerosis (FSGS) [5-7]. FSGS-linked mutations in the *ACTN4* gene, such as the K255E mutation (K256E in mice), expose a third actin-binding site, increase its affinity for actin and promote α-actinin-4/actin aggregate formation in podocytes [5, 8-10]. While the K256E-α-actinin-4 protein can homodimerize, it can also heterodimerize with wt-α-actinin-4 such that wt-α-actinin-4 bound to the mutant form can be detected in K256E-α-actinin-4/actin aggregates. While these aggregates undergo poly-ubiquitination and proteasomal degradation thereby reducing overall expression levels of K256E-α-actinin-4, over time, these become supersaturated and "choke" the ubiquitin-proteasome system (UPS) thereby leading to their accumulation, as demonstrated *in vitro* [10, 11]. Mice with podocyte-specific overexpression of K256E-α-actinin-4 develop albuminuria, podocyte foot process (FP) effacement and FSGS lesions [12]. However the precise subcellular mechanism(s) that underlie α-actinin-4/actin aggregate-dependent podocyte injury remain incompletely elucidated.

Podocyte ubiquitin C-terminal hydrolase L1 (UCHL1) is upregulated in a subset of human glomerulopathies, including primary FSGS [13]. Among an array of other ubiquitin (Ub)-regulating functions is a salvage function wherein the UCHL1 enzyme hydrolyzes small C-terminal adducts from Ub [14, 15]. UCHL1 also binds and stabilizes

mono-Ub *in vitro* and maintains intracellular Ub pools [16]. Significant UCHL1 expression has been reported in podocytes of patients with glomerular diseases, such as IgA nephropathy, FSGS etc. [13, 17, 18]. UCHL1 upregulation upon podocyte injury may serve to generate/promote availability of free monomeric Ub for poly-ubiquitination and degradation of aggregates/cytotoxic proteins via the UPS. Interestingly, UCHL1 deficiency in *gracile axonal dystrophy* (*gad*) mice, which have an in-frame deletion comprising exons 7 and 8 of the *UCHL1* gene and no detectable UCHL1 protein, is linked to the accumulation of cytotoxic proteins and impaired protein turnover in neurons [19]. Similarly, UCHL1 overexpression leads to protein inclusion formation in neuronal cells [20]. Despite conflicting findings for UCHL1 in neurons, recent findings in the kidney, specifically in a rat model of membranous nephropathy, demonstrate that UCHL1 upregulation coincides with poly-ubiquitinated protein accumulation and UPS activity decline. Pharmacological inhibition of UCHL1 in this model restores UPS activity, decreases poly-ubiquitinated proteins and ameliorates the overall glomerular pathology [21]. Taken together these data suggest a maladaptive role for UCHL1 in glomerular disease.

Based on these findings, we propose that UCHL1 induction in the presence K256E-α-actinin-4/actin aggregation is maladaptive for protein turnover. In the present study, we tested the hypothesis that *UCHL1* deletion in a mouse model of *ACTN4*-associated FSGS reduces indications of filtration barrier injury and glomerular lesions.

2. MATERIALS AND METHODS

2.1. Mice Studies

Mice were housed at the Animal Care facility at the University of Ottawa. Protocols were approved and undertaken according to Canadian Council on Animal Care guidelines. Euthanasia was performed by anesthetizing mice by inhalation of isofluorane and perfusion with 20ml PBS through the left ventricle.

2.2. Immunofluorescence / Immunohistochemistry of Paraffin-Embedded Sections

Harvested kidneys were incubated in a 4% paraformaldehyde/PBS solution for 24 hours and processed for paraffin embedding. Kidney sections were rehydrated through graded ethanol solutions (100%, 90% and 70%; v:v), boiled in 10mM/1mM/0.05% Tris/EDTA/Tween-20 pH 9.0 or sodium citrate 0.01M pH 6.0 and incubated with 0.3% H_2O_2 in MeOH. For UCHL1 immunofluorescence, 2µm sections were incubated with mouse anti-PGP9.5 1:400 (Abcam, Toronto, ON) and anti-α-actinin-4 1:200 (Abcam, Toronto, ON) o/n at 4°C, then incubated with secondary Cy3-donkey anti-mouse 1:100 and Alexa Fluor 488-donkey anti-rabbit 1:100 (Jackson ImmunoResearch Laboratories, West Grove, PA) for 1 hour at room temperature. For UCHL1 immunohistochemistry, 5µm sections were incubated with mouse anti-UCHL1 1:600 (Novus Biologicals, Oakville, ON) o/n at 4°C, then processed according to the ImmPRESS Reagent Anti-mouse Ig (rat adsorbed) kit (Vector Laboratories, Burlingame, CA) and finally processed with diaminobenzidine/H_2O_2 (Sigma-Aldrich, Oakville, ON). Cortical renal sections were visualized blinded with a Zeiss Axio Imager A1 microscope.

2.3. K256E-*ACTN4*$^{pod+}$ / *UCHL1*-/- mice

The fourth exon of the murine *UCHL1* gene was replaced by inserting a neomycin resistance gene with a selectable marker for embryonic stem cells. Mice were established on 129v/J and C57Bl/6 genetic backgrounds (Gray and Coulombe, submitted). *UCHL1*+/- mice were intercrossed with K256E-*ACTN4*$^{pod+}$ mice [12]. K256E-*ACTN4*$^{pod+}$ mice were maintained on a C3H background. The pups and littermate controls used for this study were of mixed backgrounds, including 129v/J, C57Bl/6 and C3H. Genotyping was performed by PCR of genomic DNA isolated from ear snips of 3-week-old mice. For *UCHL1*: 5'-CTGGACCACCATCTGCTTAC-3' (forward primer), 5'-CAGCTTGTCTTGGTTGTTGG-3' (wild type reverse primer) and 5'-AAGCGAAGGAGCAAAGCTGC-3' (*UCHL1*-/- reverse primer). For K256E-*ACTN4*$^{pod+}$: 5'-GAGAAAGAACTGTTAACGGG-3' (forward primer) and 5'-AGTTAGTCGCCCATGCTTC-3' (reverse primer). Mice were obtained at the expected Mendelian ratio.

2.4. RNA Isolation and Quantitative PCR

Cortical kidney tissue was homogenized with a COE Capmixer and processed for RNA isolation with the RNeasy Mini kit (Qiagen, Toronto, ON) and converted to cDNA with the High Capacity cDNA Reverse Transcription Kit (Applied Biosystems, Burlington, ON). qPCR was performed using the Real-Time qPCR Master Mix-SYBR Advantage qPCR Premix (Clontech, Mountainview, CA). UCHL1 primers were designed to span exons 4-6 of the *UCHL1* gene. UCHL1 forward primer (439F): 5'-

TGGTACCATCGGGTTGATCC-3' and reverse primer (723R): 5'-TGGTTCACTGGAAAGGGCAT-3'. Control RNA from rodent, obtained from the TaqMan Rodent GAPDH Control Reagents, served as a global control (Applied Biosystems, Burlington, ON). GAPDH served as a loading control using primers from the TaqMan Rodent GAPDH Control Reagents (Applied Biosystems, Burlington, ON).

2.5. Albumin/Creatinine Ratios

Spot urine was obtained from mice at 4 and 10 weeks of age. Albumin concentration was measured by ELISA (Bethyl Laboratories, Montgomery, TX) and normalized to creatinine content measured by the Creatinine Companion kit (Exocell, Philadelphia, PA).

2.6. Plasma Creatinine

At sacrifice, mouse blood was collected using heparinized syringes. Blood samples were centrifuged at 5000rpm for 10 minutes at 4°C and the supernatant was collected. Mouse plasma was stored at -80°C for subsequent use. For plasma creatinine determination, mouse plasma was analyzed commercially by IDEXX (IDEXX Labs, Toronto, ON).

2.7. Kidney Histology

Kidneys were dissected, cut into <0.5 cm portions and incubated in a 4% paraformaldehyde/PBS solution for 24 hours before being processed for paraffin embedding. Paraffin-embedded blocks were cut into 4-5μm sections and stained with periodic-acid Schiff (PAS) stain. Analysis of glomerulosclerosis was performed using a

Zeiss Axio Imager A1 microscope. Glomeruli were subdivided into categories based upon the proportion of mesangial matrix occupying the glomerular tuft (healthy, 25-40% matrix; segmental sclerosis, 40-75% matrix; and global sclerosis, >75% matrix). The relative difference between Bowman's capsule area and the glomerular tuft area was computed using Alpha Innotech software and was determined by substracting the total glomerular tuft area from the total Bowman's capsule area. Tubulointerstitial inflammation was scored from 0-3, where 0, healthy tubules with few interstitial cells; 1, healthy tubules with some interstitial cells (<10% of field); 2, tubulointerstitial inflammation (10-25% of field) with some tubular damage; and 3, significant tubulointerstitial inflammation (25-50% of field) with some tubular invasion and destruction. Renal sections were analyzed in a blinded fashion. For electron microscopy, dissected kidneys were incubated in 2.7% glutaraldehyde/PBS, rinsed in a sodium cacodylate buffer, followed by OsO_4, water, uranyl acetate and dehydrated with ethanol and acetone and embedded in spur resin. Sections were visualized with a Hitachi 7100 transmission electron microscope. The number of podocyte foot processes per glomerular basement membrane (GBM) length and GBM thickness was analyzed as previously described [22, 23], using Axiovision software.

2.8. Systolic Blood Pressure

Tail cuff plethysmography (BP-2000 Visitech Sytems, Apex, NC) was used to measure systolic blood pressure. Mice were trained at 5 weeks of age and baseline measurements were taken at 6 weeks of age. Blood pressure was assessed at 7 and 10 weeks of age. Measurements were collected over 3-5 consecutive days.

2.9. Cell Culture

Undifferentiated conditionally immortalized human podocytes (passage <15) were cultured at 33˚C on collagen-I-coated dishes supplemented with RPMI-1640 containing 10% fetal bovine serum, 100U/ml penicillin, 100µg/ml streptomycin (InvivoGen, San Diego, CA) and 10U/ml γ-interferon (Sigma-Aldrich, Oakville, ON). For differentiation, podocytes were thermoshifted to 37˚C and cultured on collagen-I-coated dishes supplemented with RPMI-1640 containing 2% fetal bovine serum, 100U/ml penicillin, 100µg/ml streptomycin (InvivoGen, San Diego, CA). Podocytes were differentiated on 10cm dishes at a cell density of $1x10^5$ cells per dish, for a minimum of 10 days. COS7 cells were cultured in DMEM containing 10% fetal bovine serum, 100U/ml penicillin, 100µg/ml streptomycin (InvivoGen, San Diego, CA). Cells were grown on 10cm dishes at a starting cell density of $2x10^5$ cells per dish and harvested after a maximum of 2 days during which appropriate treatments took place.

2.10. Adenoviral Infection

At day 10 post-thermoshift or 24 hours after seeding, differentiated podocytes or COS7 cells, respectively, were incubated with adenovirus at an appropriate multiplicity of infections (MOI) to yield overexpression of GFP, WT- and K256E-α-actinin-4 as previously described [8]. The adenoviral infection was incubated for 24, 48 or 72 hours where appropriate.

2.11. UCHL1 siRNA Knockdown

UCHL1 siRNA oligonucleotides (Qiagen, Toronto, ON) and scrambled oligonucleotides (Santa Cruz Biotechnology, Santa Cruz, CA) were incubated in serum-free RPMI-1640 with HiPerfect transfection reagent (Qiagen, Toronto, ON), as per the manufacturer's instructions, for 10 minutes at room temperature to allow complex formation. Complexes were added to differentiated conditionally immortalized human podocytes seeded on 10cm dishes. Complexes were incubated for 72 hours at which time cells were harvested and processed for western immunoblotting. For co-transfection/infection, cells were incubated with the appropriate siRNA for 24 hours at which time the appropriate adenovirus was administered (without changing the media). Cells were incubated for an additional 48 hours, for a total of 72 hours.

2.12. Protein Isolation

Cortical kidney tissue was homogenized with a COE Capmixer and resuspended in RIPA lysis buffer (150mM NaCl, 1% Triton X-100, 0.5% sodium deoxycholate, 0.1% SDS and 50mM Tris pH 8.0), supplemented with protease inhibitor cocktail 1:100 (Sigma-Aldrich, Oakville, ON). Glomeruli were isolated from kidney as previously described [24]. Differentiated conditionally immortalized human podocytes and COS7 cells were washed once with PBS and scraped in lysis buffer (10mM Tris, pH 7.4, 150mM NaCl, 1mM ethyleneglycol tetraacetate, 1mM ethylenediaminetetraacetic acid, 1% Triton X-100, 0.5% Nonidet P-40) and RIPA lysis buffer (150mM NaCl, 1% Triton X-100, 0.5% sodium deoxycholate, 0.1% SDS and 50mM Tris pH 8.0), respectively, and supplemented with protease inhibitor cocktail 1:100 (Sigma-Aldrich, Oakville, ON).

Protein lysates were incubated at 4°C for 10 minutes. Extracted proteins (50μg of renal lysates and 20μg of glomerular and cellular lysates) were processed for SDS-PAGE on appropriate percentage gels.

2.13. Immunoblotting

Immunoblotting of renal tissue was performed using rabbit anti-Ub (Cederlane, Burlington, ON) or rabbit anti-UCHL1 1:1000 (Millipore, Darmstadt, Germany) or rabbit anti-HA 1:125 (Invitrogen, Burlington, ON) o/n at 4°C. For cells, immunoblotting was performed using mouse anti-HA7 1:10000 (Sigma-Aldrich, Oakville, ON) for 1 hour at room temperature and rabbit anti-UCHL1 1:1000 (Millipore, Darmstadt, Germany) o/n at 4°C. β-actin served as a loading control for all immunoblots, using mouse anti-β-actin 1:10000 (Sigma-Aldrich, Oakville, ON) for 1 hour at room temperature. Secondary antibodies included HRP-goat anti-rabbit 1:10000 (Jackson ImmunoResearch Laboratories, West Grove, PA), HRP-goat anti-mouse 1:10000 (Jackson ImmunoResearch Laboratories, West Grove, PA) and were added appropriately following primary antibody incubations, for 1 hour at room temperature. Densitometry of western blots was computed using Alpha Innotech software.

2.14. Immunofluorescence on Frozen Sections

Dissected kidneys were frozen in Tissue Tek O.C.T. compound (Sakura Finetek, Torrance, CA) in 2-methylbutane. Embedded kidney tissues were sectioned at 10μm. For immunofluorescence, sections were dried, washed with PBS and blocked with 10% donkey serum (Jackson ImmunoResearch Laboratories, West Grove, PA) in 1%

BSA/PBS for 1 hour at room temperature. Sections were incubated with rabbit anti-WT1 1:200 (Santa Cruz Biotechnology, Santa Cruz, CA) o/n at 4°C. After washing with PBS, sections were incubated with Alexa Fluor 488-donkey anti-rabbit 1:500 (Jackson ImmunoResearch Laboratories, West Grove, PA) for 1 hour at room temperature. WT1-positive nuclei were quantified by counting the total number per glomerulus using Axiovision software. Sections were visualized with a Zeiss Axioskop 2 MOT epifluorescence microscope (Zeiss, Germany).

2.15. TUNEL

Dissected kidneys were incubated in a 4% paraformaldehyde/PBS solution for 24 hours before being processed for paraffin embedding. Kidneys were cut into 4-5μm sections and stained according to the TUNEL Apoptosis Detection for paraffin-embedded tissue sections, biotin-labeled POD protocol (GenScript, Piscataway, NJ). Apoptosis was quantified by counting the number of TUNEL-positive tubular nuclei per renal section and the total TUNEL-positive glomerular nuclei per glomerular section. Sections were analyzed in a blinded manner.

2.16 Differential Centrifugation

Differentiated conditionally immortalized human podocytes were scraped in lysis buffer (10mM Tris, pH 7.4, 150mM NaCl, 1mM ethyleneglycol tetraacetate, 1mM ethylenediaminetetraacetic acid, 1% Triton X-100, 0.5% Nonidet P-40) supplemented with protease inhibitor cocktail at 1:100 (Sigma-Aldrich, Oakville, ON). A volume of the whole cell lysate was reserved for the input (I) and for protein determination. The

remaining volume was centrifuged for 15 minutes at 13000rpm to isolate Triton-soluble (TS) and Triton-insoluble (TI) fractions. The supernatant (the TS fraction) was collected and the pellet (the TI fraction) was resuspended in an equal volume of lysis buffer. 20μg of protein was resolved by SDS-PAGE. Densitometry was computed as described above and by normalizing HA/β-actin for all fractions before normalizing TS/TI.

2.17. Statistics

Values are expressed as the mean or mean percentage ± SE. Statistical comparisons were carried out by one-way ANOVA followed by either Bonferroni or Newman-Keuls post-tests or with a t-test for analyses including exclusively two groups. For albuminuria, a longitudinal analysis using a random coefficients model and a linear trend for the mean response statistical test was performed.

3. RESULTS

3.1. UCHL1 is expressed in glomeruli of K256E-*ACTN4*$^{pod+}$ / *UCHL1*+/+ mice

UCHL1 induction is associated with podocyte injury in a subset of glomerulopathies, including FSGS [13, 17, 18]. While healthy podocytes express little UCHL1, podocyte injury may trigger UCHL1 upregulation for degradation of cytotoxic proteins. We verified UCHL1 expression in glomeruli of mice with *ACTN4*-associated FSGS. Immunohistochemistry revealed 3±2 UCHL1-positive cells per glomerulus in nonTG / *UCHL1*+/+ mice which was significantly increased to 7±4 UCHL1-positive cells per glomerulus in K256E-*ACTN4*$^{pod+}$ / *UCHL1*+/+ albuminuric mice ($p<0.001$) (Figure 1a and b). To verify podocyte-specific expression of UCHL1, a double immunofluorescence staining procedure was performed using appropriate antibodies against UCHL1 and the podocyte marker α-actinin-4. Indeed, podocyte-specific expression of UCHL1 was detectable in glomeruli of K256E-*ACTN4*$^{pod+}$ / *UCHL1*+/+ mice. UCHL1 expression appeared mainly nuclear but was occasionally detectable in podocyte cytoplasm (Figure 1c). Immunoblotting of glomerular lysates also revealed increased UCHL1 protein levels, associated with increased poly-ubiquitinated proteins, in K256E-*ACTN4*$^{pod+}$ / *UCHL1*+/+ glomeruli as compared to nonTG / *UCHL1*+/+ mice ($p<0.001$) (Figure 1d-f). We next tested whether increases in UCHL1 were observable in cell lines expressing the K256E-α-actinin-4 mutant. We infected COS7 cells with adenovirus containing constructs for WT- and K256E-α-actinin-4 at a range of MOI and found that the levels of WT- or K256E-α-actinin-4 increased as the MOI increased. COS7 cells overexpressing K256E-α-actinin-4 showed UCHL1 protein upregulation versus uninfected and WT-α-actinin-4

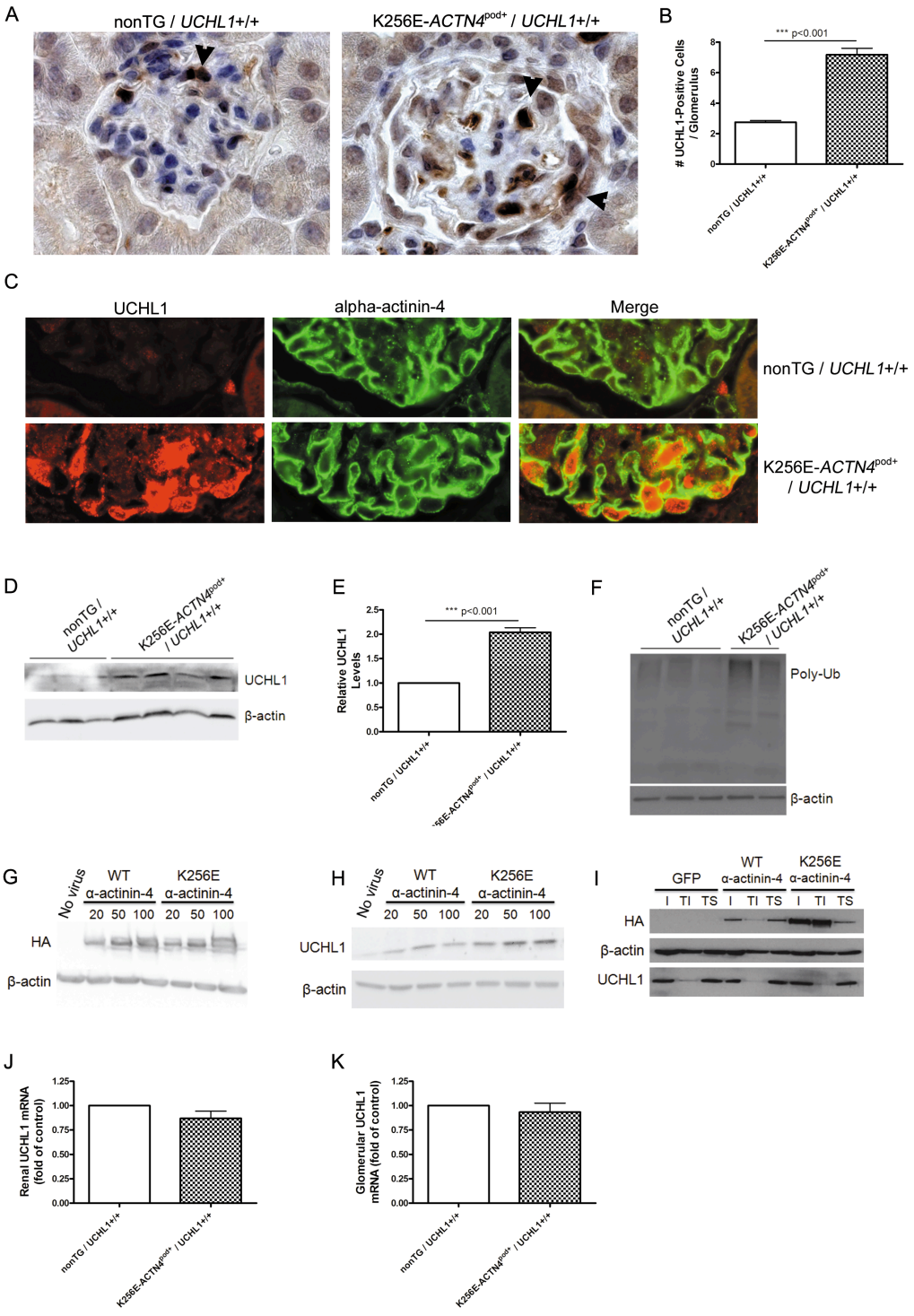

Figure 1. UCHL1 is expressed in glomeruli of K256E-*ACTN4*$^{pod+}$ / *UCHL1*+/+ mice. (**a**) Immunohistochemistry reveals extensive UCHL1 induction in glomeruli (likely podocytes, arrowheads) of 10-week-old K256E-*ACTN4*$^{pod+}$ / *UCHL1*+/+ mice (n=3 per group). A minimum of 20 glomeruli were analyzed per mouse. Magnification, 640x. (**b**) Graph depicting increased UCHL1-positive glomerular cells

in K256E-*ACTN4*$^{pod+}$ / *UCHL1*+/+ mice ($p<0.001$ vs. nonTG / *UCHL1*+/+ mice). (**c**) UCHL1 induction in glomeruli is confirmed in podocytes of K256E-*ACTN4*$^{pod+}$ / *UCHL1*+/+ mice, as determined by double immunofluorescence using antibodies against UCHL1 and the podocyte marker α-actinin-4 (n=3-4 per group). A minimum of 20 glomeruli were analyzed per mouse. Magnification, 630x. (**d-e**) UCHL1 induction in glomeruli of K256E-*ACTN4*$^{pod+}$ / *UCHL1*+/+ mice is confirmed by western immunoblotting of glomerular lysates ($p<0.001$ vs. nonTG / *UCHL1*+/+ mice) (n=3-4 per group). (**f**) Representative immunoblot showing elevated poly-ubiquitinated protein levels in 10-week-old K256E-*ACTN4*$^{pod+}$ / *UCHL1*+/+ mice as compared to nonTG / *UCHL1*+/+ mice (n=3 per group). (**g**) COS7 cells overexpressing HA-tagged K256E-α-actinin-4, infected at various MOI (20, 50 and 100) for 24 hours, illustrate increased UCHL1 protein levels as compared to WT-α-actinin-4 and uninfected controls. β-actin served as a loading control (n=3). (**h**) Graph depicting UCHL1 protein levels, as determined by densitometry, that are significantly increased in K256E-α-actinin-4 overexpressing COS7 cells as compared to WT-α-actinin-4 overexpressing COS7 cells at equivalent MOI ($p<0.01$ for MOI=20, $p<0.001$ for MOI=50 and $p<0.01$ for MOI=100). (**i**) Human podocytes overexpressing GFP, WT- and K25E-α-actinin-4 (MOI=30) and subjected to differential centrifugation show no differences in UCHL1. A representative immunoblot using anti-HA confirms the infection efficacy (n=3). β-actin served as a loading control for all immunoblots. UCHL1 mRNA levels were not significantly different in renal (**j**) and glomerular (**k**) lysates of K256E-*ACTN4*$^{pod+}$ / *UCHL1*+/+ mice as determined by qPCR. UCHL1 mRNA levels were normalized to GAPDH mRNA (n=3 per group).

infected controls (Figure 1g). Specifically, COS7 cells overexpressing K256E-α-actinin-4 at a MOI of 20, 50 and 100 show significant UCHL1 protein induction (by approximately 2-fold) as compared to COS7 cells overexpressing WT-α-actinin-4 at equivalent MOI ($p<0.01$, $p<0.001$ and $p<0.01$, respectively) (Figure 1h). No differences in UCHL1 levels were observed in conditionally immortalized human podocytes overexpressing either GFP, WT- or K256E-α-actinin-4 and subjected to differential centrifugation, suggesting that podocytes may behave differently *in vitro* (Figure 1i). Finally, to test whether UCHL1 upregulation results from increased transcription, qPCR was performed and confirmed no differences in UCHL1 mRNA levels in renal and glomerular lysates of K256E-*ACTN4*$^{pod+}$ / *UCHL1*+/+ mice (Figure 1j and k), suggesting that UCHL1 levels

are increased post-translationally.

3.2. Development of *UCHL1* knockout mice

In *ACTN4*-associated FSGS, UCHL1 induction may promote formation of poly-ubiquitinated K256E-α-actinin-4 aggregates that choke the UPS [11]. *UCHL1* deletion is predicted to restore the UPS. To test this hypothesis, we used mice generated by Coulombe and Gray with global *UCHL1* deletion (*UCHL1*-/-), where a selectable marker conferring neomycin resistance was inserted within the catalytically essential 4th exon of the mouse *UCHL1* gene (Coulombe and Gray, in preparation). UCHL1 mRNA expression in renal cortex of nonTG / *UCHL1*+/+ mice was not detected by qPCR in nonTG / *UCHL1*-/- mice (Figure 2a). Furthermore, UCHL1 protein levels were undetectable by western blot (Figure 2b and c) and immunohistochemistry (Figure 2d) of renal cortex of nonTG / *UCHL1*-/- mice, while nonTG / UCHL1+/+ mice exhibited some detectable UCHL1. Similar to the phenotype observed with *gad* mice, homozygous *UCHL1* null mice show progressive neurodegeneration that affects gait around 6-12 weeks of age. These mice are fertile, although the females fail to care for pups, and are generally viable for 6 months.

3.3. Albuminuria is reduced in K256E-*ACTN4*$^{pod+}$ / *UCHL1*-/- mice

K256E-*ACTN4*$^{pod+}$ / *UCHL1*+/+ mice were intercrossed with *UCHL1*+/- mice to generate K256E-*ACTN4*$^{pod+}$ / *UCHL1*-/- mice. Urinary albumin/creatinine ratios (ACR) were determined at 4 and 10 weeks of age. As previously reported, ~50% of K256E-*ACTN4*$^{pod+}$ / *UCHL1*+/+ mice develop albuminuria at 4 weeks of age that is maintained

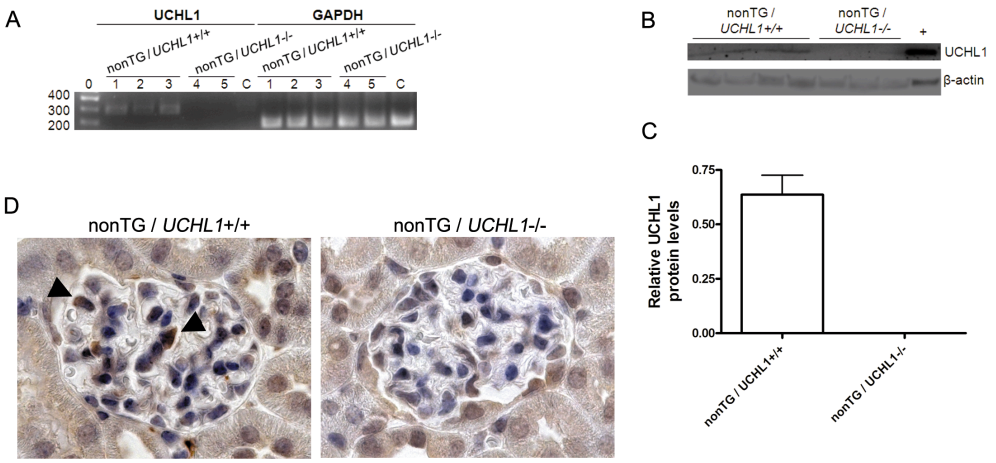

Figure 2. UCHL1 is absent from renal cortex of nonTG / *UCHL1*-/- mice. (**a**) qPCR reveals an amplicon migrating at ~300bp, likely UCHL1 mRNA (predicted amplicon size ~284bp) in renal cortex of nonTG / *UCHL1*+/+ mice (lanes 1-3), that is absent in nonTG / *UCHL1*-/- mice (lanes 4 and 5). Control RNA from rodent, obtained commercially, served as a global control (lane C). GAPDH mRNA served as an internal control. DNA markers (bp) are depicted in lane 0. (**b-c**) While the UCHL1 protein is detectable in nonTG / *UCHL1*+/+ mice, western immunoblotting and densitometry analysis reveals its absence in renal cortex of nonTG / *UCHL1*-/- mice (n=3-4 per group). Differentiated human podocytes infected with adenovirus containing a construct for K256E-α-actinin-4, to yield overexpression of K256E-α-actinin-4, served as a positive control for UCHL1 protein detection (+). β-actin served as a loading control. (**d**) Immunohistochemistry of UCHL1 confirms its absence in glomeruli of nonTG / *UCHL1*-/- mice. UCHL1-positive cells are indicated in glomeruli of nonTG / *UCHL1*+/+ mice by arrowheads (n=3 per group). Magnification, 640x.

through 10 weeks of age. In this model, albuminuria correlates with K256E-α-actinin-4 transgene mRNA levels [12]. nonTG / *UCHL1*+/+ and nonTG / *UCHL1*-/- mice littermate controls were not albuminuric. nonTG / *UCHL1*+/+ mice displayed mean ACR values of 152±11μg/mg and 173±30μg/mg at 4 and 10 weeks of age, respectively. Similarly, nonTG / *UCHL1*-/- mice displayed mean ACR values of 131±14μg/mg and 107±15μg/mg at 4 and 10 weeks of age, respectively. In contrast, mean ACR values for K256E-*ACTN4*$^{pod+}$ / *UCHL1*+/+ mice were elevated at 4 and 10 weeks (2905±1592μg/mg and 2519±1037μg/mg). ACR levels for K256E-*ACTN4*$^{pod+}$ / *UCHL1*-/- mice were also

elevated to K256E-*ACTN4*$^{pod+}$ / *UCHL1*+/+ mice levels at 4 weeks (4406±2998μg/mg). However, by 10 weeks, ACR values were significantly reduced to 569±131μg/mg for K256E-*ACTN4*$^{pod+}$ / *UCHL1*-/- mice ($p<0.01$ vs. K256E-*ACTN4*^{pod} / *UCHL1*-/- mice mean ACR at 4 weeks of age) (Figure 3a). Of note, while the ACR levels of 4-week-old K256E-*ACTN4*$^{pod+}$ / *UCHL1*-/- mice were greater than ACR levels of K256E-*ACTN4*$^{pod+}$ / *UCHL1*+/+ mice at 4 weeks, this difference was not statistically significant. Similar findings showing albuminuria amelioration in *UCHL1* deleted mice were obtained when urine samples were resolved by SDS-PAGE (Figure 3b). Plasma creatinine concentrations for nonTG / *UCHL1*+/+ and K256E-*ACTN4*$^{pod+}$ / *UCHL1*+/+ mice were determined to be 15.4±1.3 and 16.2±1.4μM, respectively. Plasma creatinine levels for nonTG / *UCHL1*-/- mice (14.2±2.1μM) were slightly higher than K256E-*ACTN4*$^{pod+}$ / *UCHL1*-/- mice (11.2±0.7μM), however no significant statistical differences were determined between all four mice groups (Figure 3c).

3.4. Glomerular pathology and filtration barrier damage are attenuated in K256E-*ACTN4*$^{pod+}$ / *UCHL1*-/- mice

K256E-*ACTN4*$^{pod+}$ / *UCHL1*+/+ mice present with characteristic histopathological features of FSGS that include glomerular scarring and downstream tubular damage [12]. Indeed, analysis of PAS-stained renal sections of 10-week-old mice confirmed these findings. K256E-*ACTN4*$^{pod+}$ / *UCHL1*+/+ mice displayed features of glomerular and tubular damage, including tubular dilatation and accumulation of proteinaceous casts [12]. K256E-*ACTN4*$^{pod+}$ / *UCHL1*-/- mice showed evidence of attenuated glomerular injury and ameliorations in overall renal pathology (Figure 4a, Supplemental Figure 1).

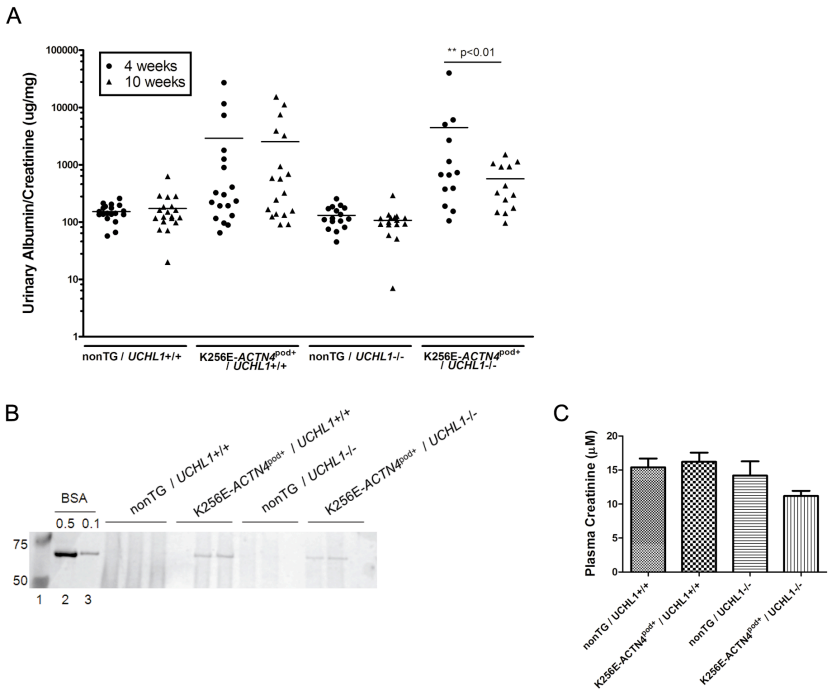

Figure 3. Reduced albuminuria in K256E-*ACTN4*$^{pod+}$ / *UCHL1*-/- mice.
(**a**) Urinary albumin levels, normalized to creatinine content were elevated in a subset of K256E-*ACTN4*$^{pod+}$ / *UCHL1*+/+ mice (n=18) at 4 and 10 weeks of age. While urinary albumin/creatinine ratios (ACR) were elevated in K256E-*ACTN4*$^{pod+}$ / *UCHL1*-/- mice at 4 weeks of age, these were attenuated significantly by 10 weeks (n=13; $p<0.01$ vs. K256E-*ACTN4*$^{pod+}$ / *UCHL1*-/- mice ACR at 4 weeks). No significant changes were observed for nonTG / *UCHL1*+/+ and nonTG / *UCHL1*-/- mice between 4 and 10 weeks of age, n=19 and n=16, respectively. (**b**) Coomassie Brilliant blue staining of urine samples processed by SDS-PAGE indicates an intense band migrating at ~67kDa (likely albumin) in K256E-*ACTN4*$^{pod+}$ / *UCHL1*+/+ mice which is reduced in samples obtained from K256E-*ACTN4*$^{pod+}$ / *UCHL1*-/- mice at 10 weeks (n=3 per group). Molecular weight markers (kDa) are depicted in lane 1 while standard concentrations (μg) of bovine serum albumin (BSA) are depicted in lanes 2 and 3. (**c**) Plasma creatinine concentrations were not significantly different between mice groups at 10 weeks of age (n=5 per group).

Since non-albuminuric K256E-*ACTN4*$^{pod+}$ / *UCHL1*+/+ mice do not display histologic features of FSGS, only mice that exhibited ACR > 500 μg/mg were selected for analysis. In K256E-*ACTN4*$^{pod+}$ / *UCHL1*+/+ mice the proportion of healthy glomeruli was significantly reduced (33±5%; $p<0.01$) while the proportion of glomeruli exhibiting segmental and global sclerosis were significantly increased (36±4% and 31±9%,

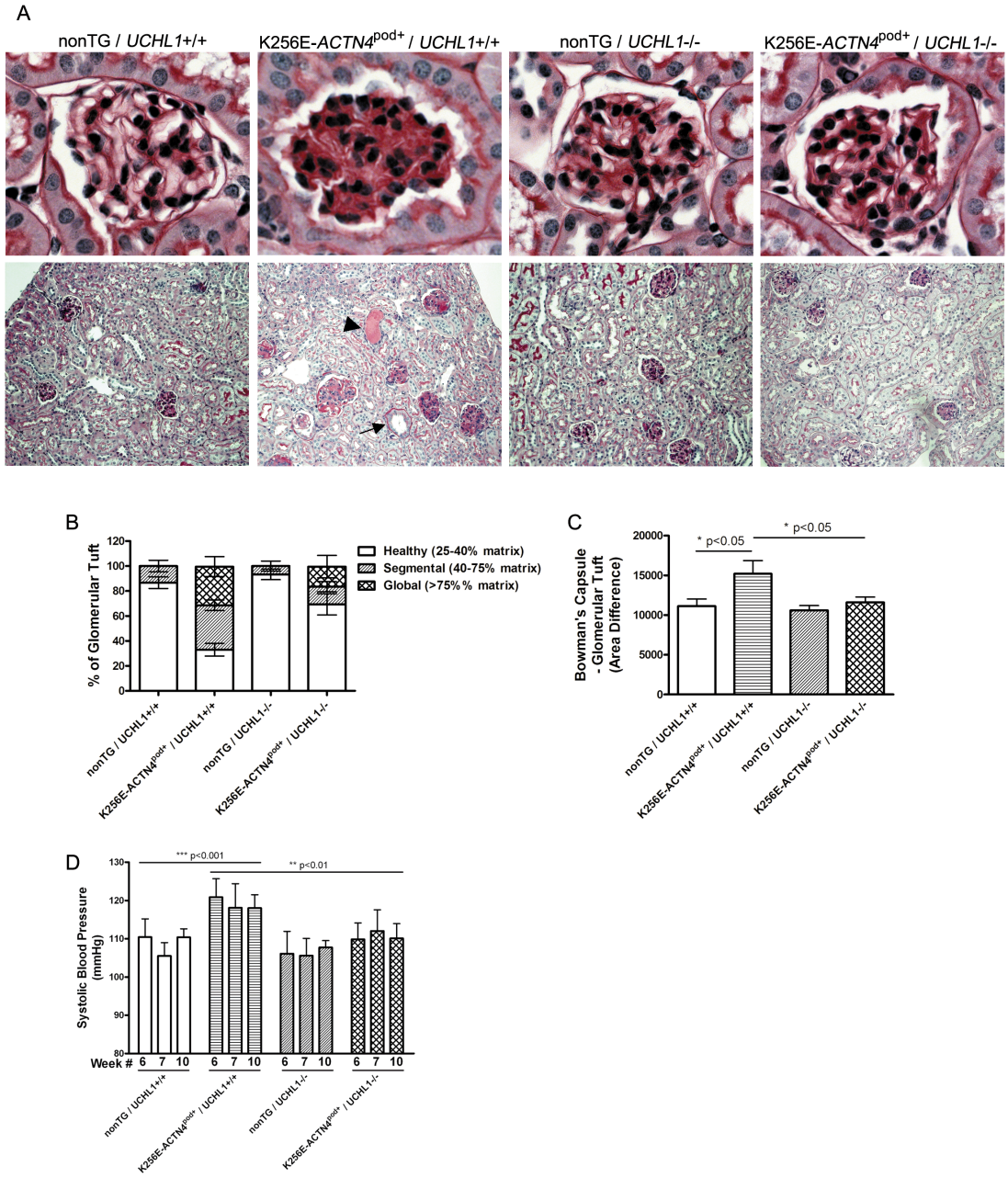

Figure 4. Glomerulosclerosis is attenuated in K256E-*ACTN4*$^{pod+}$ / *UCHL1*-/- mice. (**a**) A representative PAS-stained glomerular section (upper panel) and renal cortical section (lower panel) of a 10-week-old mouse from each mouse group. PAS stained sections indicate widespread renal pathology in 10-week-old K256E-*ACTN4*$^{pod+}$ / *UCHL1*+/+ mice, consisting of glomerulosclerosis, proteinaceous casts (arrowhead) and tubular dilatation (arrow). Tubulointerstitial damage was less frequent in K256E-*ACTN4*$^{pod+}$ / *UCHL1*-/- mice. Magnification, 640x (upper panel) and 200x (lower panel). (**b**) Glomerular scoring reveals a reduced proportion of healthy glomeruli ($p<0.001$ vs. nonTG / *UCHL1*+/+ mice) and an increased proportion of segmental ($p<0.05$ vs. nonTG / *UCHL1*+/+ mice) and globally sclerotic ($p<0.05$ vs. nonTG /

UCHL1+/+ mice) glomeruli in K256E-*ACTN4*$^{pod+}$ / *UCHL1*+/+ mice. K256E-*ACTN4*$^{pod+}$ / *UCHL1*-/- mice displayed an increased proportion of healthy ($p<0.01$) and a decreased proportion of segmental ($p<0.05$) and global sclerotic glomeruli vs. K256E-*ACTN4*$^{pod+}$ / *UCHL1*+/+ mice. A minimum of 60 glomeruli were analyzed per mouse (n=5 per group). (**c**) The relative difference between the Bowman's capsule area and the glomerular tuft area is increased in K256E-*ACTN4*$^{pod+}$ / *UCHL1*+/+ mice at 10 weeks (n=8; $p<0.05$ vs. nonTG / *UCHL1*+/+ mice) and normalized in K256E-*ACTN4*$^{pod+}$ / *UCHL1*-/- mice (n=8; $p<0.05$ vs. K256E-*ACTN4*$^{pod+}$ / *UCHL1*+/+ mice). n=10 and n=9 for nonTG / *UCHL1*+/+ and nonTG / *UCHL1*-/- mice, respectively. (**d**) Systolic blood pressure is increased in K256E-*ACTN4*$^{pod+}$ / *UCHL1*+/+ mice (n=7; $p<0.001$ vs. nonTG / *UCHL1*+/+ mice) at 6, 7 and 10 weeks of age. This increase is attenuated in K256E-*ACTN4*$^{pod+}$ / *UCHL1*-/- mice (n=8; $p<0.01$ vs. K256E-*ACTN4*$^{pod+}$ / *UCHL1*+/+ mice). n=7 and n=9 for nonTG / *UCHL1*+/+ and nonTG / *UCHL1*-/- mice respectively.

---

respectively; $p<0.05$) vs. nonTG / *UCHL1*+/+ mice. In contrast, K256E-*ACTN4*$^{pod+}$ / *UCHL1*-/- mice exhibited an ameliorated glomerular phenotype. Specifically, segmental and global glomerulosclerosis were significantly reduced (14±4%; $p<0.05$ and 17±9% of glomeruli, respectively), while 69±9% of glomeruli exhibited healthy histology ($p<0.01$) as compared to K256E-*ACTN4*$^{pod+}$ / *UCHL1*+/+ mice. >85% glomeruli were scored as healthy in nonTG / *UCHL1*+/+ and nonTG / *UCHL1*-/- mice (Figure 4b). A similar difference was seen with relative glomerular tuft to Bowman's capsule surface area. K256E-*ACTN4*$^{pod+}$ / *UCHL1*+/+ mice showed a significantly increased surface area between Bowman's capsule and the glomerular tuft ($p<0.05$) as compared to nonTG / *UCHL1*+/+. This relative area was normalized in K256E-*ACTN4*$^{pod+}$ / *UCHL1*-/- mice ($p<0.05$) (Figure 4c). No significant systolic blood pressure differences were observed in nonTG / *UCHL1*+/+ (115±5, 109±3 and 112±3 mmHg at 6, 7 and 10 weeks) or nonTG / *UCHL1*-/- mice (106±6, 106±5 and 108±2 mmHg at 6, 7 and 10 weeks). However systolic blood pressure was significantly elevated in K256E-*ACTN4*$^{pod+}$ / *UCHL1*+/+ mice to 121±5, 118±6 and 118±4 mmHg at 6, 7 and 10 weeks of age respectively, vs. nonTG / *UCHL1*+/+ mice ($p<0.001$). This elevation was attenuated in K256E-*ACTN4*$^{pod+}$

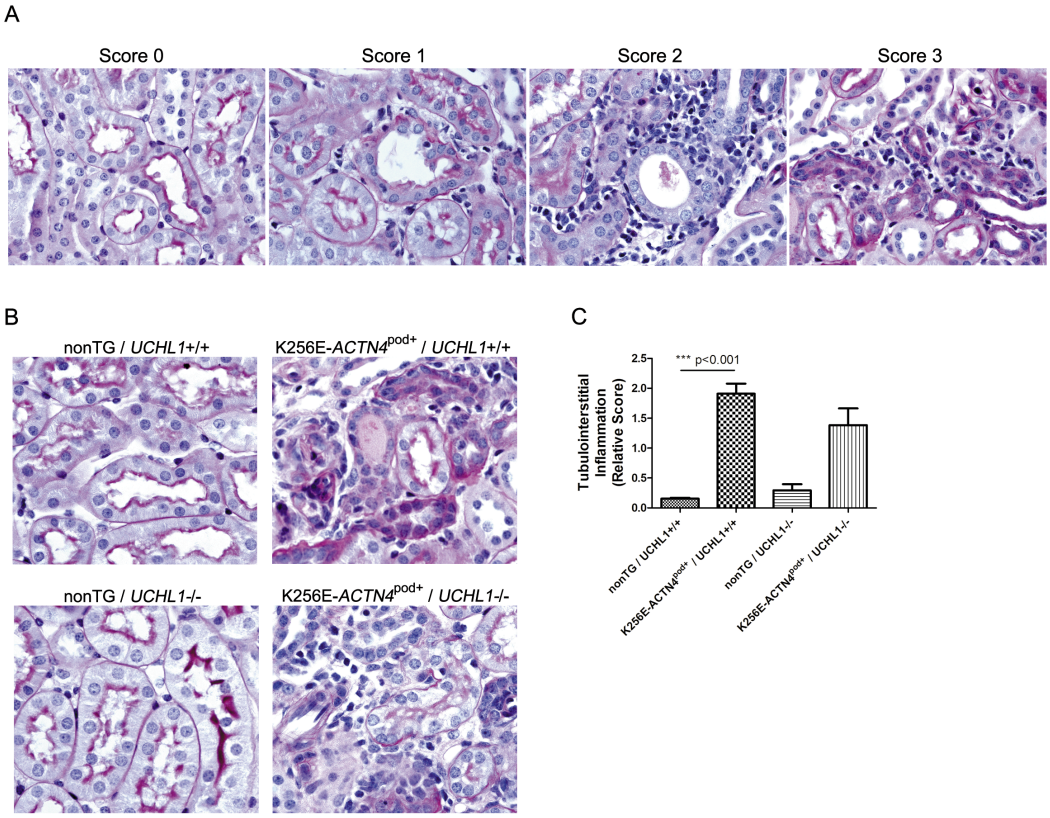

Supplemental Figure 1. Tubulointerstitial inflammation was mildly attenuated in in K256E-*ACTN4*$^{pod+}$ / *UCHL1*-/- mice. (**a**) Representative images of PAS-stained renal sections depicting the tubulointerstitial inflammation scoring system employed. Score 0 is defined by normal renal tubules with few visible interstitial cells, score 1 is defined by the accumulation of monocytes in the interstitial space, occupying <10% field, with relatively intact tubules, score 2 is defined by interstitial inflammation (10-25% field of view) and some tubular damage while score 3 defines significant tubulointerstitial inflammation (25-50% field of view), comprising tubular invasion and destruction. Magnification, 640x. (**b**) Representative images of PAS-stained renal sections for all mice groups. Magnification, 640x. (**c**) Graph depicting tubulointerstitial inflammation scoring, which was significantly increased in K256E-*ACTN4*$^{pod+}$ / *UCHL1*+/+ mice as compared to nonTG / *UCHL1*+/+ mice ($p<0.01$). This increase was attenuated (but not significantly) in K256E-*ACTN4*$^{pod+}$ / *UCHL1*-/- mice. A minimum of 10 fields of view were analyzed per mouse. n=3-4 per group.

/ *UCHL1*-/- mice to 112±5, 112±6 and 111±4 mmHg at the same time points ($p<0.01$ vs. K256E-*ACTN4*$^{pod+}$ / *UCHL1*+/+ mice) (Figure 4d). Electron microscopy analyses of K256E-*ACTN4*$^{pod+}$ / *UCHL1*+/+ mice glomeruli (ACR > 500 µg/mg) revealed significant podocyte FP effacement and GBM thickening, similar to previous observations [12]

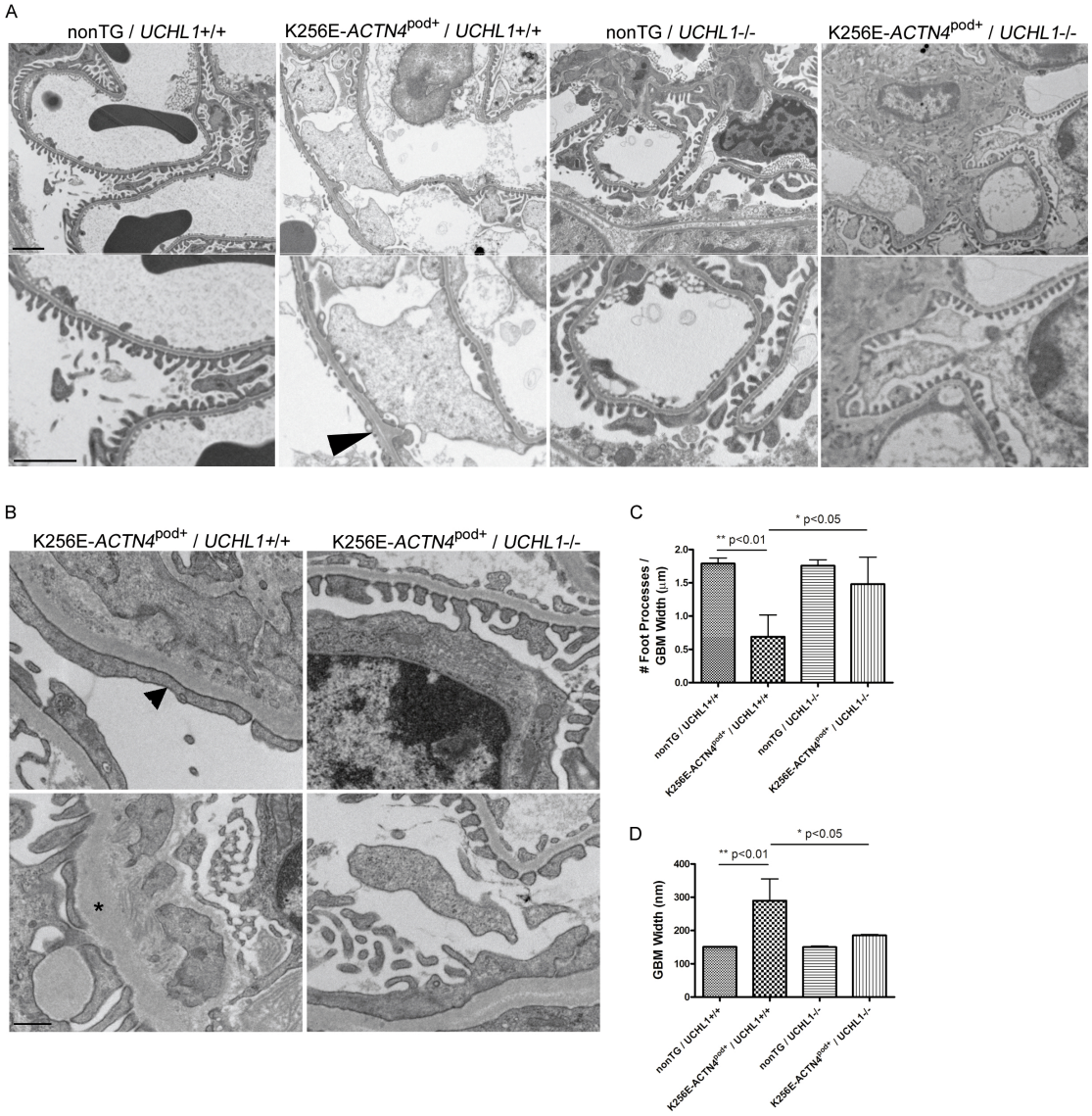

Figure 5. Foot process fusion is ameliorated in K256E-*ACTN4*$^{pod+}$ / *UCHL1*-/- mice. (**a**) Electron microscopy reveals foot process (FP) effacement and some irregular glomerular basement membrane (GBM) blebbing (arrowhead) in K256E-*ACTN4*$^{pod+}$ / *UCHL1*+/+ mice at 10 weeks. FP architecture appears relatively intact in K256E-*ACTN4*$^{pod+}$ / *UCHL1*-/- mice (n=3 per group). Scale bar represents 2μm. (**b**) Representative micrographs depicting areas of severe podocyte FP effacement (arrowhead, upper left panel) and GBM thickening (asterisk, lower left panel) in 10-week-old K256E-*ACTN4*$^{pod+}$ / *UCHL1*+/+ mice which are attenuated in K256E-*ACTN4*$^{pod+}$ / *UCHL1*-/- mice (upper and lower right panels). Scale bar represents 500nm. n=3 per group (**c**) Graph depicting the number of podocyte FP per micron of GBM length. The number of FP per GBM length were significantly decreased in K256E-*ACTN4*$^{pod+}$ / *UCHL1*+/+ mice ($p<0.01$) vs. nonTG / *UCHL1*+/+ mice. The decrease in FP per GBM length was attenuated in K256E-*ACTN4*$^{pod+}$ / *UCHL1*-/- mice ($p<0.05$ vs. K256E-*ACTN4*$^{pod+}$ / *UCHL1*+/+ mice). 2-3 glomeruli were analyzed per

group. (**d**) Graph depicting GBM width, where K256E-*ACTN4*$^{pod+}$ / *UCHL1*+/+ mice exhibited a significant increase in GBM width ($p<0.01$) vs. nonTG / *UCHL1*+/+ mice controls. K256E-*ACTN4*$^{pod+}$ / *UCHL1*-/- mice exhibit a relatively normalized GBM width ($p<0.05$) vs. K256E-*ACTN4*$^{pod+}$ / *UCHL1*+/+ mice. 2-3 glomeruli were analyzed per group.

(Figure 5a and b). In fact, while nonTG / *UCHL1*+/+ and nonTG / *UCHL1*-/- mice showed 1.78±0.05 and 1.76±0.06 FP/μm GBM, K256E-*ACTN4*$^{pod+}$ / *UCHL1*+/+ mice exhibited a decrease to 0.69±0.20 FP/μm GBM ($p<0.01$ vs. nonTG / *UCHL1*+/+ mice). Loss of *UCHL1* in K256E-*ACTN4*$^{pod+}$ / *UCHL1*-/- mice restored foot process architecture as these exhibited 1.48±0.20 FP/μm GBM ($p<0.05$ vs. K256E-*ACTN4*$^{pod+}$ / *UCHL1*+/+ mice) (Figure 5b and c). Additionally, GBM thickness was significantly increased in K256E-*ACTN4*$^{pod+}$ / *UCHL1*+/+ mice to 290±38nm ($p<0.01$ vs. nonTG / *UCHL1*+/+ mice) vs. 151±0.39nm for nonTG / *UCHL1*+/+ and 150±2.1nm for nonTG / *UCHL1*-/- mice. GBM thickening was significantly reduced in K256E-*ACTN4*$^{pod+}$ / *UCHL1*-/- mice to 185±1.6nm ($p<0.05$ vs. K256E-*ACTN4*$^{pod+}$ / *UCHL1*+/+ mice) (Figure 5b and d).

3.5. UCHL1 expression positively correlated with poly-ubiquitinated proteins but negatively correlated with K256E-α-actinin-4

In vitro data show that UCHL1 levels positively correlate with Ub expression, suggesting that UCHL1 may in fact fuel the UPS and activate protein degradation [16]. Since UCHL1 is increased in *ACTN4*-associated FSGS, we tested whether increased UCHL1 in glomeruli of K256E-*ACTN4*$^{pod+}$ / *UCHL1*+/+ mice correlated with increased Ub levels. Immunoblotting for Ub revealed slightly elevated levels of renal poly-ubiquitinated proteins in K256E-*ACTN4*$^{pod+}$ / *UCHL1*+/+ mice renal lysates vs. nonTG / *UCHL1*+/+ mice. In contrast, K256E-*ACTN4*$^{pod+}$ / *UCHL1*-/- mice exhibited significantly reduced

($p<0.05$) renal ubiquitinated protein levels (Figure 6a and b). Accordingly, immunoblotting for HA-tagged K256E-α-actinin-4 revealed increased levels in K256E-*ACTN4*$^{pod+}$ / *UCHL1*-/- mice as compared to K256E-*ACTN4*$^{pod+}$ / *UCHL1*+/+ mice ($p<0.05$), suggesting K256E-α-actinin-4 aggregate accumulation and UPS impairment when UCHL1 is absent (Figure 6c and d). Interestingly, while increased poly-Ub content is consistent with UPS failure, the decreased K256E-α-actinin-4 levels in podocytes of K256E-*ACTN4*$^{pod+}$ / *UCHL1*+/+ mice suggests an activated UPS. Conversely, the decreased Ub content in addition to increased K256E-α-actinin-4 levels suggests decreased UPS activity in K256E-*ACTN4*$^{pod+}$ / *UCHL1*-/- mice. Since K256E-α-actinin-4 levels are increased in K256E-*ACTN4*$^{pod+}$ / *UCHL1*-/- mice, we sought to determine if this increase correlated with changes in K256E-α-actinin-4/actin aggregation. To test if our findings were reproducible *in vitro*, we used differentiated conditionally immortalized human podocytes and transfected these with either scrambled or UCHL1 siRNA oligonucleotides. We first determined by western immunoblotting that 2.5 and 5nM of UCHL1 siRNA yielded optimal knockdown of UCHL1 levels in podocytes (Figure 6e). Choosing 2.5nM as the optimal dose for UCHL1 knockdown, we pursued co-infection/transfection experiments in podocytes overexpressing K256E-α-actinin-4 or WT-α-actinin-4 and determined whether knocking down UCHL1 levels impacted the expression of K256E-α-actinin-4. Western immunoblotting revealed no significant changes in the expression of both WT- and K256E-α-actinin-4 (Figure 6f). While the expression pattern of K256E-α-actinin-4 remained unchanged following UCHL1 knockdown, we tested whether the aggregation of K256E-α-actinin-4 was affected. Differential centrifugation experiments revealed no changes in the distribution

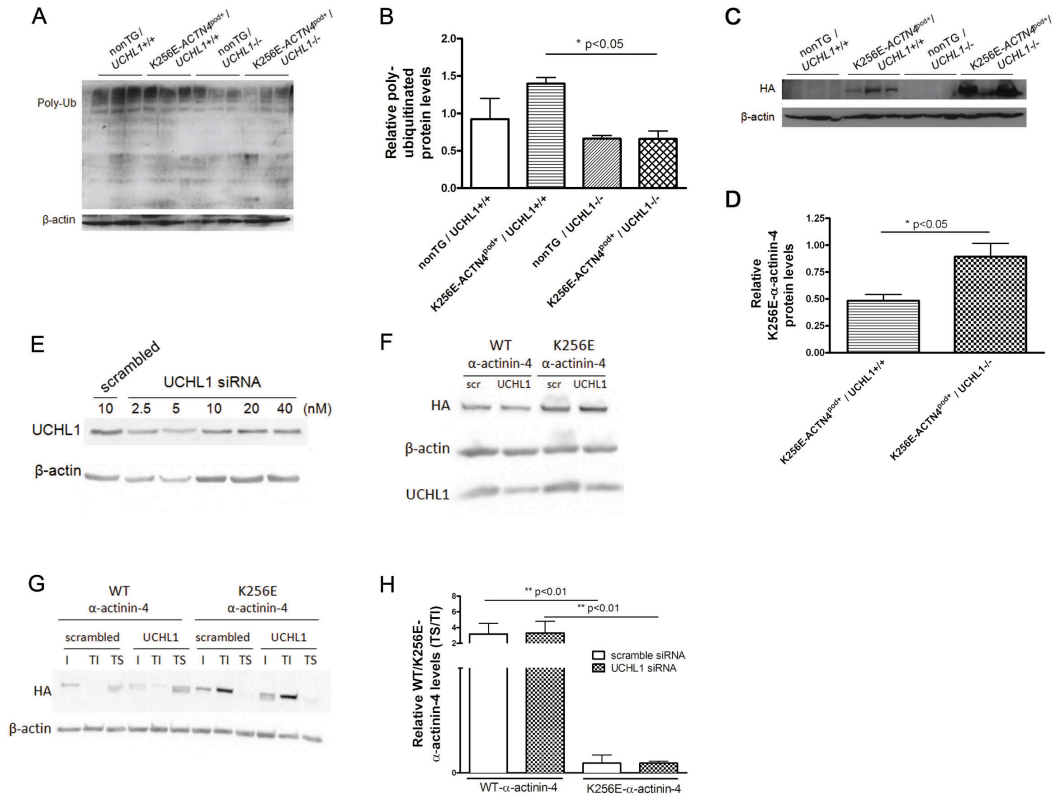

Figure 6. UCHL1 expression positively correlated with poly-ubiquitinated protein levels but negatively correlated with K256E-α-actinin-4 levels.
(**a**) Representative immunoblot showing poly-ubiquitinated proteins in renal cortical lysates of each mouse group at 10 weeks of age. (**b**) Graph depicting slightly elevated poly-ubiquitinated protein levels in K256E-*ACTN4*$^{pod+}$ / *UCHL1*+/+ mice as determined by densitometry. Poly-ubiquitinated proteins are significantly reduced in K256E-*ACTN4*$^{pod+}$ / *UCHL1*-/- mice ($p<0.05$ vs. K256E-*ACTN4*$^{pod+}$ / *UCHL1*+/+ mice). (**c**) Representative immunoblot showing HA-tagged K256E-α-actinin-4 levels in renal cortical lysates of each mouse group at 10 weeks of age. (**d**) Graph depicting decreased HA-tagged K256E-α-actinin-4 levels in K256E-*ACTN4*$^{pod+}$ / *UCHL1*+/+ mice as compared to K256E-*ACTN4*$^{pod+}$ / *UCHL1*-/- mice which exhibit significantly elevated levels of HA-tagged K256E-α-actinin-4 levels ($p<0.05$) (n=3 per group). (**e**) A 72-hour UCHL1 siRNA dose course in human podocytes showing optimal UCHL1 knockdown between 2.5-5nM of UCHL1 siRNA as compared to scrambled siRNA-treated controls (n=4) (**f**) Human podocytes overexpressing K256E-α-actinin-4 (MOI=30) and treated with 2.5nM UCHL1 siRNA for 72 hours showed no differences in HA-tagged K256E-α-actinin-4 versus scrambled (scr) controls. A slight decrease was observed in levels of WT-α-actinin-4 in human podocytes treated with UCHL1 siRNA but this was not significant. (**g**) A representative immunoblot showing the distribution of either HA-tagged WT- or K256E-α-actinin-4 in WT- or K256E-α-actinin-4 overexpressing human podocytes (MOI=30) and transfected with UCHL1 siRNA (2.5nM) and subjected to differential centrifugation. I, TI and TS represent the

input, triton-soluble and triton-insoluble isolated fractions. (**h**) Densitometry confirms decreased K256E-α-actinin-4 in the TS relative to the TI cellular fractions of human podocytes overexpressing K256E-α-actinin-4 and transfected with UCHL1 siRNA. No differences were observed compared to scrambled controls. Conversely, in human podocytes overexpressing WT-α-actinin-4 and transfected with UCHL1 siRNA, WT-α-actinin-4 was mainly distributed to the TS fraction versus the TI fraction. No differences were observed as compared to scrambled controls. Podocytes overexpressing WT-α-actinin-4 transfected with either scrambled or UCHL1 siRNA showed significantly increased WT-α-actinin-4 levels in the TS fraction as compared to K256E-α-actinin-4 expressing human podocytes treated with scrambled or UCHL1 siRNA, respectively ($p<0.001$). β-actin served as a loading control for all western blots.

of K256E-α-actinin-4. Specifically, K256E-α-actinin-4 remained associated with the triton-insoluble (TI) fraction as compared to the triton-soluble (TS) fraction following incubation with both scrambled and UCHL1 siRNA, suggesting that K256E-α-actinin-4 aggregation/association with large cytoskeletal fragments was unaffected by UCHL1 knockdown. The distribution of WT-α-actinin-4 remained associated with the TS fraction even following UCHL1 knockdown. WT-α-actinin-4 TS/TI fraction distribution remained greater in scrambled and UCHL1 siRNA transfected conditions versus K256E-α-actinin-4 scrambled and UCHL1 siRNA transfected podocytes ($p<0.001$) (Figure 6g and h). Similarly, immunofluorescence of podocytes overexpressing K256E-α-actinin-4 + UCHL1 knockdown and subjected to 10% equibiaxial stretch for 24 hours confirmed no differences in K256E-α-actinin-4 aggregation as compared to scrambled controls (data not shown).

3.6. Tubular and glomerular cell apoptosis are decreased in K256E-*ACTN4*$^{pod+}$ / *UCHL1*-/- mice

K256E-α-actinin-4 aggregation and misfolding lead to cytotoxicity and apoptosis [11]. Accordingly, enhanced UCHL1 expression stabilizes Ub levels, thereby over-fuelling the

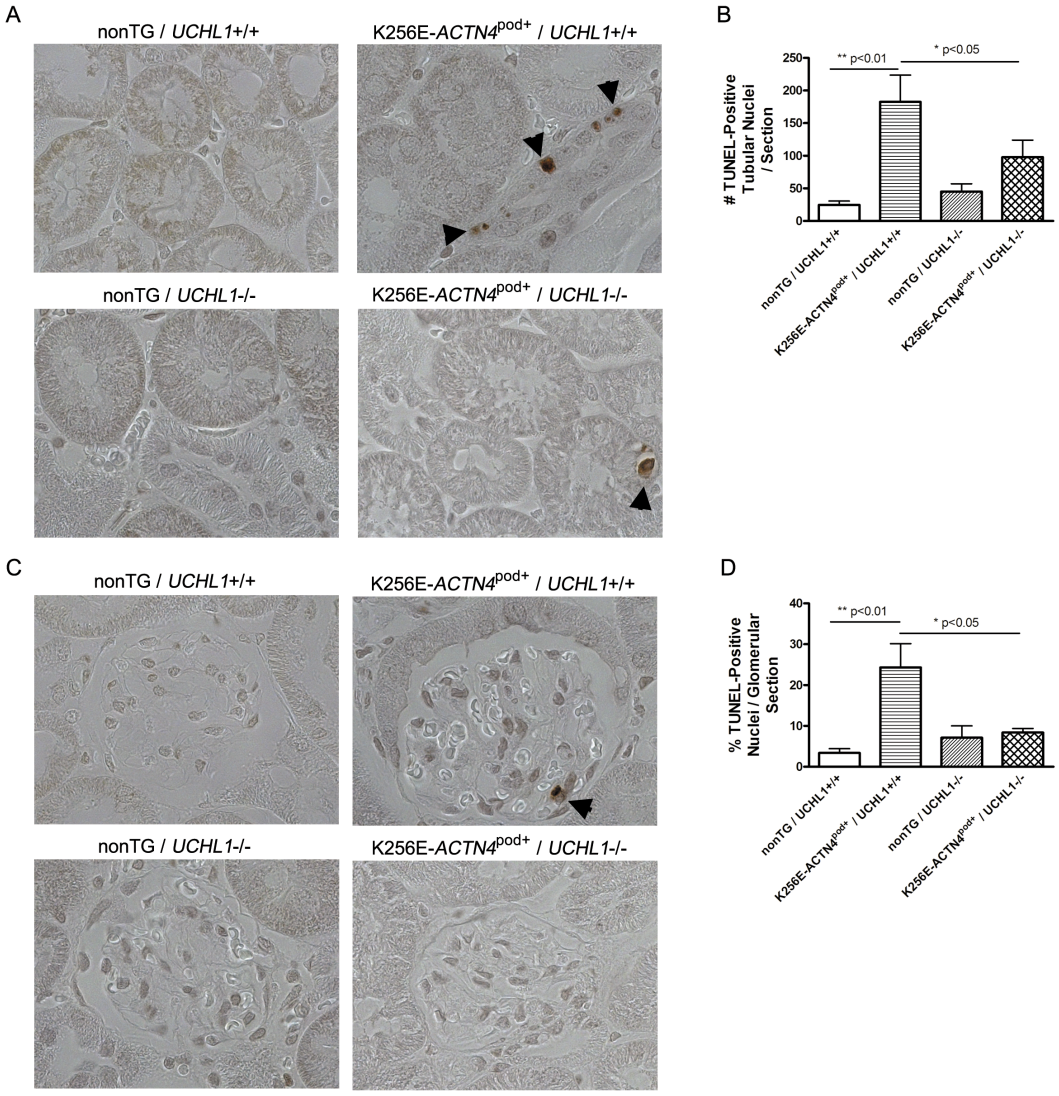

Figure 7. Tubular and glomerular cell apoptosis are decreased in K256E-*ACTN4*$^{pod+}$ / *UCHL1*-/- mice. (**a**) Representative images of renal cortex for each mouse group revealing TUNEL-positive nuclei in tubules (arrowheads). Magnification, 640x. (**b**) Graph depicting the total number of TUNEL-positive tubular nuclei per renal section in 10-week-old mice. Tubular TUNEL-positive nuclei numbers were increased in K256E-*ACTN4*$^{pod+}$ / *UCHL1*+/+ mice (n=6; p<0.01 vs. nonTG / *UCHL1*+/+ mice) and decreased in K256E-*ACTN4*$^{pod+}$ / *UCHL1*-/- mice (n=5; p<0.05 vs. K256E-*ACTN4*$^{pod+}$ / *UCHL1*+/+ mice). n=5 for nonTG / *UCHL1*+/+ and nonTG / *UCHL1*-/- mice. (**c**) Representative glomeruli showing TUNEL-positive nuclei (arrowhead) in 10-week old mice. Magnification, 640x. (**d**) Graph depicts the number of TUNEL-positive nuclei per glomerulus. The number of glomerular TUNEL-positive nuclei was elevated in K256E-*ACTN4*$^{pod+}$ / *UCHL1*+/+ mice (n=6; p<0.01 vs. nonTG / *UCHL1*+/+ mice) and decreased in K256E-*ACTN4*$^{pod+}$ / *UCHL1*-/- mice (n=5; p<0.01 vs. K256E-*ACTN4*$^{pod+}$ / *UCHL1*+/+ mice). n=5 for nonTG / *UCHL1*+/+ and nonTG / *UCHL1*-/- mice. A minimum of 20 glomeruli were analyzed per mouse.

UPS, and would be predicted to lead to cellular stress and apoptosis. We therefore assayed for apoptosis following *UCHL1* deletion in *ACTN4*-associated FSGS. TUNEL staining of renal sections revealed increased TUNEL-positive tubular nuclei per section (183±41) in K256E-*ACTN4*$^{pod+}$ / *UCHL1*+/+ mice ($p<0.01$ vs. nonTG / *UCHL1*+/+ mice). The increase was partly attenuated to 98±26 TUNEL-positive tubular nuclei per section in K256E-*ACTN4*$^{pod+}$ / *UCHL1*-/- mice ($p<0.05$ vs. K256E-*ACTN4*$^{pod+}$ / *UCHL1*+/+ mice). nonTG / *UCHL1*+/+ and nonTG / *UCHL1*-/- mice displayed <50 TUNEL-positive tubular cells per section (Figure 7a and b). Similarly, TUNEL staining revealed a 24±6% induction in TUNEL-positive nuclei per glomerular section in K256E-

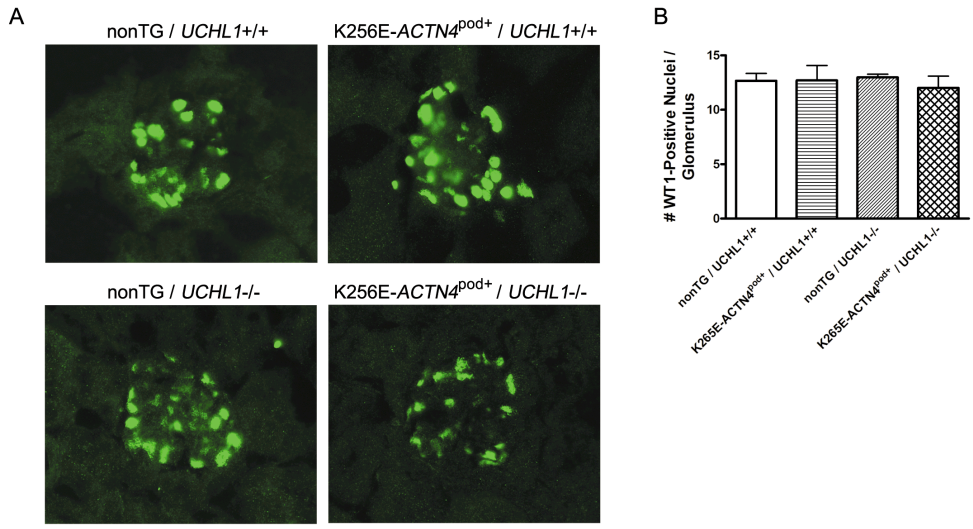

Figure 8. WT1-positive nuclei are unchanged in all mice groups. (**a**) Glomerular sections of 10-week-old mice representative of each mouse group, depicting immunoreactive WT1-positive nuclei. Magnification, 200x. (**b**) Graph representing the number of WT1-positive nuclei per glomerular section, which was not significantly different between mouse groups. n=3 per group and a minimum of 20 glomeruli were analyzed per mouse.

ACTN4^{pod+} / *UCHL1*+/+ mice ($p<0.01$ vs. nonTG / *UCHL1*+/+ mice). The increase in TUNEL-positive nuclei per glomerular section was blunted to 8±1% in K256E-*ACTN4*$^{pod+}$ / *UCHL1*-/- mice ($p<0.01$ vs. K256E-*ACTN4*$^{pod+}$ / *UCHL1*+/+ mice). Both

nonTG / *UCHL1*+/+ and nonTG / *UCHL1*-/- mice displayed <8% of TUNEL-positive glomerular cells per glomerular section (Figure 7c and d). Interestingly, K256E-*ACTN4*$^{pod+}$ / *UCHL1*+/+ mice showed no differences in WT1-positive nuclei per glomerulus in comparison to nonTG / *UCHL1*+/+ mice controls. In fact, no significant differences were observed for all four mice groups, suggesting that the glomerular apoptosis in K256E-*ACTN4*$^{pod+}$ / *UCHL1*+/+ mice is not podocyte-specific (Figure 8).

4. DISCUSSION

In our mouse model of *ACTN4*-associated FSGS, UCHL1 expression was increased in podocytes. *UCHL1* deletion ameliorated the renal phenotype, indicating that its activity may play a detrimental role in the etiology of this FSGS model.

The K256E mutation imposes a conformational change on the α-actinin-4 molecule leading to cytotoxic α-actinin-4/actin aggregate formation. Nonetheless, K256E-α-actinin-4 is a rapidly degraded cytoskeletal protein with a half-life of 15 hours, as compared to wt-α-actinin-4, which has a half-life >30 hours [5, 8-10]. In *ACTN4*-associated FSGS, UCHL1 induction may serve to fuel the UPS to help eliminate K256E-α-actinin-4. In contrast to findings in other glomerular disease models that show an inverse correlation between UCHL1 expression and proteasome activity, our findings suggest that UCHL1 expression positively correlates with proteasome activity as K256E-α-actinin-4 levels were significantly lower in podocytes of K256E-*ACTN4*$^{pod+}$ / *UCHL1*+/+ mice as compared to K256E-*ACTN4*$^{pod+}$ / *UCHL1*-/- mice. Interestingly, UPS impairment in podocytes of *UCHL1* knockout mice resembles the phenotype observed in *gad* mice, where UPS impairment and protein inclusions have been described [19, 25]. In light of our findings we postulate the following: In the absence of UCHL1, monomeric Ub levels are significantly reduced thereby diminishing K256E-α-actinin-4 poly-ubiquitination and degradation via the UPS. Over time however, the K256E-α-actinin-4 protein will form aggregates despite the absence of UCHL1. Without sufficient monomeric Ub to fuel UPS-mediated K256E-α-actinin-4 degradation, this mutant protein

will form aggregates that choke the proteasome in podocytes of K256E-*ACTN4*$^{pod+}$ / *UCHL1*-/- mice. Our *in vitro* results are consistent with this hypothesis in that mutant α-actinin-4 continues to associate with large cytoskeletal fragments (i.e., TI fraction) regardless of UCHL1 expression in conditionally immortalized human podocytes. In contrast, if UCHL1 upregulation promotes proteolysis in K256E-*ACTN4*$^{pod+}$ / *UCHL1*+/+ mice, K256E-α-actinin-4 aggregates can be degraded via the UPS. While K256E-α-actinin-4 degradation should be beneficial in relieving podocyte cytotoxicity, the histopathological and albuminuria data does not correspond to an ameliorated phenotype in K256E-*ACTN4*$^{pod+}$ / *UCHL1*+/+ mice. In fact, since K256E-α-actinin-4 can heterodimerize with wild type α-actinin-4 (in addition to homodimerizing to itself) both K256E- and wt-α-actinin-4 can be degraded by the proteasome in heterodimeric form [10]. As a result, the cytoskeleton of podocytes from K256E-*ACTN4*$^{pod+}$ / *UCHL1*+/+ mice would resemble that of an α-actinin-4 deficient podocyte [6, 10]. In fact, α-actinin-4 knockout mice develop podocyte FP effacement, proteinuria and glomerular disease, similar to K256E-*ACTN4*$^{pod+}$ / *UCHL1*+/+ mice [6]. Conversely, UPS impairment in K256E-*ACTN4*$^{pod+}$ / *UCHL1*-/- mice would preserve mutant and wt-α-actinin-4 expression, thereby partially stabilizing the cytoskeleton. This might explain why albuminuria in K256E-*ACTN4*$^{pod+}$ / *UCHL1*-/- mice is initially elevated at 4 weeks of age, but was significantly decreased by 10 weeks of age. Furthermore, K256E-*ACTN4*$^{pod+}$ / *UCHL1*-/- mice may not develop the same degree of filtration barrier injury as K256E-*ACTN4*$^{pod+}$ / *UCHL1*+/+ mice, limiting FP fusion and the development of FSGS lesions.

Interestingly, conditionally immortalized human podocytes overexpressing K256E-α-actinin-4 do not exhibit significant differences in UCHL1 protein levels as compared to WT-α-actinin-4 and GFP overexpressing podocyte controls. In fact, since Meyer-Schwesinger *et al* (2009) showed that UCHL1 expression inversely correlates with the differentiation status of conditionally immortalized human podocytes, we compared UCHL1 protein levels in undifferentiated and differentiated human podocyte cell line [13]. We found no differences in UCHL1 expression, regardless of podocyte differentiation status (verified by immunoblotting with anti-synaptopodin) (data not shown), suggesting that UCHL1 levels are consistently elevated in our conditionally immortalized human podocyte cell line. We reproduced these experiments in conditionally immortalized mouse podocytes and observed similar findings (data not shown). Therefore, the presence of K256E-α-actinin-4 in our human podocytes may not have been sufficient to further upregulate UCHL1 levels, given that UCHL1 levels were initially elevated. Conversely, the presence of K256E-α-actinin-4 in K256E-*ACTN4*$^{pod+}$ / *UCHL1*+/+ mice lead to UCHL1 upregulation, suggesting that podocytes lose some of the characteristics they exhibit *in vivo* [26, 27]. We therefore undertook UCHL1 silencing-based approaches in podocytes overexpressing K256E-α-actinin-4 to better model our findings *in vivo*. In addition, we overexpressed K256E-α-actinin-4 in COS7 cells and observed UCHL1 upregulation confirming that K256E-α-actinin-4 can lead to UCHL1 upregulation in other cell types *in vitro*.

The blood pressure elevation (~10 mmHg) in K256E-*ACTN4*$^{pod+}$ / *UCHL1*+/+ mice corresponds to previous findings by Michaud *et al* (2006) and on initial analysis, may be

a result secondary to compromised filtration barrier integrity along with downstream tubular damage, leading to activation of the renin-angiotensin-aldosterone system (RAAS). However, non-albuminuric mice also show blood pressure elevations without the histopathological features of FSGS thereby refuting this hypothesis [12]. Furthermore, increased aldosterone production may lead to edema which would likely result in blood pressure elevations. However, no significant body weight changes were observed for all four mice groups, suggesting that K256E-*ACTN4*$^{pod+}$ / *UCHL1*+/+ mice are not edemic (data not shown). As such, we cannot conclusively determine a role for the RAAS in the context of blood pressure elevation in K256E-*ACTN4*$^{pod+}$ / *UCHL1*+/+ mice. The blood pressure normalization in K256E-*ACTN4*$^{pod+}$ / *UCHL1*-/- mice may in fact be regulated through other mechanisms related specifically to the nature of the *UCHL1* null phenotype.

While UCHL1 has a long half-life (48h) and its expression is largely regulated by macroautophagy [28], it can also be degraded by the UPS [29]. Our findings suggest that UCHL1 may be induced through other regulators, such as NFκB, which may be increased in this diseased setting [30]. Moreover, we cannot rule out the possibility that reduced promoter methylation, which normally silences UCHL1 expression in non-neuronal tissues, underlies the FSGS-associated induction [31]. While the specific triggers that lead to increased UCHL1 expression and its precise enzymatic function(s) remain unclear, our data strongly support the notion that UCHL1 carries out a detrimental role in FSGS lesion development in *ACTN4*-associated FSGS, as supported by the ameliorated phenotype of K256E-*ACTN4*$^{pod+}$ / *UCHL1*-/- mice.

In summary, UCHL1 is expressed in podocytes of K256E-*ACTN4*$^{pod+}$ / *UCHL1*+/+ mice. *UCHL1* deletion in *ACTN4*-associated FSGS reduced albuminuria, glomerulosclerosis, FP effacement, GBM thickening, glomerular and tubular cell apoptosis, and ameliorated the overall renal pathology. These observations coincide with decreased poly-ubiquitinated protein levels and increased K256E-α-actinin-4 levels in K256E-*ACTN4*$^{pod+}$ / *UCHL1*-/- mice kidneys, suggesting impaired proteolysis of K256E-α-actinin-4. As a result, endogenous α-actinin-4 may be protected from degradation, preserving the podocyte's architectural integrity and improving glomerular function.

ACKNOWLEDGEMENTS

The authors thank Julie Zhu for her indispensable technical support (mice colonies and cell culture) and Laure Tessier for computing statistical analyses on the mice ACR. We thank Jeff McClintock at the Children's Hospital of Eastern Ontario and Peter Rippstein at the University of Ottawa's Heart Institute for their help with processing the renal samples for electron microscopy and Steve Callaghan for the adenoviruses.

N.C.R is a recipient of the Kidney Foundation of Canada Graduate Fellowship Award-Agostino Montedoro Endowment Fund. This study was supported by grants from the Kidney Foundation of Canada (KFOC) to C. R. J. K. and D. A. G.

REFERENCES

[1] K. Djinovic-Carugo, P. Young, M. Gautel, M. Saraste, Structure of the alpha-actinin rod: molecular basis for cross-linking of actin filaments, Cell, 98 (1999) 537-546.
[2] O. Pelletier, E. Pokidysheva, L.S. Hirst, N. Bouxsein, Y. Li, C.R. Safinya, Structure of actin cross-linked with alpha-actinin: a network of bundles, Phys. Rev. Lett., 91 (2003) 148102.
[3] Z. Rajfur, P. Roy, C. Otey, L. Romer, K. Jacobson, Dissecting the link between stress fibres and focal adhesions by CALI with EGFP fusion proteins, Nat. Cell Biol., 4 (2002) 286-293.
[4] M.P. Winn, P.J. Conlon, K.L. Lynn, D.N. Howell, B.D. Slotterbeck, A.H. Smith, F.L. Graham, M. Bembe, L.D. Quarles, M.A. Pericak-Vance, J.M. Vance, Linkage of a gene causing familial focal segmental glomerulosclerosis to chromosome 11 and further evidence of genetic heterogeneity, Genomics, 58 (1999) 113-120.
[5] J.M. Kaplan, S.H. Kim, K.N. North, H. Rennke, L.A. Correia, H.Q. Tong, B.J. Mathis, J.C. Rodriguez-Perez, P.G. Allen, A.H. Beggs, M.R. Pollak, Mutations in ACTN4, encoding alpha-actinin-4, cause familial focal segmental glomerulosclerosis, Nat. Genet., 24 (2000) 251-256.
[6] C.H. Kos, T.C. Le, S. Sinha, J.M. Henderson, S.H. Kim, H. Sugimoto, R. Kalluri, R.E. Gerszten, M.R. Pollak, Mice deficient in alpha-actinin-4 have severe glomerular disease, J. Clin. Invest., 111 (2003) 1683-1690.
[7] S. Dai, Z. Wang, X. Pan, X. Chen, W. Wang, H. Ren, Q. Feng, J.C. He, B. Han, N. Chen, ACTN4 gene mutations and single nucleotide polymorphisms in idiopathic focal segmental glomerulosclerosis, Nephron Clin. Pract., 111 (2009) c87-94.
[8] J.L. Michaud, K.M. Chaisson, R.J. Parks, C.R. Kennedy, FSGS-associated alpha-actinin-4 (K256E) impairs cytoskeletal dynamics in podocytes, Kidney Int., 70 (2006) 1054-1061.
[9] A. Weins, J.S. Schlondorff, F. Nakamura, B.M. Denker, J.H. Hartwig, T.P. Stossel, M.R. Pollak, Disease-associated mutant alpha-actinin-4 reveals a mechanism for regulating its F-actin-binding affinity, Proc. Natl. Acad. Sci. U. S. A., 104 (2007) 16080-16085.
[10] J. Yao, T.C. Le, C.H. Kos, J.M. Henderson, P.G. Allen, B.M. Denker, M.R. Pollak, Alpha-actinin-4-mediated FSGS: an inherited kidney disease caused by an aggregated and rapidly degraded cytoskeletal protein, PLoS Biol., 2 (2004) e167.
[11] A.V. Cybulsky, T. Takano, J. Papillon, K. Bijian, J. Guillemette, C.R. Kennedy, Glomerular epithelial cell injury associated with mutant alpha-actinin-4, Am. J. Physiol. Renal Physiol., 297 (2009) F987-995.
[12] J.L. Michaud, L.I. Lemieux, M. Dube, B.C. Vanderhyden, S.J. Robertson, C.R. Kennedy, Focal and segmental glomerulosclerosis in mice with podocyte-specific expression of mutant alpha-actinin-4, J. Am. Soc. Nephrol., 14 (2003) 1200-1211.
[13] C. Meyer-Schwesinger, T.N. Meyer, S. Munster, P. Klug, M. Saleem, U. Helmchen, R.A. Stahl, A new role for the neuronal ubiquitin C-terminal hydrolase-L1 (UCH-L1) in podocyte process formation and podocyte injury in human glomerulopathies, J. Pathol., 217 (2009) 452-464.

[14] K.D. Wilkinson, K.M. Lee, S. Deshpande, P. Duerksen-Hughes, J.M. Boss, J. Pohl, The neuron-specific protein PGP 9.5 is a ubiquitin carboxyl-terminal hydrolase, Science, 246 (1989) 670-673.
[15] Z.R. Zhou, Y.H. Zhang, S. Liu, A.X. Song, H.Y. Hu, Length of the active-site crossover loop defines the substrate specificity of ubiquitin C-terminal hydrolases for ubiquitin chains, Biochem. J., 441 (2012) 143-149.
[16] H. Osaka, Y.L. Wang, K. Takada, S. Takizawa, R. Setsuie, H. Li, Y. Sato, K. Nishikawa, Y.J. Sun, M. Sakurai, T. Harada, Y. Hara, I. Kimura, S. Chiba, K. Namikawa, H. Kiyama, M. Noda, S. Aoki, K. Wada, Ubiquitin carboxy-terminal hydrolase L1 binds to and stabilizes monoubiquitin in neuron, Hum. Mol. Genet., 12 (2003) 1945-1958.
[17] Y. Liu, H. Wu, J. Wu, S. Wang, Y. Liu, Z. Zhao, X. Zhang, R. Li, M. Guo, Z. Zhang, Detection of UCH-L1 expression by pre-embedding immunoelectron microscopy with colloidal gold labeling in diseased glomeruli, Ultrastruct. Pathol., 32 (2008) 5-9.
[18] Y. Liu, J. Wu, H. Wu, T. Wang, H. Gan, X. Zhang, Y. Liu, R. Li, Z. Zhao, Q. Chen, M. Guo, Z. Zhang, UCH-L1 expression of podocytes in diseased glomeruli and in vitro, J. Pathol., 217 (2009) 642-653.
[19] K. Saigoh, Y.L. Wang, J.G. Suh, T. Yamanishi, Y. Sakai, H. Kiyosawa, T. Harada, N. Ichihara, S. Wakana, T. Kikuchi, K. Wada, Intragenic deletion in the gene encoding ubiquitin carboxy-terminal hydrolase in gad mice, Nat. Genet., 23 (1999) 47-51.
[20] C.J. Proctor, P.J. Tangeman, H.C. Ardley, Modelling the role of UCH-L1 on protein aggregation in age-related neurodegeneration, PLoS One, 5 (2010) e13175.
[21] C. Meyer-Schwesinger, T.N. Meyer, H. Sievert, E. Hoxha, M. Sachs, E.M. Klupp, S. Munster, S. Balabanov, L. Carrier, U. Helmchen, F. Thaiss, R.A. Stahl, Ubiquitin C-terminal hydrolase-l1 activity induces polyubiquitin accumulation in podocytes and increases proteinuria in rat membranous nephropathy, Am. J. Pathol., 178 (2011) 2044-2057.
[22] M.L. Chiang, E.P. Hawkins, P.L. Berry, J. Barrish, L.L. Hill, Diagnostic and prognostic significance of glomerular epithelial cell vacuolization and podocyte effacement in children with minimal lesion nephrotic syndrome and focal segmental glomerulosclerosis: an ultrastructural study, Clin. Nephrol., 30 (1988) 8-14.
[23] Y.K. Lee, T. Kwon, D.J. Kim, W. Huh, Y.G. Kim, H.Y. Oh, H. Kawachi, Ultrastructural study on nephrin expression in experimental puromycin aminonucleoside nephrosis, Nephrol. Dial. Transplant., 19 (2004) 2981-2986.
[24] M. Takemoto, N. Asker, H. Gerhardt, A. Lundkvist, B.R. Johansson, Y. Saito, C. Betsholtz, A new method for large scale isolation of kidney glomeruli from mice, Am. J. Pathol., 161 (2002) 799-805.
[25] N. Ichihara, J. Wu, D.H. Chui, K. Yamazaki, T. Wakabayashi, T. Kikuchi, Axonal degeneration promotes abnormal accumulation of amyloid beta-protein in ascending gracile tract of gracile axonal dystrophy (GAD) mouse, Brain Res., 695 (1995) 173-178.
[26] S.J. Shankland, J.W. Pippin, J. Reiser, P. Mundel, Podocytes in culture: past, present, and future, Kidney Int., 72 (2007) 26-36.
[27] M.A. Saleem, M.J. O'Hare, J. Reiser, R.J. Coward, C.D. Inward, T. Farren, C.Y. Xing, L. Ni, P.W. Mathieson, P. Mundel, A conditionally immortalized human podocyte cell line demonstrating nephrin and podocin expression, J. Am. Soc. Nephrol., 13 (2002) 630-638.

[28] T. Kabuta, A. Furuta, S. Aoki, K. Furuta, K. Wada, Aberrant interaction between Parkinson disease-associated mutant UCH-L1 and the lysosomal receptor for chaperone-mediated autophagy, J. Biol. Chem., 283 (2008) 23731-23738.
[29] H.C. Ardley, G.B. Scott, S.A. Rose, N.G. Tan, P.A. Robinson, UCH-L1 aggresome formation in response to proteasome impairment indicates a role in inclusion formation in Parkinson's disease, J. Neurochem., 90 (2004) 379-391.
[30] H. Zhang, Y. Sun, R. Hu, W. Luo, X. Mao, Z. Zhao, Q. Chen, Z. Zhang, The regulation of the UCH-L1 gene by transcription factor NF-kappaB in podocytes, Cell. Signal., 25 (2013) 1574-1585.
[31] J. Yu, Q. Tao, K.F. Cheung, H. Jin, F.F. Poon, X. Wang, H. Li, Y.Y. Cheng, C. Rocken, M.P. Ebert, A.T. Chan, J.J. Sung, Epigenetic identification of ubiquitin carboxyl-terminal hydrolase L1 as a functional tumor suppressor and biomarker for hepatocellular carcinoma and other digestive tumors, Hepatology, 48 (2008) 508-518.

CHAPTER 2

Hyperfiltration in *Ubiquitin C-Terminal Hydrolase L1*-Deleted Mice

General Description

UCHL1 is one of the most abundant proteins expressed in neurons where it plays a role in Ub maintenance and axonal transport. The kidney relies on rich innervation by sympathetic nerves wherein neurostimulation promotes renin release, sodium reabsorption and importantly, maintenance of renal artery and arteriole tone. While it appears that UCHL1 is abundantly expressed in the human kidney (after brain and testes), the role of UCHL1 in the renal nerves and how it may impact renal function is not known. Mice lacking *Uchl1* demonstrate significant neurodegeneration of axonal processes, accompanied by progressive sensory and motor ataxia. These also display significant neurodegeneration of the dorsal root ganglion of the gracile tract where renal afferent nerves traverse. Furthermore, it is not known whether renal efferent nerves become impacted by neurodegeneration as the disorder progresses to motor ataxia. Since renal sympathetic input is an important regulator of renal and glomerular hemodynamics, we sought to investigate whether neuronal UCHL1 is required for these processes. We hypothesized that neurodegeneration in mice lacking *Uchl1* leads to dysregulated renal sympathetic tone, resulting in loss of renal vascular tone and altered renal hemodynamics.

Hyperfiltration in *Ubiquitin C-Terminal Hydrolase L1*-Deleted Mice

Naomi Boisvert[1,4], Chet E. Holterman[1], Jean-François Thibodeau[1,4], Rania Nasrallah[4], Eldjonai Kamto[1], Cesar H. Comin[5], Luciano da F. Costa[6,] Anthony Carter[2,4,7], Richard L. Hébert[4], Alex Gutsol[1], Gregory O. Cron[3], Baptiste Lacoste[4,8,9], Douglas A. Gray[2,10], and Chris R. Kennedy[1,4]

[1]Kidney Research Centre, [2]Ottawa Hospital Research Institute, [3]The Ottawa Hospital, Ottawa, Ontario, Canada
[4]Department of Cellular and Molecular Medicine, Faculty of Medicine, University of Ottawa, Ottawa, Ontario, Canada
[5]São Carlos Institute of Physics, University of São Paulo, São Carlos, Brazil
[6]IFSC, University of São Paulo, São Carlos, Brazil
[7]Canadian Partnership for Stroke Recovery, Ottawa, Canada
[8]Neuroscience Program, Ottawa Hospital Research Institute, Ottawa, Ontario, Canada
[9]University of Ottawa Brain and Mind Research Institute, Ottawa, Ontario, Canada
[10]Department of Biochemistry, Microbiology and Immunology, Faculty of Medicine, University of Ottawa, Ottawa, Ontario, Canada.

Corresponding Author:
Dr. Chris R. Kennedy
Kidney Research Centre, Ottawa Hospital Research Institute, The Ottawa Hospital
Department of Cellular and Molecular Medicine, Faculty of Medicine, University of Ottawa
451 Smyth Rd, Roger-Guindon Hall, room 2515
Ottawa, Ontario, Canada, K1H 8M5
Phone: 1-613-562-5800, extension 8529
Fax: 1-613-562-5487
E-mail: ckennedy@uottawa.ca

Running Title: *Uchl1*-deleted mice hyperfilter

Abstract Word Count: 233

Text Word Count: 4221

Author Contributions

Naomi Boisvert	▪ Planned and performed the bulk of the experiments ▪ Wrote the manuscript
Chet E. Holterman	▪ Performed most of the mice procedures/sacrifices ▪ Provided guidance to the project
Jean-François Thibodeau	▪ Performed wire myography experiments ▪ Assisted with ELISA experiments
Rania Nasrallah	▪ Conducted the Western immunoblotting experiments for SGLT2, NKCC2 and COX-2
Eldjonai Kamto	▪ Assisted with ELISA experiments
Cesar H. Comin	▪ Analyzed the renal nerves ▪ Assisted with processing the renal nerve images
Luciano da F. Costa	▪ Analyzed the renal nerves ▪ Assisted with processing the renal nerve images
Anthony Carter	▪ Conducted the mice surgeries for DCE-MRI experiments
Richard L. Hébert	▪ Supervisor to Rania Nasrallah ▪ Provided resources for Western immunoblotting experiments
Alex Gutsol	▪ Performed the renin and nNOS immunohistochemistry experiments
Greg O. Cron	▪ Performed the DCE-MRI procedure ▪ Analyzed the results from the DCE-MRI
Baptiste Lacoste	▪ Provided significant guidance for renal nerve immunofluorescence experiments ▪ Finalized UCHL1/neurofilament immunofluorescence images
Douglas A. Gray	▪ Co-supervised the project ▪ Assisted with manuscript revisions
Chris R.J. Kennedy	▪ Supervised the project ▪ Assisted with manuscript revisions

Abstract

Neuronal ubiquitin C-terminal hydrolase L1 (UCHL1) is a deubiquitinating enzyme that maintains intracellular ubiquitin pools and promotes axonal transport. *Uchl1* deletion in mice leads to progressive axonal degeneration, affecting the dorsal root ganglion that harbours axons emanating to the kidney. Innervation is a crucial regulator of renal hemodynamics, though the contribution of neuronal UCHL1 to this is unclear. Immunofluorescence revealed significant neuronal UCHL1 expression in mouse kidney, including the axons surrounding the juxtaglomerular region. Glomerular filtration rate trended higher in 6-week-old *Uchl1*-/- mice, and by twelve weeks of age, these displayed significant glomerular hyperfiltration, coincident with the onset of neurodegeneration. Angiotensin converting enzyme inhibition had no effect on glomerular filtration rate of *Uchl1*-/- mice indicating that the renin angiotensin system does not contribute to the observed hyperfiltration. DCE-MRI revealed increased cortical renal blood flow in *Uchl1*-/- mice, suggesting that hyperfiltration results from afferent arteriole dilation. Nonetheless, hyperglycemia, cyclooxygenase-2 and nitric oxide synthases were ruled out as sources of hyperfiltration in *Uchl1*-/- mice as glomerular filtration rate remained unchanged following insulin treatment, and cyclooxygenase-2 and nitric oxide synthase inhibition. Finally, renal nerve dysfunction in *Uchl1*-/- mice is suggested as renal nerve arborization was increased and urinary norepinephrine was decreased. Moreover, vascular constriction in isolated mesenteric arteries was impaired following adrenergic stimulation. Altogether *Uchl1*-deleted mice demonstrate glomerular hyperfiltration

associated with renal neuronal dysfunction, suggesting that neuronal UCHL1 plays a crucial role in regulating renal hemodynamics.

Introduction

Ubiquitin C-terminal hydrolase L1 (UCHL1) is a deubiquitinating enzyme that salvages ubiquitin from substrates and preserves intracellular ubiquitin pools. UCHL1 is largely expressed in neurons and is most abundant in the brain where it comprises 1-5% of total soluble protein.[1] Studies in the gracile axonal dystrophy (*gad)* mouse, a mouse model that stems from a spontaneous deletion in exons 7-8 of the *Uchl1* gene, yielding no functional UCHL1 protein, have provided insight into the role of UCHL1 in neurons. Mice lacking *Uchl1* display significantly reduced ubiquitin levels in the cerebellum among other regions.[2] Phenotypically, *gad* mice develop sensory and motor ataxia by 12 and 16 weeks of age, respectively, where motor paresis affects gait between 6-12 weeks of age.[3] Further analysis of the *gad* mouse revealed degeneration of presynaptic terminals at the neuromuscular junction, accumulation of ubiquitinated protein aggregates, absence of synaptic vesicles and presence of aggresomes and tubulovesicular structures in neurons.[4,5] Moreover, inclusion body formation is evident in the axons of the dorsal root ganglion that pass through the gracile tract.[6,7] Together these observations delineate a critical role for UCHL1 in maintaining axonal transport and neuronal function.

The dorsal root ganglion of the gracile tract (T7-L2) harbours renal afferent nerves and since loss of *Uchl1* is associated with axonal degeneration in this region, there is a likely requirement for UCHL1 in renal innervation.[6,8] Moreover, as motor ataxia develops and hind limb paralysis progresses in *Uchl1*-deleted mice, efferent nerves branching to the kidney may also become affected. While *Uchl1* loss is largely known to impact skeletal

muscle, recent findings suggest that dysregulated innervation impairs visceral organ function, and the kidney may be no exception.[9,10]

Innervation plays a crucial role in renal hemodynamics and function. Renal afferent nerves innervate the proximal ureter, renal pelvis and major renal vessels, where they mediate chemoreceptor and baroreceptor activation.[11,12] In contrast, renal efferent nerves innervate the juxtaglomerular cells, tubules and renal vasculature. Through adrenergic receptor stimulation, sympathetic activation promotes renin secretion and water and sodium reabsorption.[13] Renal sympathetic activity also promotes vasoconstriction of renal vessels, including the afferent and efferent arterioles (where innervation at the afferent arteriole is predominant), thereby reducing renal blood flow (RBF). The effects on glomerular filtration rate (GFR) are modest in this setting due to compensation by angiotensin II (Ang II) at the efferent arteriole. In fact, blocking renin secretion from juxtaglomerular cells with the β-adrenergic receptor antagonist propanolol or blocking the angiotensin converting enzyme 1 (ACE1) with captopril significantly reduced GFR following renal nerve stimulation.[14,15] Conversely, while a number of studies demonstrated that renal denervation had no effect on RBF, there is also strong evidence to suggest that renal denervation impacts renal hemodynamics. Renal nerve ablation in rats increased cortical RBF in an acute manner.[16] Accordingly, Yoshimoto *et al* showed that RBF was unchanged in resting denervated rats, however, RBF increased during daily activities such as grooming and feeding.[16] Together these findings attest to the crucial role of renal nerves in regulating renal hemodynamics and function.

The role of neuronal UCHL1 in renal hemodynamics and function remains to be determined. Among the first reports describing UCHL1 expression in the kidney, Shirato *et al* demonstrated UCHL1 expression in the axons located at the vascular pole of the rat glomerulus. Additionally, Bradbury *et al* described significant UCHL1 protein levels in human renal homogenates and we speculate that these are largely attributed to UCHL1 expression in renal neurons.[17] To our knowledge, the role of neuronal UCHL1 has not been specifically investigated in the kidney where we postulate that it is required for renal neuronal function.[18] In the present study, we characterized UCHL1 in the renal neurovasculature and hypothesized that loss of neuronal *Uchl1* in mice impacts renal hemodynamics and homeostasis.

Results

Neuronal UCHL1 Expression in the Mouse Kidney

UCHL1 expression was characterized in renal nerves. Significant UCHL1-positive immunostaining was determined in the renal nerves of wild type mice, including the fine axonal branches in the renal cortex. Neuronal UCHL1 was abundant around the major blood vessels that supply the glomeruli and was mapped to the juxtaglomerular region (Figure 1).

Uchl1-Deleted Mice Hyperfilter

Renal histology in 12-week-old *Uchl1*-/- mice was similar to wild type littermates, however a hyperplastic abnormality was observed in the juxtaglomerular region (Figure 2a). Next, we postulated that loss of *Uchl1* in the renal neurovasculature would lead to changes in renal hemodynamics. Systolic blood pressure (SBP) trended lower in *Uchl1*-/- mice at 6 weeks (109±2mmHg vs. 117±2mmHg for wild type), 9 weeks (109±3mmHg vs. 113±2mmHg for wild type) and 12 weeks of age (106±4mmHg vs. 113±2mmHg for wild type) (Figure 2b). Similarly, at 20 weeks of age and well after the onset of motor ataxia, mesenteric arteries isolated from *Uchl1*-/- mice showed decreased sensitivity to phenylephrine (Phe)-induced vasoconstriction compared to wild type mice (Figure 2c). Accordingly, Phe had reduced potency ($p<0.01$) on *Uchl1*-/- arteries (Figure 2d), as they required a greater dose to achieve EC_{50} (6.2±0.1 vs. 6.6±0.1 for wild type; $-\log EC_{50}$). FITC-inulin clearance trended higher in 6-week-old *Uchl1*-/- mice (329±34µl/min vs. 233±19µl/min for wild type), but was significantly elevated ($p<0.01$) by 12 weeks of age

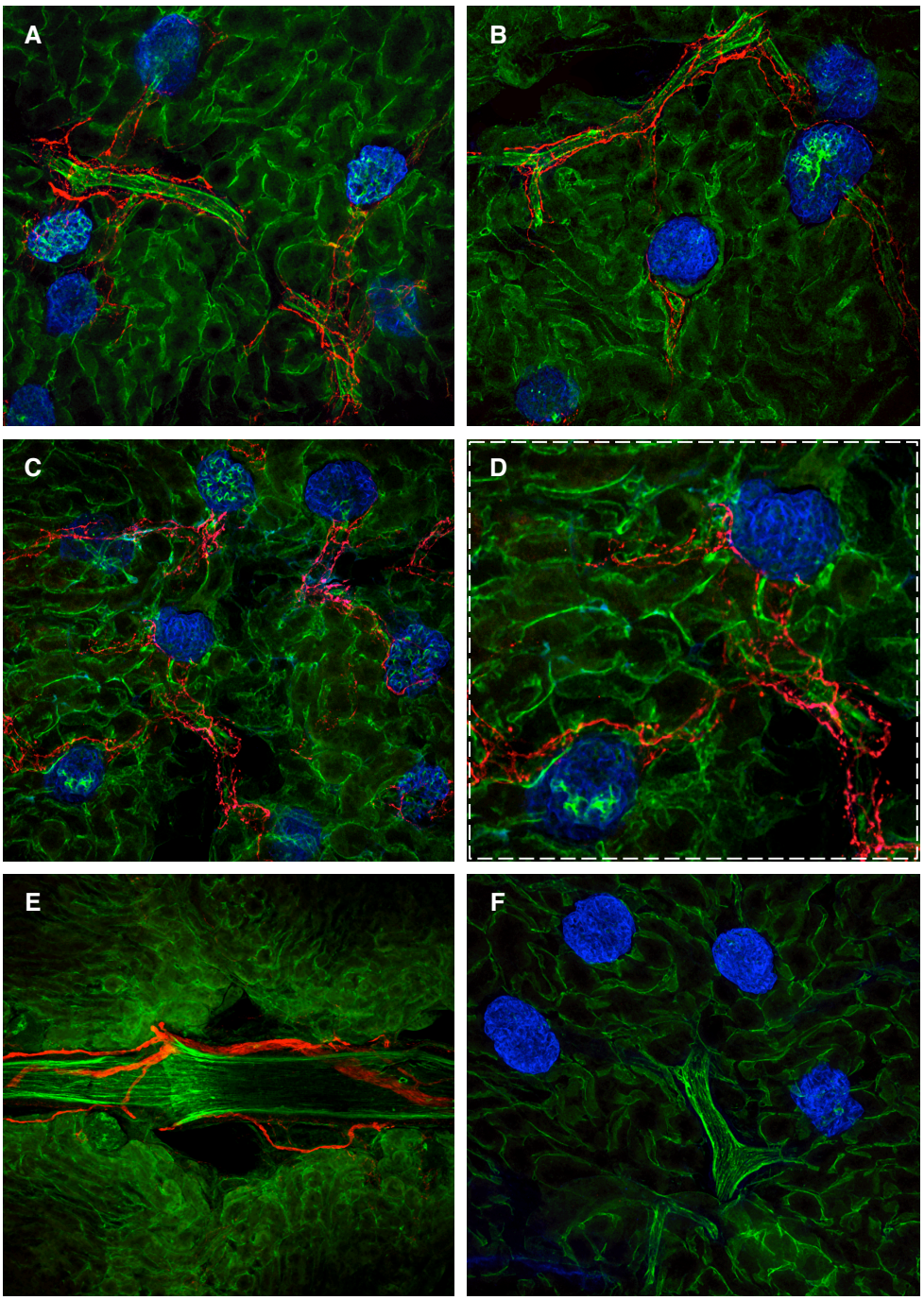

Figure 1. UCHL1 is abundantly expressed in mouse renal nerves.
Immunofluorescence microscopy revealed UCHL1-positive nerves surrounding the vasculature branching towards the glomeruli of wild type mice (**A-C, D**). **D.** Inset from (**C**) depicts significant UCHL1 immunopositive nerves branching toward and partially surrounding the glomerulus. Magnification, 200X. **E.** Larger renal vessels from wild type mice also depicted significant neural UCHL1 expression. Magnification, 100X. **F.** UCHL1 immunopositivity was absent in renal sections from *Uchl1*-/- mice. Magnification, 200X. n=5-6. UCHL1: red, CD31: green and synaptopodin: blue.

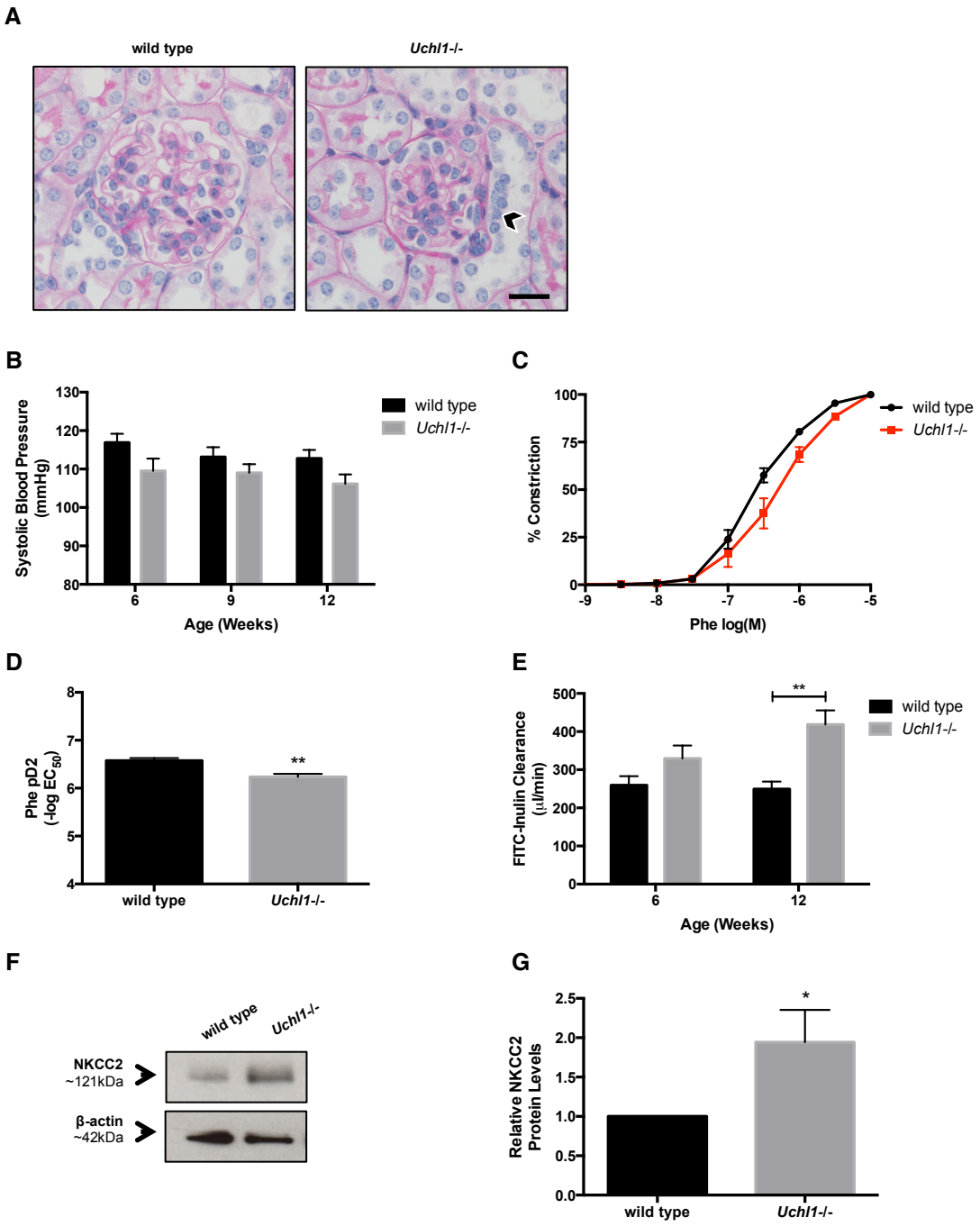

Figure 2. *Uchl1*-/- mice demonstrate loss of vascular resistance combined with glomerular hyperfiltration. A. Renal architecture was relatively intact in *Uchl1*-deleted mice, although an abnormal cellularity was observed in the juxtaglomerular region (arrowhead; n=5). Scale bar = 20µm. **B.** Blood pressure trended lower in *Uchl1*-/- mice at 6, 9 and 12 weeks of age (n=10 per group). **C.** Myography experiments revealed a delay in phenylephrine-induced constriction in mesenteric arteries of 20-week-old *Uchl1*-/- mice (n=3). **D.** -Log EC_{50} graph depicts decreased phenylephrine potency in *Uchl1*-deleted mesenteric arteries (**p<0.01; n=3).

E. Glomerular filtration rate determined by FITC-inulin clearance was significantly elevated (**p<0.01) in 12-week-old *Uchl1*-/- mice (n=9) compared to wild type mice (n=11). **F.** Renal cortical NKCC2 protein levels were increased in *Uchl1*-/- mice (n=7-8). **G.** Densitometry graph confirming elevated NKCC2 protein levels in renal cortical lysates from *Uchl1*-/- mice (*p<0.05; n=7-8).

(418±37µl/min vs. 249±19µl/min for wild type), coinciding with the onset of neurodegeneration (Figure 2e). By 12 weeks of age, *Uchl1*-/- mice demonstrated glomerular hyperfiltration (by definition: a GFR greater than twice the standard deviation above the mean of wild type control mice).[19] Consistent with the GFR findings, renal cortical Na-K-Cl cotransporter 2 (NKCC2) protein levels were elevated in *Uchl1*-/- mice by 1.9-fold (p<0.05) (Figures 2f-g). Despite the onset of hyperfiltration in *Uchl1*-/- mice, albumin/creatinine ratios were not elevated above those of wild type mice. Kidney weight trended lower in *Uchl1*-/- mice. To this end, glomerular and Bowman's capsule areas were quantified and were also reduced in *Uchl1*-/- mice. Finally, we determined that an increase in glomerular number per area does not underlie the absolute increase in GFR in *Uchl1*-/- mice (Table 1).

The Renin Angiotensin System and Hyperfiltration in *Uchl1*-/- Mice

Next, we postulated that progressive neurodegeneration and decreased vascular resistance in *Uchl1*-/- mice may lead to renin angiotensin system (RAS) activation, which would indirectly promote glomerular hyperfiltration by increasing efferent arteriole resistance. Indeed, components of the RAS were altered in *Uchl1*-/- mice. ACE1 (p<0.01) and the angiotensin type 2 receptor (AT2R; p<0.001) mRNA levels were significantly elevated, both by 3.1-fold, while the angiotensin type 1 receptor (AT1R) and mas receptor (MasR)

Table 1. Renal physiological parameters of 12-week-old wild type and *Uchl1*-/- mice.

	wild type	*Uchl1*-/-
Albumin/Creatinine Ratios (μg/mg)	23.8 ± 2.7 (n=12)	34.7 ± 6.3 (n=16)
Body Weight (g)	25.0 ± 0.6 (n=12)	21.9* ± 1.0 (n=9)
Kidney Weight/Tibia Length (mg/mm)	16.3 ± 1.1 (n=7)	14.8 ± 1.2 (n=8)
Glomerular Tuft Area (a.u.)	36147 ± 2002 (n=10)	30907* ± 1700 (n=10)
Bowman's Capsule Area (a.u.)	46674 ± 2653 (n=10)	41968 ± 1997 (n=10)
Total Glomeruli/ Cortical Area (#/mm^2)	11.3 ± 0.5 (n=3)	12.4 ± 0.3 (n=3)

Data are represented as mean ± SE, *$p<0.05$ versus wild type mice (using an unpaired T-test)

mRNA were both attenuated by 2.1-fold ($p<0.05$) and 3.7-fold ($p<0.05$), respectively (Figure 3a). Western immunoblotting confirmed increased prorenin and renin in renal cortical lysates from *Uchl1*-/- mice (Figure 3b). Immunohistochemistry with a renin antibody however did not reveal any obvious differences in the renin-positive juxtaglomerular region (Figure 3c). ACE1 protein levels were also increased in renal cortical lysates from a proportion of *Uchl1*-/- mice (Figure 3d). To further delineate the contribution of the RAS to hyperfiltration, *Uchl1*-/- mice were administered lisinopril for 14 days (Table 2). While SBP was modestly reduced in lisinopril-treated wild type mice (108±2mmHg vs. 117±3mmHg for wild type + vehicle), no changes were observed in lisinopril-treated *Uchl1*-/- mice (102±3mmHg vs. 104±1mmHg for *Uchl1*-/- + vehicle) (Figure 3e). FITC-inulin clearance was similarly unchanged in lisinopril-treated *Uchl1*-/-

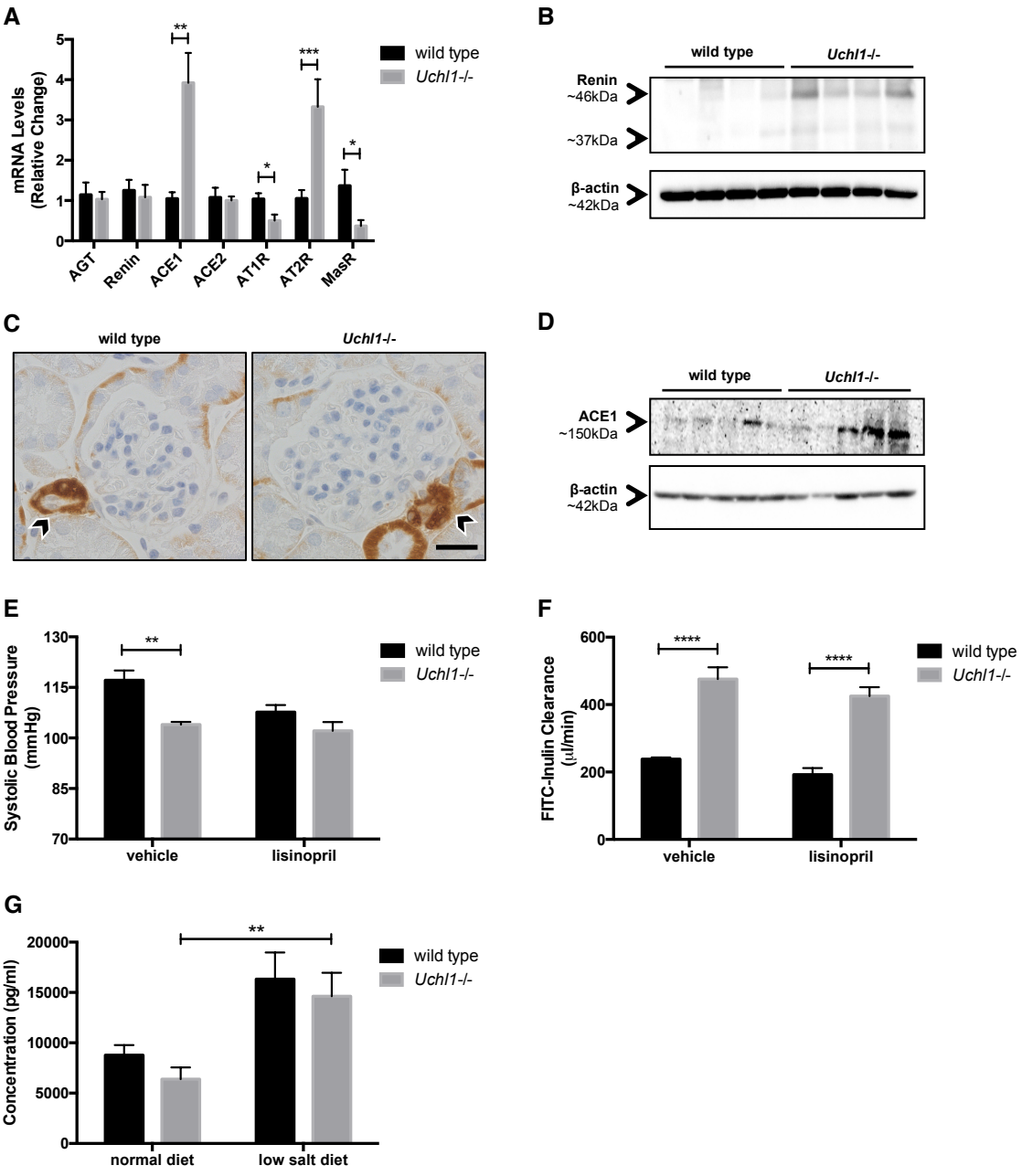

Figure 3. The RAS is not a means of glomerular hyperfiltration in *Uchl1*-/- mice. **A.** qPCR of various RAS components depicted significantly increased ACE1 (**p<0.01) and AT2R (**p<0.001) and significantly decreased AT1R (*p<0.05) and MasR (*p<0.05) mRNA (n=5-10). AGT: angiotensinogen. **B.** Prorenin (~46kDa) and renin (~37kDa) protein levels were elevated in renal cortical lysates from *Uchl1*-/- mice (n=4). **C.** Immunohistochemistry using anti-renin revealed no differences in renin-expressing juxtaglomerular cells from *Uchl1*-/- mice (n=6). Scale bar = 20μm. **D.** Renal cortical ACE1 protein levels (n=5) were increased in a proportion of *Uchl1*-/- mice. **E.** Lisinopril treatment slightly reduced systolic blood pressure in wild type mice but not in *Uchl1*-/- mice. Blood pressure in vehicle-treated *Uchl1*-/- mice was reduced compared to vehicle-treated wild type mice (**p<0.01) (n=5-6 per group).

F. Glomerular filtration rate estimated by FITC-inulin clearance was unaltered in *Uchl1*-/- mice treated with lisinopril (n=5-6 per group). **G.** Plasma renin concentration trended lower in *Uchl1*-/- mice but was significantly increased (**p<0.01; comparable to wild type + low salt diet) when these were subjected to a low salt diet (n=3-8).

Table 2. Daily and endpoint parameters of lisinopril-treated wild type and *Uchl1*-/- mice.

	vehicle		lisinopril	
	wild type (n=5)	***Uchl1*-/-** (n=5)	**wild type** (n=5)	***Uchl1*-/-** (n=5)
Water intake (ml)	4.6 ± 0.3	4.2 ± 0.37	4.1 ± 0.3	4.1 ± 0.2
Dosage (mg/kg/day)	12.5 ± 1.89	12.4 ± 1.15	11.0 ± 0.36	12.8 ± 1.12
Delta body weight (g)	-0.7 ± 0.5	0.4 ± 0.3	-0.5 ± 0.3	-0.3 ± 0.2

Data are represented as mean ± SE

mice (425±24µl/min vs. 476±35µl/min for *Uchl1*-/- + vehicle) despite a modest reduction in lisinopril-treated wild type mice (192±19µl/min vs. 238±5µl/min for wild type + vehicle) (Figure 3f). Thus, changes in the RAS do not account for hyperfiltration in *Uchl1*-/- mice.

Finally, research by Chu *et al* suggests that *Uchl1* loss combined with proteolytic stress leads to degradation of vesicle-associated membrane protein 2 (VAMP2) in pancreatic β-cells. Since VAMP2 is required for renin secretion from juxtaglomerular cells, we investigated whether renin release was impaired in *Uchl1*-/- mice.[9,20] At baseline, plasma renin concentration was lower in *Uchl1*-/- mice (6397±1155pg/ml vs. 8782±997pg/ml for

wild type). However, challenge with a sodium-deficient diet produced similar renin levels in *Uchl1*-/- mice (14631±2328pg/ml) as wild type mice (16328±2642pg/ml) (Figure 3g).

Increased RBF and Tubular Flow in *Uchl1*-/- Mice

Glomerular hyperfiltration is associated with either an increase or a decrease in RBF, depending on whether the afferent or efferent arteriole is dilated or constricted, respectively.[21] By DCE-MRI, RBF was estimated. Cortical RBF was higher in *Uchl1*-/- mice (578±137ml/100ml/min vs. 321±71ml/100ml/min for wild type) and blood volume was increased ($p<0.05$; 27.7±1.2ml/100ml for *Uchl1*-/- vs. 23.0±1.5ml/100ml for wild type) (Figure 4a-b). Conversely, blood mean transit time trended lower in the renal cortex of *Uchl1*-/- mice (3.8±1.0sec vs. 5.0±1.2sec for wild type) (Figure 4c). Medullary RBF, blood volume and blood mean transit time were comparable between groups. Consistent with the GFR findings, medullary tubular flow was increased ($p<0.05$) in *Uchl1*-/- mice (35.5±5.7ml/100ml/min vs.14.8±3.3 ml/100ml/min for wild type) while tubular mean transit time was decreased ($p<0.05$; 0.3±0.1min for *Uchl1*-/- vs. 2.4±0.7min for wild type) (Figure 4d-e). The extraction fraction was elevated to 16.9±3.4% in *Uchl1*-/- mice (vs. 8.4±2.4% for wild type) (Figure 4f). Finally, the global cortical signal intensity trended higher while the medullary signal intensity decreased more rapidly over time in *Uchl1*-/- mice (Figure 4g-i). These data suggest elevated RBF in *Uchl1*-/- mice, consistent with afferent arteriole dysfunction.

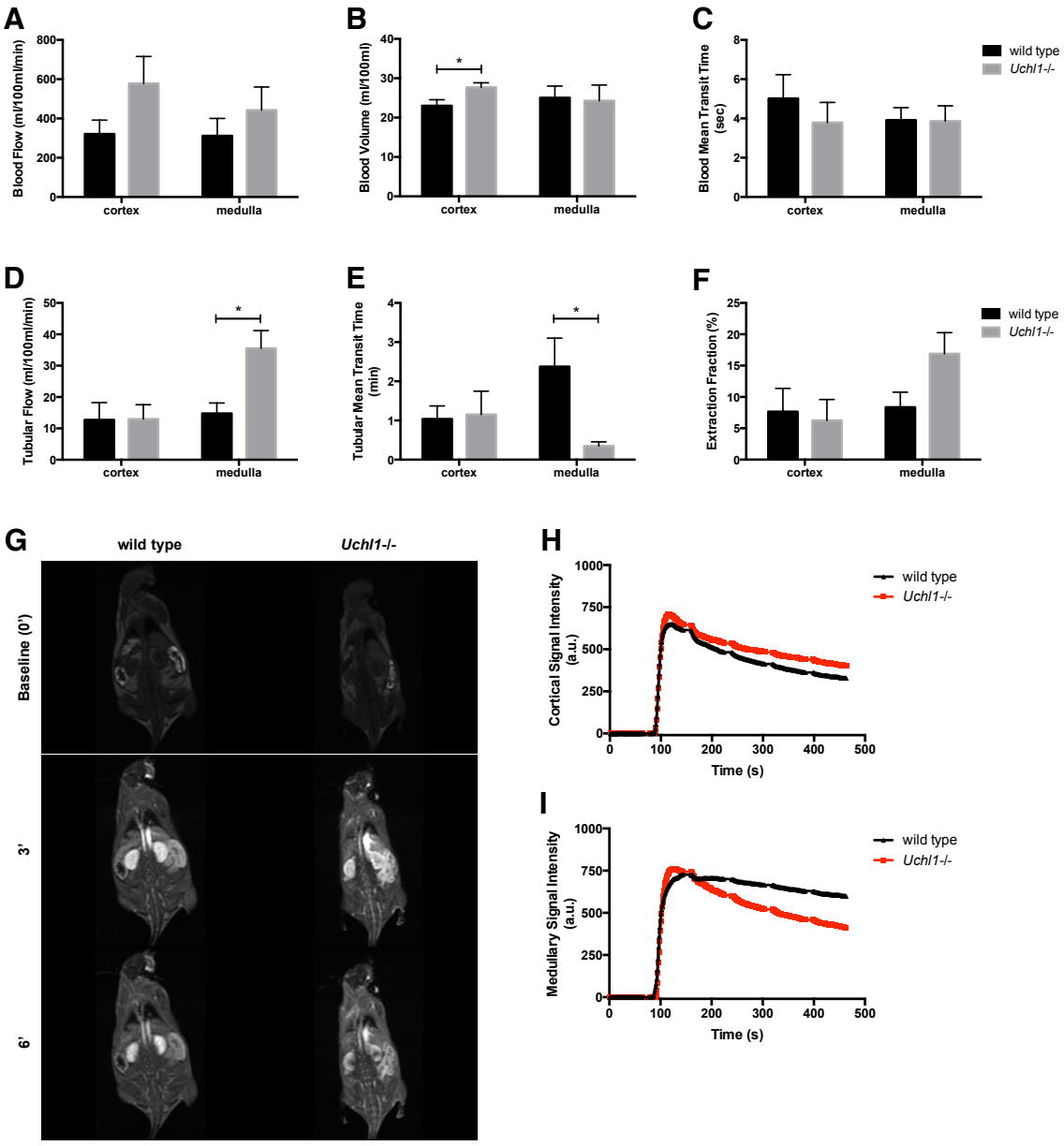

Figure 4. Contrast-enhanced magnetic resonance imaging reveals elevated renal cortical perfusion and increased gadolinium clearance in *Uchl1*-/- mice.
A. Cortical renal blood flow trended higher in *Uchl1*-/- mice. **B.** Blood volume was significantly elevated in the renal cortex of *Uchl1*-/- mice (*p<0.05). **C.** Blood mean transit time trended lower in the renal cortex of *Uchl1*-/- mice. **D.** Tubular flow rate was significantly increased in the medulla of *Uchl1*-/- mice (*p<0.05). **E.** Tubular mean transit time was significantly decreased in *Uchl1*-/- mice (*p<0.05). **F.** The medullary extraction fraction trended higher in *Uchl1*-/- mice. **G.** Representative images at baseline (0'), 3 mins (3') and 6 mins (6') post-gadolinium injection depicting gadolinium signal distribution in wild type and *Uchl1*-/- mice. **H.** Signal intensity curve depicting cortical gadolinium signal intensity trending higher in *Uchl1*-/- mice over time. **I.** Signal intensity curve depicting reduced medullary gadolinium signal intensity over time in *Uchl1*-/- mice. n=5-6 per group.

Impaired Glucose Tolerance and Hyperfiltration in *Uchl1*-/- Mice

Uchl1-deleted mice subjected to a high fat diet display impaired glucose tolerance consequent to impaired insulin release from pancreatic β-cells.[9] Interestingly, studies in the general population show that impaired glucose tolerance is positively correlated to increased GFR.[22] Although resting blood glucose levels were normal, we confirmed that glucose tolerance was slightly impaired in male *Uchl1*-/- mice (Figure 5a) and this was associated with higher HbA1c levels ($p<0.05$; 4.3±0.2% for *Uchl1*-/- vs. 3.7±0.1% for wild type) (Figure 5b). Renal cortical sodium/glucose cotransporter 2 (SGLT2) protein levels were not different between groups (Figure 5c) suggesting intact glucose handling in the proximal tubule. A sub-diabetic dose of insulin was administered to *Uchl1*-/- mice for 14 days to determine if intermittently elevated glucose levels promote hyperfiltration. Insulin treatment significantly improved glucose tolerance ($p<0.001$ at 30mins) compared to vehicle-treated *Uchl1*-/- mice and as determined by computing the area under the curve ($p<0.05$) (Figures 5d-e). However, FITC-inulin clearance was unchanged in insulin-treated *Uchl1*-/- mice (494±28µl/min vs. 419±40µl/min for *Uchl1*-/- + vehicle) (Figure 5f), indicating that impaired glucose tolerance may not account for hyperfiltration.

COX-2 and Hyperfiltration in *Uchl1*-/- Mice

Cyclooxygenase-2 (COX-2) through downstream prostaglandins, notably prostaglandin E2 (PGE2), is a potential means of hyperfiltration as it promotes afferent arteriole dilation.[21] COX-2 mRNA levels were significantly induced by 2.9-fold ($p<0.001$) in renal cortical lysates but trended lower by 2.7-fold in renal medullary lysates from *Uchl1*-/-

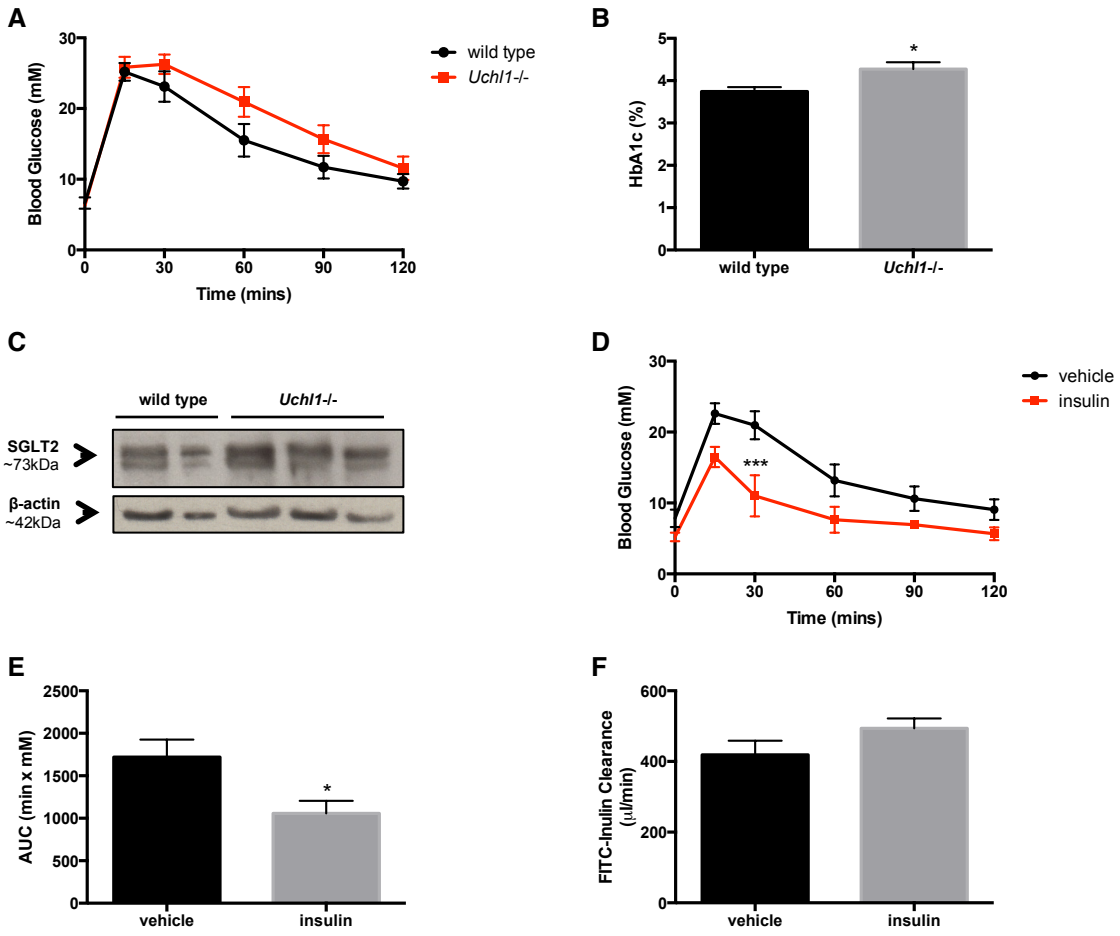

Figure 5. Impaired glucose tolerance is not linked to glomerular hyperfiltration in *Uchl1*-/- mice. A. Glucose tolerance trended higher in male *Uchl1*-/- mice (n=8). **B**. HbA1c levels were significantly elevated in blood samples from male *Uchl1*-/- mice (*p<0.05; n=5-6). **C.** Western blotting revealed no differences in renal cortical SGLT2 protein levels between groups (n=5). **D.** Low dose insulin treatment significantly improved glucose tolerance over time in *Uchl1*-/- mice as compared to vehicle-treated *Uchl1*-/- mice (**p<0.001 vs. wild type at 30 minutes; n=5). **E.** Graph depicting the area under the curve (AUC) from (**D**), which is significantly reduced in insulin-treated *Uchl1*-/- mice (*p<0.05; n=5). **F.** FITC-inulin clearance was unaltered in *Uchl1*-/- mice treated with insulin (n=5).

mice (Figure 6a). While renal cortical COX-2 protein levels were unchanged, COX-2 was significantly reduced by 1.5-fold ($p<0.05$) in the renal medulla of *Uchl1*-/- mice (Figure 6b-c). Since renal cortical COX-2-derived PGE2 contributes to GFR regulation and expression levels do not always correlate to activity, we tested whether COX-2 inhibition with NS-398 over 14 days could lower GFR in *Uchl1*-/- mice (Table 3). FITC-inulin clearance was not different in NS-398-treated *Uchl1*-/- mice (368±45µl/min vs. 380±9µl/min for *Uchl1*-/- + vehicle). Similarly, no differences were observed in NS-398-treated wild type mice (263±35µl/min vs. 252±8µl/min for wild type + vehicle) (Figure 6d). COX-2 was therefore ruled out as a means of hyperfiltration in *Uchl1*-/- mice.

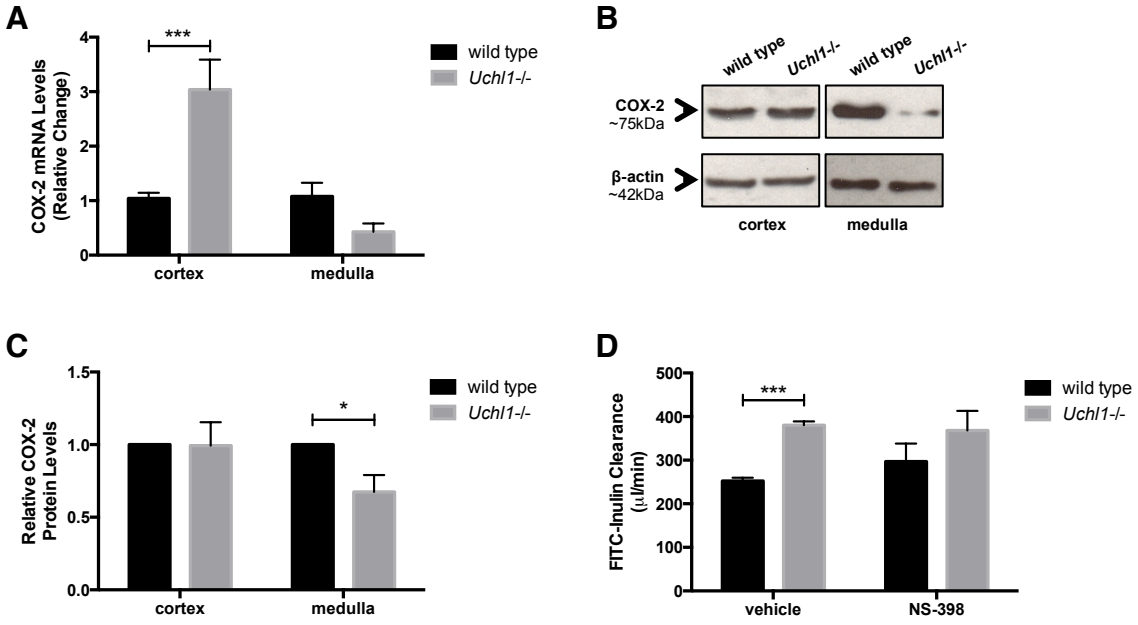

Figure 6. COX-2 does not contribute to glomerular hyperfiltration in *Uchl1*-/- mice. A. COX-2 mRNA levels were significantly increased (***$p<0.001$) in renal cortical lysates from *Uchl1*-/- mice. COX-2 mRNA levels trended lower in the renal medulla of *Uchl1*-/- mice (n=5-9). **B.** Western immunoblotting revealed unchanged COX-2 protein levels in renal cortical lysates from *Uchl1*-/- mice. Medullary COX-2 protein levels were attenuated in *Uchl1*-/- mice (n=8). **C.** Densitometry confirmed unchanged cortical COX-2 and significantly reduced (*$p<0.05$) medullary COX-2 protein levels in *Uchl1*-/- mice (n=8). **D.** FITC-inulin clearance was not different in wild type or in *Uchl1*-/- mice treated with NS-398, compared to their respective controls (n=3-4).

Table 3. Daily and endpoint parameters of NS-398-treated wild type and *Uchl1*-/- mice.

	vehicle		NS-398	
	wild type (n=4)	***Uchl1*-/-** (n=3)	**wild type** (n=4)	***Uchl1*-/-** (n=4)
Water intake (ml)	4.4 ± 0.3	4.5 ± 0.3	4.5 ± 0.2	4.2 ± 0.1
Dosage (mg/kg/day)	6.0 ± 0.6	5.8 ± 0.7	5.5 ± 0.7	5.1 ± 0.3
Delta body weight (g)	0.5 ± 0.4	0.8 ± 0.7	0.7 ± 0.4	0.4 ± 0.3

Data are represented as mean ± SE

Nitric Oxide Synthases and Hyperfiltration in *Uchl1*-/- Mice

As previously mentioned, a hypercellularity was observed in the juxtaglomerular region of *Uchl1*-/- mice. We investigated the contribution of macula densa cells to this effect. Immunohistochemistry confirmed an increase in nitric oxide synthase (nNOS)-positive nuclei (5.5±0.3 vs. 5.1±0.1 for wild type) and area (103±4μm^2 vs. 90±3μm^2 for wild type) in a proportion of *Uchl1*-/- mice (Figures 7a-c). Renal cortical nNOS protein levels were increased by 1.5-fold ($p<0.05$) in *Uchl1*-/- mice (Figure 7d-e), whereas endothelial NOS (eNOS) protein levels were unchanged (Figure 7f). No differences were observed in nNOS, eNOS or inducible NOS (iNOS) mRNA (Figure 7g). Next, to investigate the contribution of nNOS-derived NO to hyperfiltration, *Uchl1*-/- mice were administered L-NAME for 14 days (Table 4). SBP was increased to 131±5mmHg ($p<0.01$) in L-NAME-treated wild type mice (vs. 113±3mmHg for wild type + vehicle), while it trended higher in L-NAME-treated *Uchl1*-/- mice (124±3mmHg vs. 112±2mmHg for *Uchl1*-/- + vehicle) (Figure 7h). Nonetheless, GFR was not different in L-NAME-treated *Uchl1*-/-

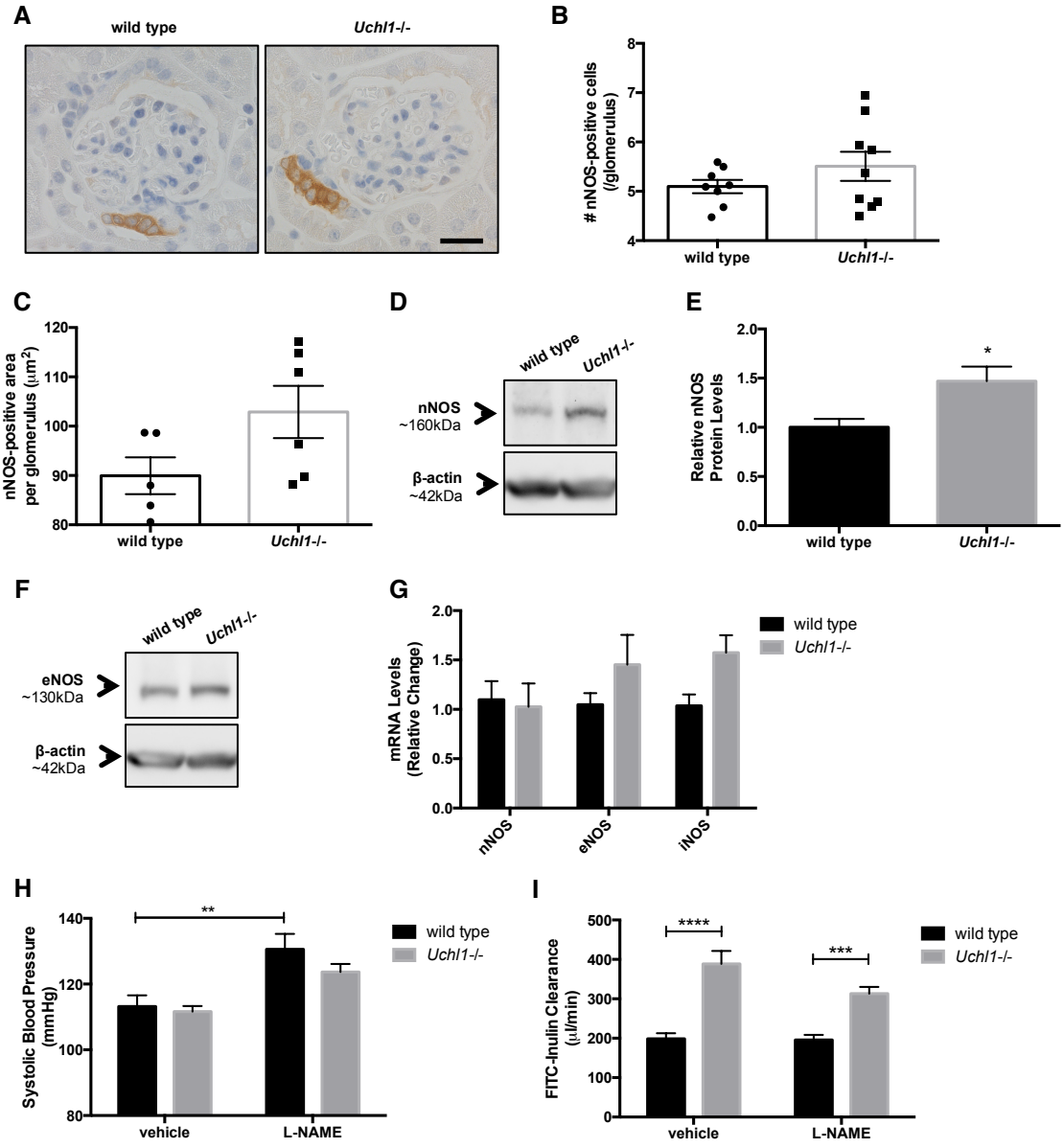

Figure 7. NOS is not a source of glomerular hyperfiltration in *Uchl1*-/- mice. **A.** Immunohistochemistry revealed an increased nNOS-positive area in the macula densa of *Uchl1*-/- mice (n=8-9). Scale bar = 20μm. **B.** Graph depicting increased nNOS-positive nuclei in a proportion of *Uchl1*-/- mice (n=8-9). **C.** Graph depicting increased nNOS-positive area in a proportion of *Uchl1*-/- mice (n=5-6). **D.** Western immunoblotting revealed elevated nNOS protein levels in renal cortical lysates from *Uchl1*-/- mice (n=4-5). **E.** Densitometry graph showing significantly elevated renal cortical nNOS protein levels in *Uchl1*-/- mice (n=4-5; *p<0.05). **F.** Renal cortical eNOS protein levels were not different in *Uchl1*-/- mice (n=5). **G.** qPCR revealed no

differences in renal cortical nNOS, eNOS or iNOS mRNA levels (n=8). **H.** Systolic blood pressure was significantly elevated in L-NAME-treated wild type mice (**p<0.01), while it trended higher in L-NAME-treated *Uchl1*-/- mice, compared to their respective controls (n=4-5). **I.** FITC-inulin clearance was not significantly different in *Uchl1*-/- mice treated with L-NAME (n=3-5).

Table 4. Daily and endpoint parameters of L-NAME-treated wild type and *Uchl1*-/- mice.

	vehicle		**L-NAME**	
	wild type (n=8)	***Uchl1*-/-** (n=7)	**wild type** (n=8)	***Uchl1*-/-** (n=9)
Water intake (ml)	4.5 ± 0.2	3.6 ± 0.1**	4.4 ± 0.2	3.8 ± 0.1
Dosage (mg/kg/day)	111.4 ± 6.4	84.3 ± 4.2**	99.1 ± 4.1	87.1 ± 4.6
Delta body weight (g)	-0.9 ± 0.4	0.1 ± 0.7	-0.4 ± 0.4	0.1 ± 0.8

Data are represented as mean ± SE, **p<0.01 vs. wild type + vehicle (using a 2-way ANOVA)

mice (313±17µl/min vs. 388±29µl/min for *Uchl1*-/- + vehicle) or L-NAME-treated wild type mice (196±13µl/min vs. 198±14µl/min for wild type + vehicle). As such, NOS' were eliminated as a source of hyperfiltration in *Uchl1*-/- mice (Figure 7i).

Neuronal Defects in *Uchl1*-Deleted Mice Kidneys

Neural structural differences were determined in *Uchl1*-/- mice. Renal nerve arborization, depicted by the neuronal marker neurofilament-L, was evident in *Uchl1*-/- mice (Figure 8a-d, Supplemental Figure 1). Analysis of axonal radii revealed a significantly increased

proportion of axons <1μm in *Uchl1*-/- mice ($p<0.0001$; 45.2±2.4% vs. 28.1±2.1% for wild type), combined with a decreased proportion of axons between 1-2μm ($p<0.0001$; 50.1±2.7% vs. 64.2±2.2% for wild type) and a decreased proportion of axons >2μm (4.7±0.8% vs. 7.7±1.1% for wild type) (Figure 8e). Finally, urinary norepinephrine (NE) was significantly reduced ($p<0.05$) to 0.14±0.01ng•kgH_2O/mosm•ml in *Uchl1*-/- mice (vs. 0.28±0.08ng•kgH_2O/mosm•ml for wild type), urinary epinephrine trended lower in *Uchl1*-/- mice (0.04±0.01ng•kgH_2O/mosm•ml vs. 0.09±0.03ng•kgH_2O/mosm•ml for wild type) while urinary dopamine was unchanged (0.28±0.03ng•kgH_2O/mosm•ml for *Uchl1*-/- vs. 0.29±0.04ng•kgH_2O/mosm•ml for wild type) (Figure 8f). Altogether, these findings provide evidence of renal neuronal dysfunction in *Uchl1*-/- mice.

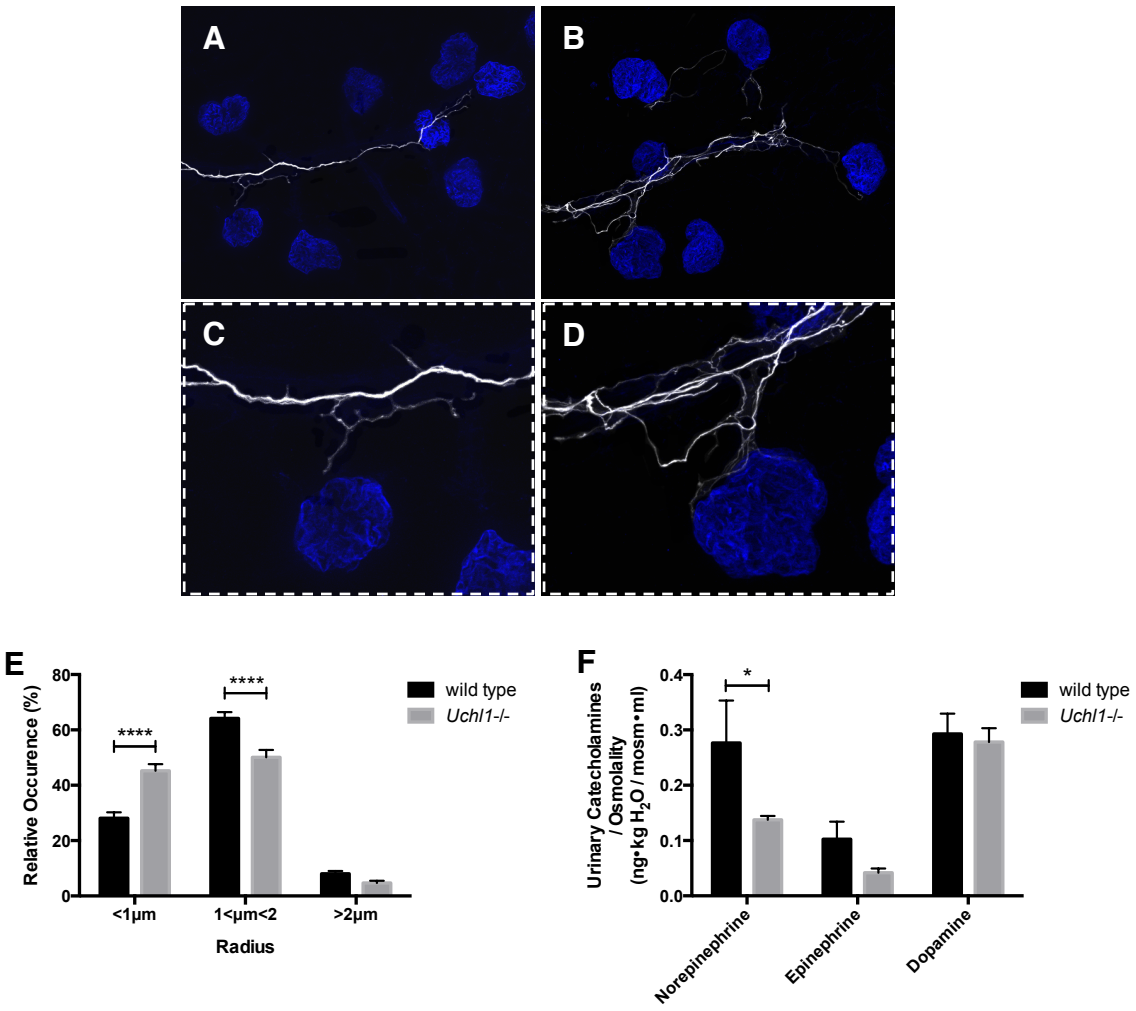

Figure 8. Evidence of renal neuronal dysfunction in *Uchl1*-/- mice.
A-D. Immunofluorescence showing neurofilament-L-positive renal nerves emanating to glomerular bundles in wild type (**A**) and *Uchl1*-/- mice (**B**) (n=10). Axonal arborization was evident in *Uchl1*-/- mice (n=10). Magnification, 200X. **C.** Inset from (**A**) and **D.** inset from (**B**) showing increased arborization of axons emanating to the glomerulus of *Uchl1*-/- mice, as compared to wild type mice (n=10). Magnification, 200X. Neurofilament-L: white and synaptopodin: blue. **E.** Quantification of renal axonal radii revealed an increased proportion of axons <1µm (****$p<0.0001$), a decreased proportion of axons between 1-2µm (****$p<0.0001$) and a slightly decreased proportion of axons >2µm in *Uchl1*-/- mice (n=10). **F.** Urinary catecholamines, specifically norepinephrine, were significantly reduced in *Uchl1*-/- mice (*$p<0.05$). Urinary epinephrine trended lower in *Uchl1*-/- mice, while urinary dopamine was unchanged between groups (n=6-8). Urine catecholamines were normalized to urine osmolality.

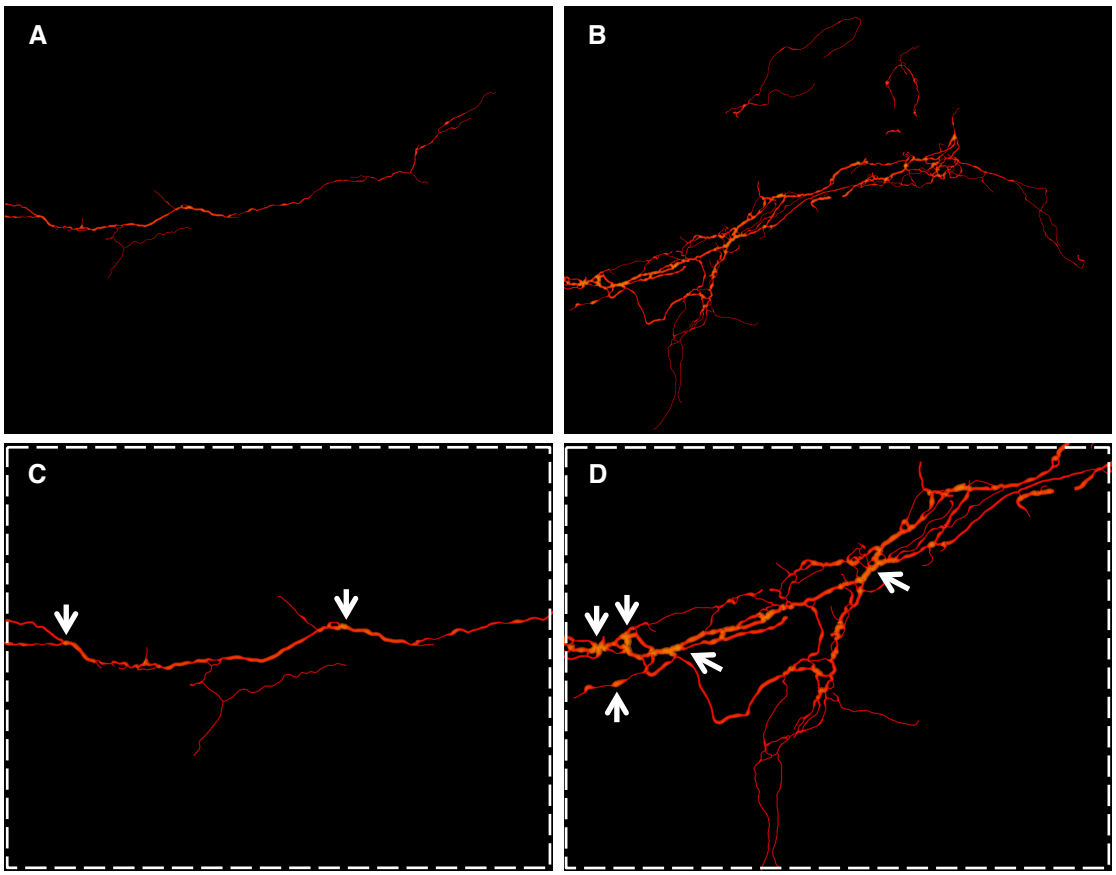

Supplemental Figure 1. Renal neural alterations in *Uchl1*-/- mice.
A-D. Reconstructed immunofluorescence images showing neurofilament-L-positive renal nerves in wild type (**A**) and *Uchl1*-/- mice (**B**) (n=10). Magnification, 200X. **C.** Inset from (**A**) and **D.** inset from (**B**) depicting increased axonal arborization in *Uchl1*-/- mice, as compared to wild type mice (n=10). Dark red depicts the regions where the axonal diameter measures from 1μm while yellow depicts the regions where the axonal diameter corresponds to 4μm (arrows). Magnification, 200X.

Discussion

Our findings show abundant UCHL1 expression in renal axons emanating to the glomeruli. 12-week-old *Uchl1*-/- mice exhibited glomerular hyperfiltration, coinciding with the onset of neurodegeneration. Despite renin and ACE1 induction, the RAS was eliminated as a source of hyperfiltration. By DCE-MRI, we determined increased cortical RBF in *Uchl1*-/- mice, suggesting that hyperfiltration stems from decreased resistance at the afferent arteriole. Nevertheless, hyperglycemia, COX-2 and NOS were eliminated as contributing sources of hyperfiltration. Finally, *Uchl1*-/- mice displayed increased renal axonal arborization, reduced urinary NE and delayed vascular reactivity to adrenergic stimulation. Our data therefore links renal nerve dysfunction to hemodynamic alterations in a mouse model of axonal degeneration where UCHL1 is absent.

Here we identified *Uchl1*-/- mice as a novel model showing an absolute increase in GFR, likely stemming from reduced renal vascular resistance consequent to progressive loss of neuronal function. Prolonged hyperfiltration may be a precursor to chronic kidney disease, as persistently elevated intraglomerular pressures correlate with glomerular hypertrophy and damage.[19] When *Uchl1*-/- mice were followed to 20 weeks of age, GFR was comparable to that of 12-week-old mice (Supplemental Figure 2a). Additionally, while albumin/creatinine ratios were unchanged in *Uchl1*-/- mice, focal areas of tubular injury and glomerular scarring were present in a proportion of mice suggesting that prolonged hyperfiltration may eventually promote glomerular damage in this model

(Supplemental Figure 2b-c). *Uchl1*-/- mice do not generally survive beyond 25 weeks of age limiting histopathological analyses at later time points.

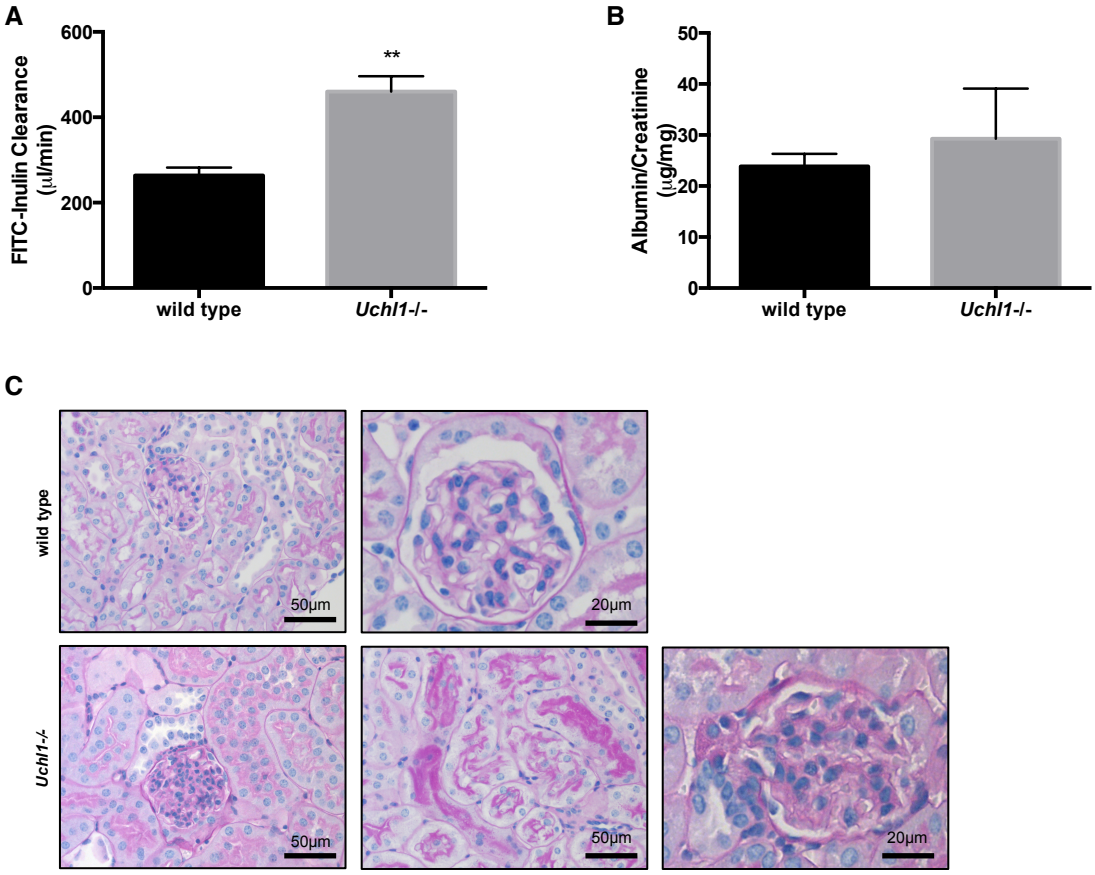

Supplemental Figure 2. A proportion of *Uchl1*-/- mice demonstrate mild renal pathology at 20 weeks of age. A. Glomerular filtration rate estimated by FITC-inulin clearance was elevated in *Uchl1*-/- mice (**p<0.01). **B.** Albumin/creatinine ratios were unchanged in *Uchl1*-/- mice. **C.** PAS-stained renal sections depicting focal areas of tubular injury and glomerulosclerosis from a subset of *Uchl1*-/- mice. n=5-6.

Mesenteric vessels from *Uchl1*-/- mice displayed reduced vascular reactivity, which may result from vessel desensitization to adrenergic stimulation following progressive loss of neuronal function. It seemed therefore likely that the RAS would be induced in this setting to counterbalance the loss of vascular resistance but this was not the case. Alternatively, we hypothesized that renin secretion may be blunted in *Uchl1*-/- mice

based on the following findings. First, neural stimulation promotes renin secretion and loss of *Uchl1* may impair this process.[13] Second, studies of pancreatic β-cells suggest that VAMP2 is ubiquitinated and degraded in *Uchl1*-deficient mice subjected to a high fat diet. Since VAMP2 is also required for renin exocytosis from juxtaglomerular cells, renin secretion may be impaired in *Uchl1*-/- mice.[14,24] The low salt diet study however refuted this hypothesis. We cannot rule out the possibility that renin secretion may become compromised should *Uchl1*-/- mice be exposed to conditions that yield high proteasomal activity (promoting VAMP2 degradation) in juxtaglomerular cells.

Presently we showed modest glucose tolerance impairment in male *Uchl1*-/- mice similar to the findings by Chu *et al*.[14] HbA1c levels were higher in *Uchl1*-/- mice and while these are not hyperglycemic, chronic elevations in post-prandial glucose levels could have a negative impact on glomerular hemodynamics.[22] The hemodynamic hypothesis stipulates that hyperglycemia increases the bioavailability of factors promoting either afferent arteriole dilation (i.e. COX-2, NO) or efferent arteriole constriction (i.e. Ang II, endothelin 1) but restoration of glucose homeostasis through insulin treatment did not impact GFR in *Uchl1*-/- mice. An important consideration in these experiments lies in that insulin has vasodilatory properties, which may have offset the effect of normalizing plasma glucose on GFR.[23,24]

The hyperplastic macula densa observed in a proportion of *Uchl1*-/- mice may reflect a developmental defect. Although the role of UCHL1 in mouse renal development is unknown, there is evidence that UCHL1 is expressed in the developing rat kidney (where

its expression is later restricted to parietal epithelial cells in adult rats).[18] Interestingly, in healthy human renal biopsies, UCHL1 expression is detectable in the macula densa; however, this was not observed in our wild type mice and may therefore represent a species difference.[26,32] Nevertheless, renal cortical nNOS induction in *Uchl1*-/- mice may be a consequence of this hyperplastic region.

Macula densa nNOS induction normally occurs under conditions of low salt delivery. nNOS-derived NO counterbalances tubuloglomerular feedback by dilating the afferent arteriole and restoring GFR. However, NKCC2 levels were elevated in *Uchl1*-/- mice suggesting active chloride reabsorption. On the other hand, since VAMP2 is also required for NKCC2 trafficking to the plasma membrane, plasma membrane NKCC2 expression may be limited.[25] Conditions of sodium restriction are also associated with renal cortical COX-2 induction. Furthermore, considering that At2R mRNA levels were elevated in *Uchl1*-/- mice (suggesting At2R-predominant signaling), this hypothesis seemed likely. However, renal cortical COX-2 protein levels were unchanged and COX-2 inhibition had no impact on GFR in *Uchl1*-/- mice. In contrast, conditions of sodium restriction are also associated with reduced medullary COX-2 that in turn inhibits natriuresis. As such, in these mice, sodium reabsorption may be compensated downstream of the macula densa by the epithelial sodium channel (ENaC). To this end no changes were found in plasma sodium or fractional excretion of sodium in *Uchl1*-/- mice (Supplemental Figure 3a-c). The hypothesis of dampened plasma membrane NKCC2 activity is supported by macula densa nNOS induction, however the lack of COX-2 induction in the renal cortical compartment suggests otherwise. Moreover, no changes were observed in SGLT2 mRNA

and protein levels, or in sodium/chloride cotransporter (NCC) and ENaC mRNA levels downstream of NKCC2 (though NKCC2 mRNA levels were elevated ($p<0.05$) in *Uchl1*-/- mice) (Supplemental Figure 3d). As such, NKCC2 activity may be elevated in our model. NKCC2 induction may reflect a response to the elevations in tubular flow rate in *Uchl1*-/- mice or a product of macula densa cell hyperplasia. Finally, nNOS induction may result from decreased neurotransmission at the juxtaglomerular apparatus as nNOS promotes NE release at this neuroeffector junction in rats.[26]

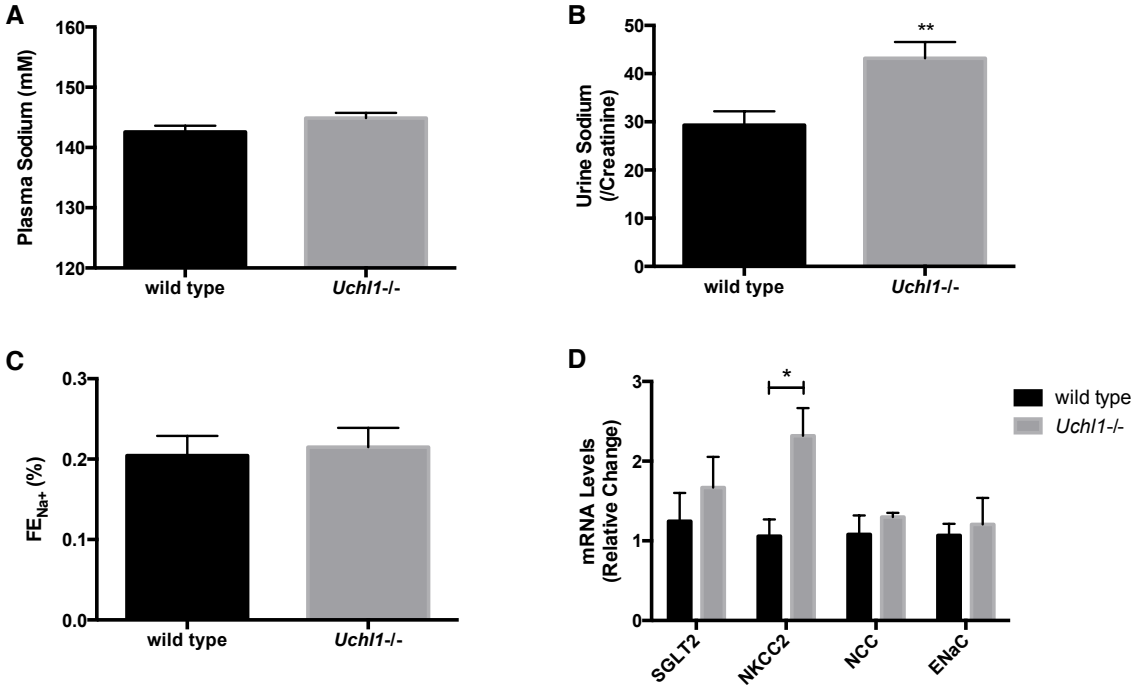

Supplemental Figure 3. Fractional excretion of sodium is unchanged in *Uchl1*-/- mice. A. Plasma sodium was not significantly different between groups (n=14-19). **B.** Urinary sodium/creatinine ratios were significantly increased in *Uchl1*-/- mice (**$p<0.01$; n=10-16). **C.** Fractional excretion of sodium was unchanged in *Uchl1*-/- mice (n=11-14). **D.** qPCR results revealed significantly elevated NKCC2 mRNA levels (*$p<0.05$) in renal cortical lysates from *Uchl1*-/- mice. SGLT2, NCC and ENaC mRNA levels were unchanged between groups (n=4-8).

It remains to be determined if *Uchl1*-/- mice depict a phenotype similar to models of direct renal denervation. Nevertheless, we cannot exclude the possibility that loss of renal sympathetic tone (associated with progressive neurodegeneration) in *Uchl1*-/- mice promotes increased RBF and GFR. UCHL1 is abundantly expressed in axons throughout the kidney and given that loss of *Uchl1* is associated with impaired signaling at various neuroeffector junctions (i.e. the neuromuscular junction), there is a strong likelihood that the kidney is not excluded from these effects. UCHL1 promotes axonal transport and loss of *Uchl1* led to increased renal nerve arborization, which may reflect early compensation to decreased neurotransmission at presynaptic termini. Moreover, urinary NE was reduced, similar to findings in models of renal denervation. Reduced renal sympathetic tone may therefore account for hemodynamic changes in *Uchl1*-/- mice.

Renal nerve dysregulation and hyperfiltration in *Uchl1*-/- mice may provide insight to the mechanism by which albuminuria and glomerular injury were ameliorated in K256E-*ACTN4*$^{pod+}$ mice lacking *Uchl1*. For instance, when denervated mice were subjected to lipopolysaccharides (LPS)-induced injury, GFR was preserved.[27] Similarly, *Uchl1* deletion in K256E-*ACTN4*$^{pod+}$ mice may preserve GFR, sparing the mice from further glomerular injury. Furthermore, albuminuria was comparably elevated in *Uchl1*-deleted K256E-*ACTN4*$^{pod+}$ mice to K256E-*ACTN4*$^{pod+}$ mice at 4 weeks of age but was significantly reduced by 10 weeks of age, coinciding with the onset of hyperfiltration and neurodegeneration in *Uchl1*-/- mice.[28]

While the specific mechanism underlying glomerular hyperfiltration in *Uchl1*-/- mice remains uncertain, we provide compelling evidence that this phenotype is associated with renal nerve dysfunction. This research yields insight as to a potential mechanism by which global *Uchl1* deletion and potentially global UCHL1 inhibition ameliorates glomerular disease. Studies employing *Uchl1* deletion or inhibition in glomerular disease models or other models will need to be informed by our findings that loss of *Uchl1* alters renal vascular resistance and GFR.

Concise Methods

Mice

Mice were housed at the Animal Care and Veterinary Services facility at the University of Ottawa. *Uchl1*-/- mice and wild type littermates were generated by intercrossing *Uchl1*+/- mice.[10,28] Mice were maintained on a mixed background (sv/129/FVB/N). At endpoint, mice were anesthetised with isofluorane and exsanguinated by cardiac puncture to collect blood and/or through perfusion with 20ml PBS through the left ventricle. All protocols and procedures were approved and carried out according to the Canadian Council on Animal Care guidelines.

SBP and FITC-Inulin Clearance

SBP was determined by tail cuff plethysmography (BP-2000 Visitech Systems, Apex, NC). Mice were trained 1 week prior to experimental measurements for a minimum of 3-4 days. Weekly values were estimated by averaging data over 3-5 days. GFR was estimated by measuring FITC-inulin clearance as previously described.[29]

Glucose Tolerance Test

The glucose tolerance test was performed in 8-12 week old male mice. Following a 16-hour fast, mice were injected with a 2g/kg b.w. D-Glucose/saline solution (i.p.). Blood glucose was determined by saphenous vein bleed at 15, 30, 60, 90 and 120 minutes.

Lisinopril, NS-398 and L-NAME Drinking Water Studies

Lisinopril (66mg/L; Cayman Chemical, Ann Arbour, MI), NS-398 (0.03mg/ml; Cayman Chemical, Ann Arbour, MI), or *N*ω-Nitro-L-arginine methyl ester (L-NAME; 0.5mg/ml; Sigma Aldrich, St. Louis, MO), was administered in the drinking water of 9-11-week-old mice for 14 days. Doses were chosen based on previous research.[30-32] Reported SBP values were determined in the second week of treatment. GFR was determined 12-14 days following the initial dosage.

Low Salt Diet Study

Mice were administered a sodium-deficient diet (0.01-0.02%; Envigo, Indianapolis, IN) *ad libitum* for 7 days. Plasma renin concentration was determined with the Mouse Ren1/Renin-1 ELISA kit (Sigma-Aldrich, Oakville, ON).

Insulin Mini Pumps Study

A sub-diabetic dose of Humulin R (Eli Lilly, Indianapolis, IN) was administered to 9-11-week-old male *Uchl1*-/- mice in Alzet mini osmotic pumps model 1002 (Durect, Cupertino, CA). Pumps were prefilled with Humulin R to 8.33U/ml or normal saline to achieve a daily dosage of 0.05U. The sub-diabetic dose of Humulin R was estimated based on previous work by reducing the optimal diabetic dose by five-fold.[33] A glucose tolerance test and FITC-inulin clearance were performed 7-8 days and 12-14 days post-implantation, respectively.

Albumin/Creatinine Ratios and Urinary Catecholamines

Spot urine was obtained from 12-week-old mice. Urine albumin was determined with the Mouse Albumin ELISA Kit (Bethyl Laboratories, Montgomery, TX) and urine creatinine was measured with the mouse Creatinine Companion kit (Exocell, Philadelphia, PA). Urinary catecholamines were determined with the 3 Catecholamines ELISA kit (ImmuSmol, Pessac, France) and the values were normalized to urine osmolality determined with a Micro-Osmometer Model 3MO Plus (Advanced Instruments Inc, Norwood, MA).

Histology and Glomerular Analysis

The glomerular tuft and Bowman's capsule areas were calculated with Alpha Innotech software (Alpha Innotech; San Leandro, CA) using PAS-stained sections. Glomerular numbers were determined by counting total cortical glomeruli per cortical area, using serial sections from both kidneys (60-63μm between levels). A total of 9 sections per kidney per mouse were analyzed. Sections were visualized with a ZEISS Axio Imager A1 (ZEISS, North York, ON) and cortical area was computed with Olympus cellSens software (Olympus; Richmond Hill, ON).

Dynamic Contrast-Enhanced Magnetic Resonance Imaging

Dynamic contrast-enhanced magnetic resonance imaging (DCE-MRI) was performed using a 7T MR901 system (Agilent Technologies, CA/GE Healthcare, WI) and analyzed as outlined in the Supplemental Methods section.[34,35] Representative images depict averaged signal intensities (±50 frames) at 0, 3 and 6 minutes.

Vessel Myography

Vascular reactivity was assessed as previously described.[36] Detailed information is available in the Supplemental Methods section.

RNA Extraction and Quantitative PCR

RNA isolation and quantitative PCR of renal cortex or medulla was performed as previously described by our laboratory.[28] Primer sequences are listed in Supplemental Table 1. All primers were obtained from Invitrogen (Burlington, ON).

Protein Extraction and Western Immunoblotting

Renal cortex or medulla protein lysates were prepared as previously described by our laboratory.[28] Antibodies used for immunoblotting are described in Supplemental Table 2.

Immunohistochemistry

Paraffin-embedded renal sections were boiled in 0.01M sodium citrate, pH 6.0 and incubated with rabbit anti-nNOS 1:200 (Cell Signaling, Beverly, MA) and goat anti-renin 1:500 (Santa Cruz Biotechnology, Santa Cruz, CA) o/n at 4°C. Sections were processed with the appropriate ImmPRESS Reagent (Vector Laboratories, Burlingame, CA) and visualized with a Zeiss Axio Imager A1 microscope (ZEISS, North York, ON). The nNOS-positive area and nuclei were determined using Olympus cellSens software (Olympus; Richmond Hill, ON).

Immunofluorescence

Paraformaldehyde-fixed kidneys were embedded in 2% agarose/PBS and cut into 60µm-thick sections with a Leica VT1000S vibratome (Leica Biosystems, Concord, ON). Sections were blocked in 10% donkey serum/0.5% cold-water fish gelatin/PBT for 2 hours and incubated with primary antibodies o/n and secondary antibodies for 3 hours (antibodies are listed in Supplemental Table 3). Sections were mounted onto slides and visualized with a Zeiss Axio Imager M2 with ApoTome.2 (ZEISS, North York, ON). Images were processed as described in the Supplemental Methods section.[37,38]

Author Contributions

N.C.B led and performed the bulk of the experiments presented in this research. C.E.H provided assistance with the mice work/surgeries. J.F.T. performed the myography experiments and assisted with ELISA experiments. R.N., supervised by R.L.H., assisted with Western blotting. E.K. assisted with ELISA experiments. A.G. performed the immunohistochemistry experiments. C.H.C. and L.d.F.C. analyzed the radius of renal nerves and refined the immunofluorescence images. G.O.C. performed the DCE-MRI experiments while A.C. led the surgeries for this procedure. B.L. provided significant guidance to renal nerve immunofluorescence and finalized the representative images. The current work is supervised and led by C.R.K. and D.A.G.

Acknowledgements

We are grateful to Julie Zhu for her support with the mice colonies. We also thank Eileen Franklin, Kim Yates and Melissa Washington for their assistance with some of the mice procedures.

This work is supported by the Kidney Foundation of Canada.

N.C.B. is a recipient of the Queen Elizabeth II Graduate Scholarship in Science and Technology (QEII-GSST).

Statement of Competing Financial Interests

Disclosures: None

Supplemental Information

Supplemental Methods

Vessel Myography

Second-order branches of mouse mesenteric artery were isolated and cleaned of adhering fat and connective tissue. Vessel segments (1.5–2mm) were mounted on a wire myography system (DMT Instruments, Crystal River, FL) and equilibrated in a physiological saline solution (in mM; 130 NaCl, 14.9 $NaHCO_3$, 4.7 KCl, 1.18 KH_2PO_4, 1.17 $MgSO_4$, 1.6 $CaCl_2$, 0.026 EDTA, and 5.5 glucose, pH 7.4, 37°C) which was bubbled continuously with 95% O_2 and 5% CO_2. Vessels were stimulated with increasing doses of phenylephrine (Phe; 1nM-10μM; Sigma-Aldrich, Oakville, ON).

Dynamic Contrast Enhanced Magnetic Resonance Imaging

Mice were anesthetized with isoflurane and a cannula was inserted into the jugular vein. A 72 mm inner diameter volume resonator coil (RAPID MR International) was used in transmit/receive mode. Dynamic contrast-enhanced magnetic resonance imaging (DCE-MRI) was performed using a Time Resolved Imaging of Contrast KineticS (TRICKS) gradient echo sequence, with the following parameters: TE=1.1 ms, TR=3.5 ms, flip=30 deg, BW=83 kHz, FOV=9 cm, slice thickness=1.6 mm, # of transverse slices = 16 (online interpolation to 32 slices at 0.8mm thick), matrix=128x128, phase FOV=0.5, frequency direction=S/I, temporal resolution=1.2s. The TRICKS sequence was run for 8 minutes, with manual *i.v.* injection of 0.1mmol/kg Gadovist contrast agent (Bayer, Mississauga,

ON) after 1 minute of scanning. The Gadovist was diluted in saline for a final volume of 100μL. Time intensity curves S(t) from the DCE dataset were converted to relative enhancement curves, (S(t) – S0)/S0, where S0 was the intensity at pre-injection baseline. Regions of interest were drawn on whole-kidney, medulla, and cortex. The average enhancement curves for these regions were analyzed with a two-compartment filtration model (A,B). For this analysis, the arterial input function was taken from a region of interest in the left ventricle of the heart.[34,35]

Renal Nerve Immunofluorescence Images

Images were processed by first smoothing the 3D images using a Gaussian kernel.[37] The images were then projected into 2D using a maximum intensity Z (depth) projection. Next, an adaptive thresholding procedure was used to binarize the images. Specifically, the value of each pixel was compared to the average intensity of a window centered on the pixel, being classified as either corresponding to a nerve fiber or the image background. Regions of interest were manually marked and extracted in order to reduce the effect of artifacts such as those caused by tissue auto-fluorescence. Small connected components were then discarded. The medial axes of the remaining components were extracted by using a thinning procedure.[38] The arc-length of each medial axis, corresponding to the length of nerve fibers, was then obtained. In addition, the number of branching points, defined as pixels belonging to a medial axis and having three or more medial axis neighbors, was also calculated. The radii of the nerve structures were obtained by first defining a perpendicular line to each medial axis pixel and then counting, along the perpendicular, the number of pixels classified as nerve.

Plasma and Urinary Sodium

Sodium-heparin derived plasma and spot urine samples were analyzed by IDEXX (IDEXX Labs, Toronto, ON). The fractional excretion percentage was determined using the following formula: ((Urinary sodium x Plasma creatinine) / (Plasma sodium x Urinary creatinine)) x 100.

Supplemental Table 1. Primer Sequences.

Gene Product	Forward Primer (5'->3')	Reverse Primer (5'->3')
ACE1	CAG AAT CTA CTC CAC TGG CAA GGT	TCG TGA GGA AGC CAG GAT GT
ACE2	TGC CCA TTT GCT TGG TGA T	AAA GGG AAC AGT CAA AGG GTA CAG
Angiotensinogen	CTG CTC CAG GCT TTC GTC TAA	AGA ACT GGG TCA GTG GAT AAA TCC
AT1R	GGG CAG TTT ATA CCG CTA TGG A	TGG CCG AAG CGA TCT TAC AT
AT2R	ATT ACC TGC ATG AGT GTC GAT AGG	AGA TGC TTG CCA GGG ATT CC
ENaC	AGA AGA GGA CCC AGG AGG AG	CCT CCC GGA CTG TTT GAC TC
MasR	TGT GGG CAC TTT CGT GCT T	AAT GAC TCT CTT CTC CGC TGT CA
NCC	CTC AAG CAG GAA GGT AGC CA	ATG AGC CAA GTC AGC ACG AT
NKCC2	GCT CTT CAT TCG CCT CTC CT	AGC CTA TTG ACC CAC CGA AC
eNOS	TGG CAT GGG CAA CTT GAA GA	CTG GGA GCC ACT CCT TTT GA
iNOS	AAG ACT GAG ACT CTG GCC CC	CGT GAG GAG CCT CAG AAG TG
nNOS	TTC TCA GCC AAG CTG ATG GG	ACC TTG TAG CTC TTC CTC TCC T
Renin	ATG AAG GGG GTG TCT GTG GGG TC	ATG TCG GGG AGG GTG GGC ACC TG
SGLT2	GCT GGA TTT GAG TGG AAT GC	CGG TCA GAT ACA CTG GCA CA

Supplemental Table 2. Western immunoblotting antibody information.

Antibody	Dilution	Blocking Solution	Manufacturer
mouse anti-renin (B-12)	1:500	5% milk/PBS-T	Santa Cruz Biotechnology, Santa Cruz, CA
goat anti-ACE1	1:500	5% milk/PBS-T	R&D Systems, Minneapolis, MN
rabbit anti-COX-2	1:500	10% milk/PBS-T	Novus Biologicals, Oakville, ON
rabbit anti-NKCC2	1:1000	5% milk/PBS-T	Abcam, Toronto, ON
rabbit anti-nNOS	1:1000	5% milk/PBS-T	Cell Signaling, Beverly, MA
rabbit anti-eNOS	1:1000	5% milk/PBS-T	Thermo Fisher Scientific, Mississauga, ON
mouse anti-β-actin	1:10,000	5% milk/PBS-T	Sigma-Aldrich, Oakville, ON
HRP-goat anti-rabbit	1:10,000	5% milk/PBS-T	Jackson ImmunoResearch, West Grove, PA
HRP-goat anti-mouse	1:10,000	5% milk/PBS-T	Jackson ImmunoResearch, West Grove, PA
HRP-mouse anti-goat	1:10,000	5% milk/PBS-T	Jackson ImmunoResearch, West Grove, PA

Supplemental Table 3. Immunofluorescence antibody information.

Antibody*	Dilution	Manufacturer
rat anti-CD31	1:200	BD Pharmingen, Mississauga, ON
rabbit anti-UCHL1	1:1000	Thermo Fisher Scientific, Mississauga, ON
rabbit anti-neurofilament-L	1:100	Thermo Fisher Scientific, Mississauga, ON
goat anti-synaptopodin	1:300	Santa Cruz Biotechnology, Santa Cruz, CA
donkey anti-rat Alexa Fluor 488	1:300	Invitrogen, Burlington, ON
donkey anti-rabbit Alexa Fluor 568	1:300	Invitrogen, Burlington, ON
donkey anti-goat Alexa Fluor 647	1:300	Invitrogen, Burlington, ON

*All antibodies were diluted in 10% donkey serum/0.5% cold-water fish gelatin/PBT

References

1. Bishop P, Rocca D, Henley JM: Ubiquitin C-terminal hydrolase L1 (UCH-L1): structure, distribution and roles in brain function and dysfunction. *Biochem J* 473: 2453-2462, 2016
2. Osaka H, Wang YL, Takada K, Takizawa S, Setsuie R, Li H, Sato Y, Nishikawa K, Sun YJ, Sakurai M, Harada T, Hara Y, Kimura I, Chiba S, Namikawa K, Kiyama H, Noda M, Aoki S, Wada K: Ubiquitin carboxy-terminal hydrolase L1 binds to and stabilizes monoubiquitin in neuron. *Hum Mol Genet* 12: 1945-1958, 2003
3. Saigoh K, Wang YL, Suh JG, Yamanishi T, Sakai Y, Kiyosawa H, Harada T, Ichihara N, Wakana S, Kikuchi T, Wada K: Intragenic deletion in the gene encoding ubiquitin carboxy-terminal hydrolase in gad mice. *Nat Genet* 23: 47-51, 1999
4. Chen F, Sugiura Y, Myers KG, Liu Y, Lin W: Ubiquitin carboxyl-terminal hydrolase L1 is required for maintaining the structure and function of the neuromuscular junction. *Proc Natl Acad Sci U S A* 107: 1636-1641, 2010
5. Ardley HC, Scott GB, Rose SA, Tan NG, Robinson PA: UCH-L1 aggresome formation in response to proteasome impairment indicates a role in inclusion formation in Parkinson's disease. *J Neurochem* 90: 379-391, 2004
6. Oda K, Yamazaki K, Miura H, Shibasaki H, Kikuchi T: Dying back type axonal degeneration of sensory nerve terminals in muscle spindles of the gracile axonal dystrophy (GAD) mutant mouse. *Neuropathol Appl Neurobiol* 18: 265-281, 1992
7. Nagamine S, Kabuta T, Furuta A, Yamamoto K, Takahashi A, Wada K: Deficiency of ubiquitin carboxy-terminal hydrolase-L1 (UCH-L1) leads to vulnerability to lipid peroxidation. *Neurochem Int* 57: 102-110, 2010
8. Ciriello J, de Oliveira CV: Renal afferents and hypertension. *Curr Hypertens Rep* 4: 136-142, 2002
9. Chu KY, Li H, Wada K, Johnson JD: Ubiquitin C-terminal hydrolase L1 is required for pancreatic beta cell survival and function in lipotoxic conditions. *Diabetologia* 55: 128-140, 2012
10. Coulombe J, Gamage P, Gray MT, Zhang M, Tang MY, Woulfe J, Saffrey MJ, Gray DA: Loss of UCHL1 promotes age-related degenerative changes in the enteric nervous system. *Front Aging Neurosci* 6: 129, 2014
11. Franco-Cereceda A, Henke H, Lundberg JM, Petermann JB, Hokfelt T, Fischer JA: Calcitonin gene-related peptide (CGRP) in capsaicin-sensitive substance P-immunoreactive sensory neurons in animals and man: distribution and release by capsaicin. *Peptides* 8: 399-410, 1987
12. Barajas L, Liu L, Powers K: Anatomy of the renal innervation: intrarenal aspects and ganglia of origin. *Can J Physiol Pharmacol* 70: 735-749, 1992
13. Johns EJ, Kopp UC, DiBona GF: Neural control of renal function. *Compr Physiol* 1: 731-767, 2011
14. Johns EJ, Lewis BA, Singer B: The sodium-retaining effect of renal nerve activity in the cat: role of angiotensin formation. *Clin Sci Mol Med* 51: 93-102, 1976

15. Handa RK, Johns EJ: Interaction of the renin-angiotensin system and the renal nerves in the regulation of rat kidney function. *J Physiol* 369: 311-321, 1985
16. Kompanowska-Jezierska E, Walkowska A, Johns EJ, Sadowski J: Early effects of renal denervation in the anaesthetised rat: natriuresis and increased cortical blood flow. *J Physiol* 531: 527-534, 2001
17. Bradbury JM, Thompson RJ: Immunoassay of the neuronal and neuroendocrine marker PGP 9.5 in human tissues. *J Neurochem* 44: 651-653, 1985
18. Shirato I, Asanuma K, Takeda Y, Hayashi K, Tomino Y: Protein gene product 9.5 is selectively localized in parietal epithelial cells of Bowman's capsule in the rat kidney. *J Am Soc Nephrol* 11: 2381-2386, 2000
19. Helal I, Fick-Brosnahan GM, Reed-Gitomer B, Schrier RW: Glomerular hyperfiltration: definitions, mechanisms and clinical implications. *Nat Rev Nephrol* 8: 293-300, 2012
20. Mendez M, Gross KW, Glenn ST, Garvin JL, Carretero OA: Vesicle-associated membrane protein-2 (VAMP2) mediates cAMP-stimulated renin release in mouse juxtaglomerular cells. *J Biol Chem* 286: 28608-28618, 2011
21. Waldum-Grevbo B: What physicians need to know about renal function in outpatients with heart failure. *Cardiology* 131: 130-138, 2015
22. Melsom T, Mathisen UD, Ingebretsen OC, Jenssen TG, Njolstad I, Solbu MD, Toft I, Eriksen BO: Impaired fasting glucose is associated with renal hyperfiltration in the general population. *Diabetes Care* 34: 1546-1551, 2011
23. Cohen AJ, McCarthy DM, Stoff JS: Direct hemodynamic effect of insulin in the isolated perfused kidney. *Am J Physiol* 257: F580-585, 1989
24. ter Maaten JC, Bakker SJ, Serne EH, ter Wee PM, Donker AJ, Gans RO: Insulin's acute effects on glomerular filtration rate correlate with insulin sensitivity whereas insulin's acute effects on proximal tubular sodium reabsorption correlation with salt sensitivity in normal subjects. *Nephrol Dial Transplant* 14: 2357-2363, 1999
25. Caceres PS, Mendez M, Ortiz PA: Vesicle-associated membrane protein 2 (VAMP2) but Not VAMP3 mediates cAMP-stimulated trafficking of the renal Na+-K+-2Cl- co-transporter NKCC2 in thick ascending limbs. *J Biol Chem* 289: 23951-23962, 2014
26. Walkowska A, Badzynska B, Kompanowska-Jezierska E, Johns EJ, Sadowski J: Effects of renal nerve stimulation on intrarenal blood flow in rats with intact or inactivated NO synthases. *Acta Physiol Scand* 183: 99-105, 2005
27. Wang W, Falk SA, Jittikanont S, Gengaro PE, Edelstein CL, Schrier RW: Protective effect of renal denervation on normotensive endotoxemia-induced acute renal failure in mice. *Am J Physiol Renal Physiol* 283: F583-587, 2002
28. Read NC, Gutsol A, Holterman CE, Carter A, Coulombe J, Gray DA, Kennedy CR: Ubiquitin C-terminal hydrolase L1 deletion ameliorates glomerular injury in mice with ACTN4-associated focal segmental glomerulosclerosis. *Biochim Biophys Acta* 1842: 1028-1040, 2014
29. Thibodeau JF, Holterman CE, He Y, Carter A, Cron GO, Boisvert NC, Abd-Elrahman KS, Hsu KJ, Ferguson SS, Kennedy CR: Vascular Smooth Muscle-Specific EP4 Receptor Deletion in Mice Exacerbates Angiotensin II-Induced Renal Injury. *Antioxid Redox Signal* 25: 642-656, 2016

30. Chen K, Wei Y, Sharp GC, Braley-Mullen H: Inhibition of TGFbeta1 by anti-TGFbeta1 antibody or lisinopril reduces thyroid fibrosis in granulomatous experimental autoimmune thyroiditis. *J Immunol* 169: 6530-6538, 2002
31. Giani JF, Janjulia T, Kamat N, Seth DM, Blackwell WL, Shah KH, Shen XZ, Fuchs S, Delpire E, Toblli JE, Bernstein KE, McDonough AA, Gonzalez-Villalobos RA: Renal angiotensin-converting enzyme is essential for the hypertension induced by nitric oxide synthesis inhibition. *J Am Soc Nephrol* 25: 2752-2763, 2014
32. Tabatabaie T, Waldon AM, Jacob JM, Floyd RA, Kotake Y: COX-2 inhibition prevents insulin-dependent diabetes in low-dose streptozotocin-treated mice. *Biochem Biophys Res Commun* 273: 699-704, 2000
33. Grant CW, Duclos SK, Moran-Paul CM, Yahalom B, Tirabassi RS, Arreaza-Rubin G, Spain LM, Guberski DL: Development of standardized insulin treatment protocols for spontaneous rodent models of type 1 diabetes. *Comp Med* 62: 381-390, 2012
34. Eikefjord E, Andersen E, Hodneland E, Hanson EA, Sourbron S, Svarstad E, Lundervold A, Rorvik JT: Dynamic contrast-enhanced MRI measurement of renal function in healthy participants. *Acta Radiol* 58: 748-757, 2017
35. Sourbron SP, Michaely HJ, Reiser MF, Schoenberg SO: MRI-measurement of perfusion and glomerular filtration in the human kidney with a separable compartment model. *Invest Radiol* 43: 40-48, 2008
36. Burger D, Turner M, Munkonda MN, Touyz RM: Endothelial Microparticle-Derived Reactive Oxygen Species: Role in Endothelial Signaling and Vascular Function. *Oxid Med Cell Longev* 2016: 5047954, 2016
37. Gonzalez RC, Woods RE: Digital Image Processing. 3rd ed., edited by McDonald M, New Jersey, Pearson Prentice Hall, 2007, pp 1-976
38. Palagyi K, Kuba A: A 3D 6-subiteration thinning algorithm for extracting medial lines. *Pattern Recog Lett* 19: 613-627, 1998

CHAPTER 3

Ubiquitin C-terminal hydrolase L1 deletion is associated with renal α-klotho deficiency and perturbed phosphate homeostasis

General Description

While studying the renal phenotypes in *Uchl1*-deleted mice it became apparent that these mice displayed disrupted phosphate homeostasis. *Uchl1*-/- mice displayed hyperphosphatemia associated with increased fractional excretion of phosphate. As such, we investigated the potential mechanisms that contribute to the perturbations in phosphate homeostasis in *Uchl1*-/- mice.

Circulating phosphate levels are tightly maintained by intestinal absorption of phosphate and renal reabsorption/excretion of phosphate (Figure A). Parathyroid hormone (PTH),

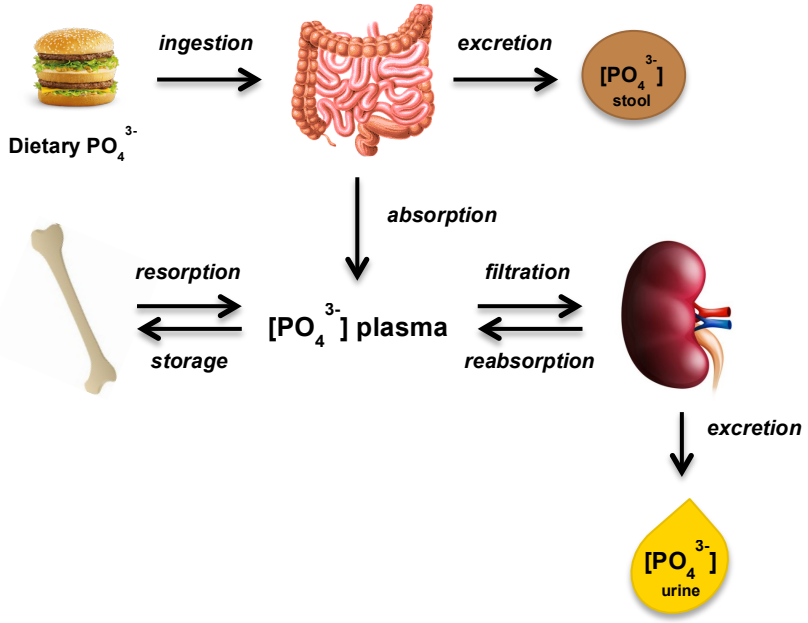

Figure A. Regulation of phosphate homeostasis. The small intestine regulates dietary phosphate absorption into the blood, while a smaller percentage is excreted into the feces. Plasma phosphate levels are maintained through renal phosphate reabsorption and excretion into the urine. Resorption/storage of phosphate from/into the bone also regulates plasma phosphate levels.

calcitriol (1,25-$(OH)_2$-D_3), fibroblast growth factor 23 (FGF23) and α-klotho are the primary phosphaturic hormones that interplay under conditions of hyperphosphatemia (Figure B) (Fukumoto, 2014). An increase in plasma phosphate levels is typically associated with the production and release of FGF23 from the bone. FGF23 acts through the fibroblast growth factor receptors 1 and 4 (FGFR1 and FGFR4)/ α-klotho complex in the kidney and promotes the internalization of the renal sodium-phosphate cotransporters 2a and 2c (Npt2a and Npt2c), thereby inhibiting phosphate reabsorption while promoting phosphate excretion into the urine (Gattineni et al., 2014, Hu et al., 2010, Ide et al., 2016, Olauson et al., 2012). PTH also has phosphaturic actions, similar to FGF23, however, it acts primarily as a calcitropic hormone. Nonetheless PTH contributes to intestinal absorption of phosphate, also by inducing 1,25-$(OH)_2$-D_3, to increase circulating phosphate levels (Fukumoto, 2014).

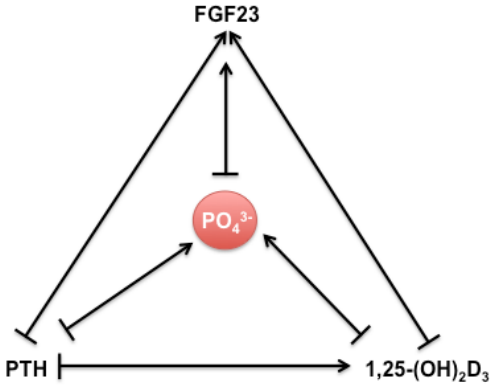

Figure B. Hormonal control of phosphate homeostasis. Parathyroid hormone (PTH) and the active form of vitamin D (1,25-$(OH)_2$-D_3) promote increased plasma phosphate levels. Fibroblast growth factor 23 (FGF23), on the other hand, negatively regulates plasma phosphate levels while suppressing both PTH and 1,25-$(OH)_2$-D_3. Adapted from Fukumoto, 2014.

In the present study, we investigated whether signaling components of the pathways involved in phosphate homeostasis were altered in *Uchl1*-/- mice, as to determine the mechanisms contributing to perturbed phosphate homeostasis in *Uchl1*-/- mice.

Ubiquitin C-terminal hydrolase L1 deletion is associated with renal α-klotho deficiency and perturbed phosphate homeostasis

Naomi Boisvert[1,2,3], Chet E. Holterman[1,2], Alex Gutsol[1,2], Josée Coulombe[2], Wanling Pan[4], Todd Alexander[4,5,6], Douglas A. Gray[2,7] and Chris R. Kennedy[1,2,3]

[1]Kidney Research Centre, [2]Ottawa Hospital Research Institute, The Ottawa Hospital, Ottawa, Ontario, Canada
[3]Department of Cellular and Molecular Medicine, Faculty of Medicine, University of Ottawa, Ottawa, Ontario, Canada
[4]Department of Physiology, University of Alberta, Edmonton, Alberta, Canada.
[5]Membrane Protein Disease Research Group, University of Alberta, Edmonton, Alberta, Canada.
[6]Department of Pediatrics, University of Alberta, Edmonton, Alberta, Canada
[7]Department of Biochemistry, Microbiology and Immunology, Faculty of Medicine, University of Ottawa, Ottawa, Ontario, Canada.

Corresponding Author:
Dr. Chris R. Kennedy
Kidney Research Centre, Ottawa Hospital Research Institute, The Ottawa Hospital
Department of Cellular and Molecular Medicine, Faculty of Medicine, University of Ottawa
451 Smyth Rd, Roger-Guindon Hall, room 2515
Ottawa, Ontario, Canada, K1H 8M5
Phone: 1-613-562-5800, extension 8529
Fax: 1-613-562-5487
E-mail: ckennedy@uottawa.ca

Running Head: Perturbed phosphate homeostasis in *Uchl1*-deleted mice

Word Count: 3917

Keywords: UCHL1, UCH-L1, phosphate, hyperphosphatemia, α-klotho

Author Contributions

Naomi Boisvert	▪ Planned and performed the bulk of the experiments ▪ Wrote the manuscript
Chet E. Holterman	▪ Performed most of the mice sacrifices
Alex Gutsol	▪ Performed the Np2b immunofluorescence ▪ Performed the Npt2a and α-klotho immunohistochemistry experiments
Josée Coulombe	▪ Provided assistance with some blood collections
Wanling Pan	▪ Conducted the PTH and FGF23 ELISAs
Todd Alexander	▪ Provided significant guidance to the project ▪ Conducted the PTH and FGF23 ELISAs
Douglas A. Gray	▪ Co-supervised the project ▪ Assisted with manuscript revisions
Chris R.J. Kennedy	▪ Supervised the project ▪ Assisted with manuscript revisions

Abstract

Loss of ubiquitin C-terminal hydrolase L1 (UCHL1), a deubiquitinating enzyme required for neuronal function, led to hyperphosphatemia accompanied by phosphaturia in mice, while calcium homeostasis remained intact. We therefore investigated the mechanisms underlying the phosphate imbalance in *Uchl1*-/- mice. Interestingly, phosphaturia was not a result of lower renal brush border membrane sodium-phosphate cotransporter expression as sodium-phosphate cotransporter 2a and 2c expression levels were similar to wild type levels. Plasma parathyroid hormone and fibroblast growth factor 23 levels were not different; however, fibroblast growth factor 23 mRNA levels were significantly increased in femur homogenates from *Uchl1*-/- mice. By immunohistochemistry, α-klotho levels were comparable in renal sections from wild type and *Uchl1*-/- mice; however, Western immunoblotting depicted attenuated full length and soluble forms of α-klotho in renal cortical lysates from *Uchl1*-/- mice. Consistent with unchanged components of 1,25-$(OH)_2$-D_3 metabolism (i.e. CYP27B1 and CYP24A1), sodium-phosphate cotransporter 2b protein levels were not different in ileum brush borders from *Uchl1-/-* mice, suggesting that the intestine is not the source of hyperphosphatemia. Nonetheless, when *Uchl1*-/- mice were fed a low phosphate diet, plasma phosphate, urinary phosphate and fractional excretion of phosphate were significantly attenuated and comparable to levels of low phosphate diet-fed wild type mice. Our findings demonstrate that *Uchl1*-deleted mice exhibit perturbed phosphate homeostasis, likely consequent to loss of renal α-klotho, which can be rescued with a low phosphate diet. *Uchl1*-/- mice may provide a useful mouse model to study mild perturbations in phosphate homeostasis.

Introduction

Phosphate homeostasis is tightly regulated by the actions of several phosphaturic hormones including parathyroid hormone (PTH), the active form of vitamin D (calcitriol; 1,25-$(OH)_2$-D_3) and fibroblast growth factor 23 (FGF23). The interplay of these hormones counterbalances perturbations in phosphate homeostasis by adjusting intestinal phosphate absorption, bone metabolism and renal phosphate reabsorption. Circulating phosphate levels are maintained in a narrow range (0.8-1.45mM) in humans (31).

Hyperphosphatemia is a disorder wherein circulating phosphate levels achieve concentrations >1.45mM. Prolonged hyperphosphatemia is detrimental as it leads to vascular calcification, cardiovascular disease, metabolic bone disease and secondary hyperparathyroidism (32). Furthermore, phosphate concentrations >2.0mM are associated with all-cause mortality. Hyperphosphatemia causes include hypoparathyroidism or chronic kidney disease (CKD), which are associated with overactive phosphate reabsorption in the renal proximal tubule via the sodium-phosphate cotransporters 2a and 2c (Npt2a and Npt2c) (31).

PTH, well established as a calcitropic hormone, negatively regulates Npt2a and Npt2c while stimulating 1,25-$(OH)_2$-D_3-mediated calcium/phosphate absorption and resorption from the intestine and the bone, respectively. PTH release from the parathyroid gland occurs in response to reduced circulating calcium levels, while its phosphaturic actions counteract the secondary phosphate increases (7). FGF23, on the other hand, is produced

and released by osteoblasts and osteocytes to increased circulating phosphate levels or by direct stimulation from 1,25-$(OH)_2$-D_3 (26, 33). FGF23 suppresses renal Npt2a expression, inhibiting renal phosphate reabsorption and promoting urinary phosphate excretion (33). FGF23 also reduces CYP27B1 and enhances CYP24A1, the enzymes involved in 1,25-$(OH)_2$-D_3 metabolism, thereby attenuating 1,25-$(OH)_2$-D_3 along with intestinal calcium/phosphate absorption (33). In the kidney, the actions of FGF23 are mediated primarily through the FGF receptors 1 and 4 (FGFR1 and FGFR4), which require the coreceptor klotho (17, 34). FGF23-null mice show marked growth retardation, abnormal bone morphology, a shorter lifespan and elevated serum phosphate and 1,25-$(OH)_2$-D_3 levels (34). Double mutant *Fgfr1*$^{-/-}$/*Fgfr4*$^{-/-}$ mice display a milder phenotype, but consistent with FGF23's role in the kidney, these mice display elevated serum phosphate levels, increased Npt2c and increased phosphate reabsorption in renal brush border membrane vesicles (BBMVs) (8).

Klotho is crucial to FGF23 signaling as it forms a binary complex with FGFR1/4 and increases FGF23 affinity for the FGFR complex (37). In the kidney, α-klotho is predominantly expressed in the distal tubule where it stabilizes the transient receptor potential cation channel subfamily V member 5 (TRPV5) to promote calcium reabsorption (3). α-Klotho is also expressed in the proximal tubule alongside FGFRs. As the coreceptor for FGFR1/4 in the kidney, klotho enables adequate FGF23-induced signaling, which in turn promotes Npt2a inhibition and internalization (10). Loss of klotho impairs renal FGF23-mediated signaling. Indeed, phosphate homeostasis is disrupted in klotho-deficient mice (kl/kl), accompanied by a gross ageing-like phenotype

characterized by arteriosclerosis, osteoporosis, emphysema and a short lifespan (34, 36, 40). The ageing phenotype is absent in mice with distal tubule-specific deletion of klotho (Ksp-KL$^{-/-}$); however, serum phosphate and FGF23 are increased. Phosphate excretion is unchanged, as Npt2a expression is elevated in renal brush border membranes (BBMs) (23). In CKD, circulating phosphate and FGF23 levels are elevated, accompanied by reduced klotho levels, which likely contributes to cardiovascular morbidity/mortality (9, 11, 13).

In the present study, we describe a novel phenotype in mice lacking *ubiquitin C-terminal hydrolase L1* (*Uchl1*-/- mice) wherein these display phosphaturia associated with mild hyperphosphatemia. Ubiquitin C-terminal hydrolase L1 (UCHL1) is a deubiquitinating enzyme that hydrolyses ubiquitin tagged to substrates and maintains intracellular ubiquitin pools (39). Mice lacking *Uchl1* show marked decreases in ubiquitin pools and significant neurodegeneration of axonal processes leading to motor deficits (5, 25, 29). To our knowledge, there is no previous association between *Uchl1*-/- mice and perturbed phosphate homeostasis. As such, we assessed the role of the PTH, 1,25-$(OH)_2$-D_3 and FGF23/α-klotho axis to determine how the interplay of these contributes to the phosphate imbalance in *Uchl1*-/- mice.

Materials and Methods

Mice

Mice were housed at the Animal Care facility at the University of Ottawa. *Uchl1*-/- mice and wild type littermates were generated by intercrossing *Uchl1*+/- mice of mixed background, including FVB/N and sv/129. For the low phosphate diet study, eleven-week-old mice were fed a low phosphate diet (0.02% phosphate; Envigo, Indianapolis, IN) or a normal diet *ad libitum* for 7 days. At endpoint, 12-week-old mice were anesthetised with isofluorane and blood was collected. Mice were also perfused with 20ml PBS through the left ventricle, for appropriate experiments. Mice procedures were approved and carried out according to Canadian Council on Animal Care guidelines.

Plasma and Urine Analysis

Sodium-heparin derived plasma or spot urine samples were analysed by IDEXX (IDEXX Labs, Toronto, ON). The fractional excretion percentage was determined using the following formula: ((Urinary phosphate or calcium x Plasma creatinine) / (Plasma phosphate or calcium x Urinary creatinine)) x 100. Plasma PTH was determined with the Mouse PTH 1-84 ELISA Kit (Immunotopics, Athens, OH) and plasma FGF23 was determined with the FGF23 ELISA Kit (Kainos Laboratories, Tokyo, Japan). The plasma used for the PTH and FGF23 assays was collected using lithium-heparin-coated tubes.

Immunohistochemistry and Immunofluorescence

Paraffin-embedded sections were dewaxed and rehydrated through interchanges of

ethanol. For immunohistochemistry experiments, renal sections were boiled in sodium citrate pH 6.0 for 30 minutes and processed with the ImmPRESS Reagent kit (Vector Laboratories, Burlingame, CA). Sections were incubated with mouse anti-SLC34A1 1:100 (Npt2a; Novus Biologicals, Oakville, ON) diluted in 1% BSA/PBS o/n at 4°C. Immunohistochemistry for α-klotho was performed as previously described (12). Sections were incubated with rat anti-α-klotho 1:200 (Trans Genic Inc., Kobe, Japan) diluted in 1% BSA/PBS o/n at 4°C. Sections were visualized with a Zeiss Axio Imager A1 microscope and images were captured using Olympus cellSens software (Olympus; Richmond Hill, ON).

Immunofluorescence was performed on paraffin-embedded ileum sections. Samples were blocked in 10% donkey serum/1% BSA/PBS (Jackson ImmunoResearch, West Grove, PA) for 1 hour and incubated with rabbit anti-Npt2b 1:1000 (generously provided by Dr. Yves Sabbagh) diluted in 1% BSA/PBS o/n at 4°C. The following day, samples were incubated with donkey anti-rabbit-Cy3 1:200 (Jackson ImmunoResearch, West Grove, PA) diluted in 1% BSA/PBS for 1 hour and counterstained with Hoescht 1:7000 (Invitrogen, Burlington, ON). Sections were visualized with Zeiss Axioskop 2 MOT epifluorescence microscope (Zeiss, North York, ON) and images were captured using Axiovision software.

BBMV Isolation

Renal and ileum BBMVs were isolated from mice as previously described (2). Alkaline phosphatase activity was assessed as a quality control. Prior to the ileum BBMVs

isolation, the last 10cm of the small intestine was removed and flushed with PBS using a P1000 pipette. The ileum was opened and the brush border was scraped and removed using the edge of a glass slide.

Western Immunoblotting

The renal cortex was homogenized using a TP-103 Amalgamator COE Capmixer (GC America, Alsip, IL). The powderized kidney was resuspended in RIPA buffer (150mM NaCl, 1% NP-40, 0.5% sodium deoxycholate, 0.1% SDS and 50mM Tris, pH 8.0) containing 1:100 protease inhibitor cocktail (Sigma-Aldrich, Oakville, ON) and incubated on ice for 15 minutes. Protein lysates were centrifuged for 10 minutes and the supernatent was collected. Renal protein lysates and renal/ileum BBMVs were resuspended in 6X Laemmli buffer and boiled for 2 minutes. For SDS-PAGE, 20-60µg of protein lysate was loaded on an appropriate percentage gel. For spot urine immunoblotting, 25µl of urine was resuspended in 6X Laemmli buffer, boiled and loaded onto an SDS-PAGE.

Primary antibodies included mouse anti-SLC34A1 1:500 (Npt2a; Novus Biologicals, Oakville, ON) diluted in 1% BSA/PBS-T, rabbit anti-SLC34A3 1:500 (Npt2c; Abcam, Toronto, ON), diluted in 5% milk/PBS-T, rat anti-α-klotho 1:100 (Trans Genic Inc., Kobe, Japan), diluted in 5% milk/PBS-T and rabbit anti-SLC34A2 1:200 (Npt2b; generously provided by Dr. Yves Sabbagh), diluted in 5% BSA/PBS-T. Mouse anti-β-actin 1:10,000 (Sigma-Aldrich, Oakville, ON) diluted in the appropriate blocking solution was used as a loading control. Primary antibodies were incubated o/n at 4°C.

Secondary antibodies included HRP-goat anti-mouse 1:10,000, HRP-goat anti-rabbit 1:10,000 and HRP-goat anti-rat 1:10,000 (Jackson ImmunoResearch, West Grove, PA) diluted in appropriate blocking solutions. Densitometry was computed using Alpha Innotech software (Alpha Innotech; San Leandro, CA). Urinary densitometry values were normalized to creatinine, as determined by the Creatinine Companion kit (Exocell, Philadelphia, PA).

Quantitative Real Time PCR

The ileum was collected (by conserving the last 10cm of the small intestine) and flushed with PBS using a P1000 pipette. The renal cortex or ileum was homogenized using a TP-103 Amalgamator COE Capmixer (GC America, Alsip, IL) and quickly resuspended in RLT supplemented with β-mercaptoethanol 1:100. Femur samples were also homogenized accordingly, resuspended in TRI Reagent and processed according to the manufacturer's instructions (Sigma-Aldrich, Oakville, ON). Renal/ileum homogenates were processed through a Qiashredder (Qiagen, Toronto, ON) and RNA isolation was performed using an RNeasy Mini Kit (Qiagen, Toronto, ON). RNA was then converted to cDNA using the High Capacity cDNA Reverse Transcription Kit (Applied Biosystems, Burlington, ON). Quantitative Real Time PCR was performed using the SYBR Advantage Premix (Clontech, Mountainview, CA) and fluorescence was detected using the ABI Prism 7000 Sequence Detection System. All primers were obtained from Invitrogen (Burlington, ON). Primer sequences are available in Table 1.

Table 1. Primer Sequences.

Gene Product	Forward Primer (5'->3')	Reverse Primer (5'->3')
CYP24A1	TGGGAAGATGATGGTGACCC	ACTGTTCCTTTGGGTAGCGT
CYP27B1	CCGCGGGCTATGCTGGAAC	CTCTGGGCAAAGGCAAACATC TGA
FGFR1	CAGCTGACTCCAGTGCATCC	TGCGTCGGACTTCAACATCT
FGFR4	GGTGGTCAGTGGGAAGTCTG	TCTTGCTGCTCCAGGATTGG
FGF23	ATCAGACCATCTACAGTGCC C	GAGAGCAGGATACAGGCACA
Pit2	CGTCAAGATTGTCGCCTCCT	TGGAGACCGTTTGGAACAGG
SLC34A1	GTCTCATTCGGATTTGGTGT CA	GCCGATGGCCTCTACCCT
SLC34A2	TGCTTCTTCATTGCTGACGGT	CAGAGGCAAGAGCACGAACA
SLC34A3	TAATCTTCGCAGTTCAGGTT GCT	CAGTGGAATTGGCAGTCTCAA G
TRPV5	CAATTGGTGGGTCAGAGACC A	CAGAGCTCCTCTTTGCCGGA
TRPV6	TTGCCCATGAGCGAGATGAG	TCTTCCACCCTCAAGAACCA
VDR	CTGCTCGATGCCCACCACAAG ACCTACG	GTGGGGCAGCATGGAGAGCGGA GACAG

Fecal Calcium and Phosphate

Mice were housed in metabolic cages for 24 hours and feces were collected and processed as described previously with some modifications (28). Stool samples were dried in a ventilated chemical hood overnight and resuspended in 0.6M HCl to 50mg/ml. Samples were placed on a shaker for 72 hours at 4°C. After 48 hours, samples were homogenized and continued to mix for the remaining 24 hours. Stool samples were then centrifuged at 2000xg for 5 minutes and the supernatant was collected and diluted 1:80 in HPLC-grade water (Sigma-Aldrich, Oakville, ON). Fecal phosphate and calcium were

measured using the Phosphorus Liquid-UV test and the Calcium (Arsenazo) LiquiColor Test (Stanbio Laboratories, Boerne, TX).

Femur Histology

At endpoint, femurs were preserved in 10% formalin for 1 week, dehydrated in ethanol and decalcified prior to being submitted to standard staining procedures (i.e. Masson's trichrome). Sections were visualized with a Zeiss Axio Imager A1 microscope and images were captured using Olympus cellSens software (Olympus; Richmond Hill, ON).

Statistical Analyses

Values are expressed as mean ± standard error. Statistical comparisons were computed using a t-test, a one-way ANOVA or a two-way ANOVA with Sidak's post-test where appropriate.

Results

Phosphate Homeostasis is Disrupted in *Uchl1*-/- Mice

At 12 weeks of age, *Uchl1*-/- mice displayed hyperphosphatemia, as plasma phosphate was increased ($p<0.001$) to 1.6±0.0mM compared to 1.3±0.1mM in wild type mice (Figure 1A). Plasma calcium in *Uchl1*-/- mice (2.0±0.1mM) was comparable to wild type mice (1.9±0.1mM) (Figure 1B). Urinary phosphate/creatinine ratios were significantly elevated ($p<0.0001$) in the phosphaturia range to 13.7±1.6 in *Uchl1*-/- mice, compared to 2.1±0.6 in wild type mice (Figure 1C). Urinary calcium/creatinine ratios trended lower in *Uchl1*-/- mice to 0.48±0.04 compared to 0.67±0.12 for wild type mice, but this was not statistically significant (Figure 1D). Finally, fractional excretion of phosphate was significantly elevated ($p<0.001$) in *Uchl1*-/- mice to 7.80±1.18% compared to 1.04±0.33% in wild type mice (Figure 1E). Fractional excretion of calcium was lowered in *Uchl1*-/- mice to 0.36±0.08% compared to 0.90±0.31% in wild type mice but this did not achieve statistical significance (Figure 1F).

Renal Sodium-Phosphate Cotransporter Levels are Maintained in *Uchl1*-/- Mice

Loss of renal proximal tubule sodium-phosphate cotransporter (Npt) expression leads to phosphaturia (1, 14, 30). As such, renal Npt expression levels were determined. Npt2c mRNA levels were elevated by 2.5-fold ($p<0.001$) in renal cortical lysates from *Uchl1*-/- mice. Npt2a and phosphate transporter 2 (Pit2) mRNA levels were not different between groups (Figure 2A). Immunohistochemistry using anti-Npt2a revealed similar Npt2a distribution in renal proximal tubules of both groups (Figure 2B). Accordingly, both

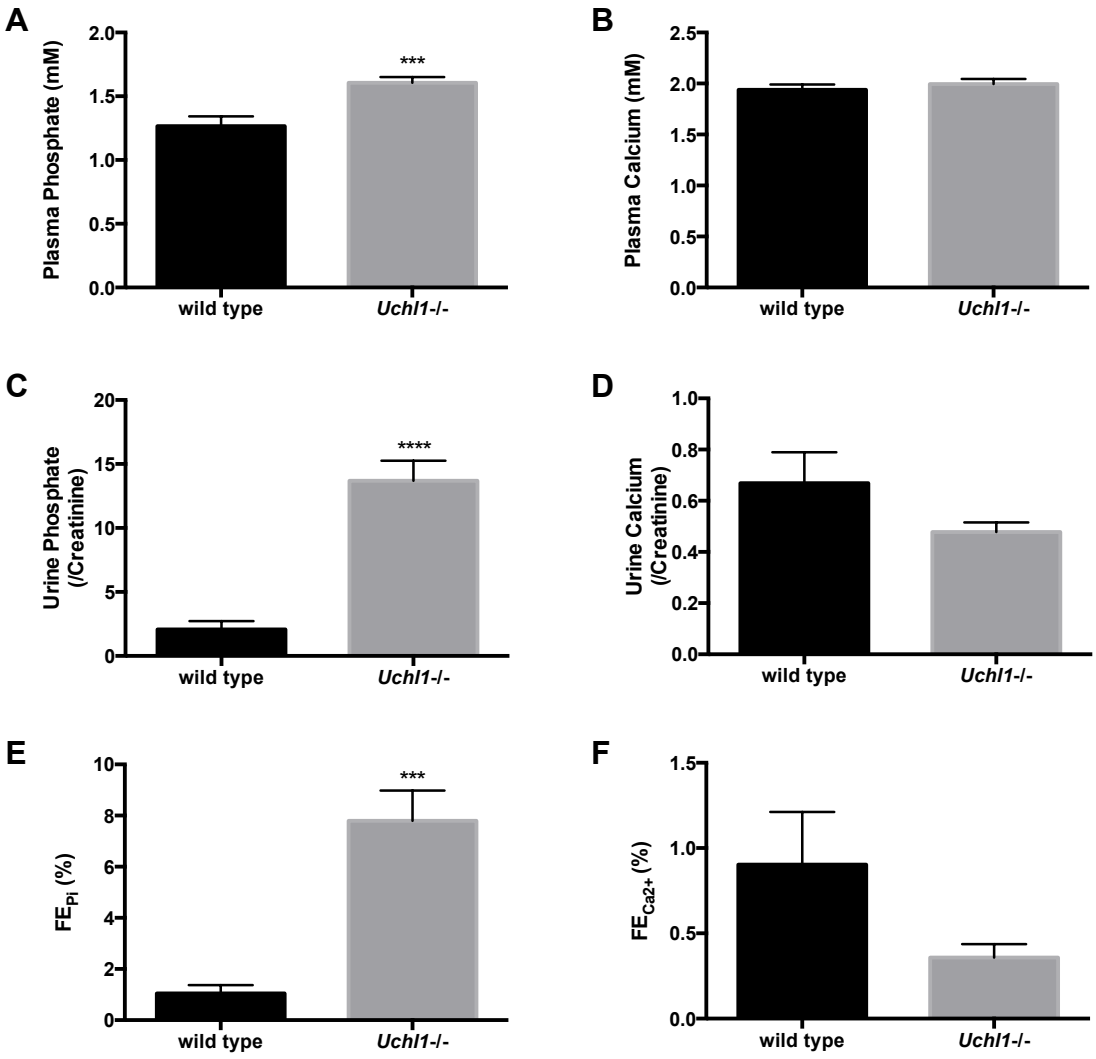

Figure 1. *Uchl1*-/- mice exhibit hyperphosphatemia accompanied by phosphaturia. A. Plasma phosphate was significantly increased in *Uchl1*-/- mice ($p<0.001$; n=13-19). **B.** Plasma calcium was unaltered in *Uchl1*-/- mice (n=13-19). **C.** Urinary phosphate to creatinine ratios were increased in *Uchl1*-/- mice ($p<0.0001$; n=11-19). **D.** Urinary calcium to creatinine ratios were modestly decreased in *Uchl1*-/- mice (n=11-19). **E.** Fractional excretion of phosphate (FE_{Pi}) was elevated in *Uchl1*-/- mice ($p<0.001$; n=9-15). **F.** Fractional excretion of calcium (FE_{Ca2+}) trended lower in *Uchl1*-/- mice (n=10-15). Data depicts mean ± SE, analyzed by unpaired t-test.

Npt2a and Npt2c protein levels trended higher in renal BBMVs isolated from *Uchl1*-/- mice, however this was not statistically significant (Figure 2C-F). As such, phosphaturia in *Uchl1*-/- mice does not result from reduced Npt expression in the renal proximal tubule.

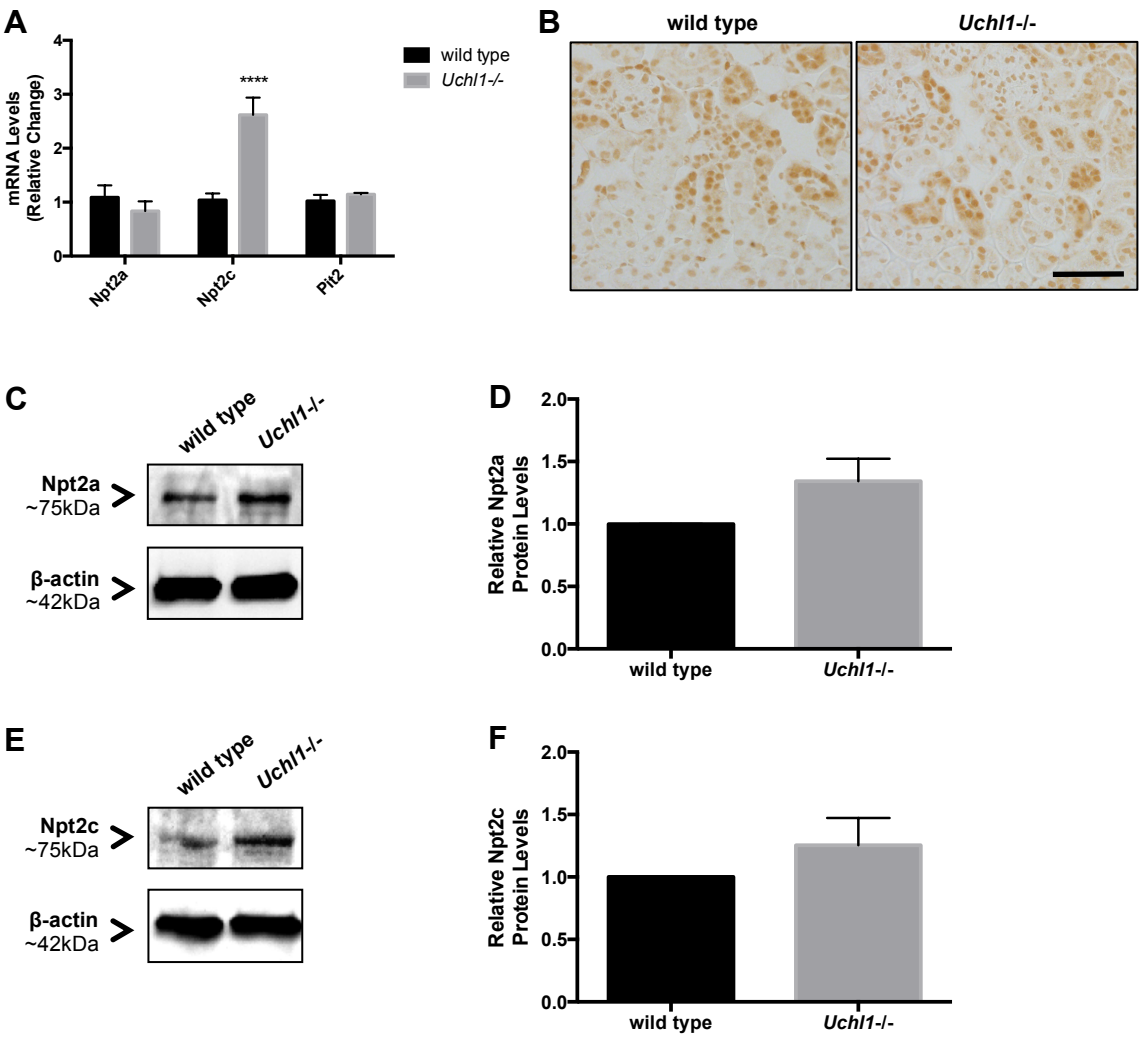

Figure 2. Renal Npt protein expression levels are unchanged in *Uchl1*-/- mice. **A.** Npt2c mRNA levels were significantly increased in renal cortical lysates from *Uchl1*-/- mice ($p<0.0001$) while Npt2a and Pit2 mRNA remained unchanged between groups (n=5). Data depicts mean ± SE, analyzed by 2-way ANOVA with Sidak's multiple comparisons test. **B.** Immunohistochemistry using anti-Npt2a revealed no differences in renal cortical Npt2a expression in *Uchl1*-/- mice (n=3). Scale bar = 50μm. **C.** Npt2a protein levels were not different in renal BBMVs isolated from *Uchl1*-/- mice, as determined by Western immunoblot (n=6). **D.** Densitometry graph depicting renal BBMV Npt2a protein levels in *Uchl1*-/- mice (n=6). Data depicts mean ± SE, analyzed by unpaired t-test. **E**. Npt2c protein levels were not different in renal BBMVs isolated from *Uchl1*-/- mice, as determined by Western immunoblot (n=6). **F.** Densitometry graph depicting renal BBMV Npt2c protein levels in *Uchl1*-/- mice (n=6). Data depicts mean ± SE, analyzed by unpaired t-test.

PTH and FGF23 Signaling are not Different in *Uchl1*-/- Mice

Next, we verified the levels of the phosphaturic hormones PTH and FGF23. Plasma PTH trended lower in *Uchl1*-/- mice to 116.6±16.4pg/ml compared to wild type mice (242.0±71.5pg/ml), but the difference was not significant (Figure 3A). Plasma FGF23 levels were unchanged between groups (*Uchl1*-/- mice: 161.1±12.7pg/ml, wild type mice: 154.5±11.0pg/ml) (Figure 3B); however, FGF23 mRNA levels were significantly induced ($p<0.05$) by 6.4-fold in femur homogenates from *Uchl1*-/- mice (Figure 3C).

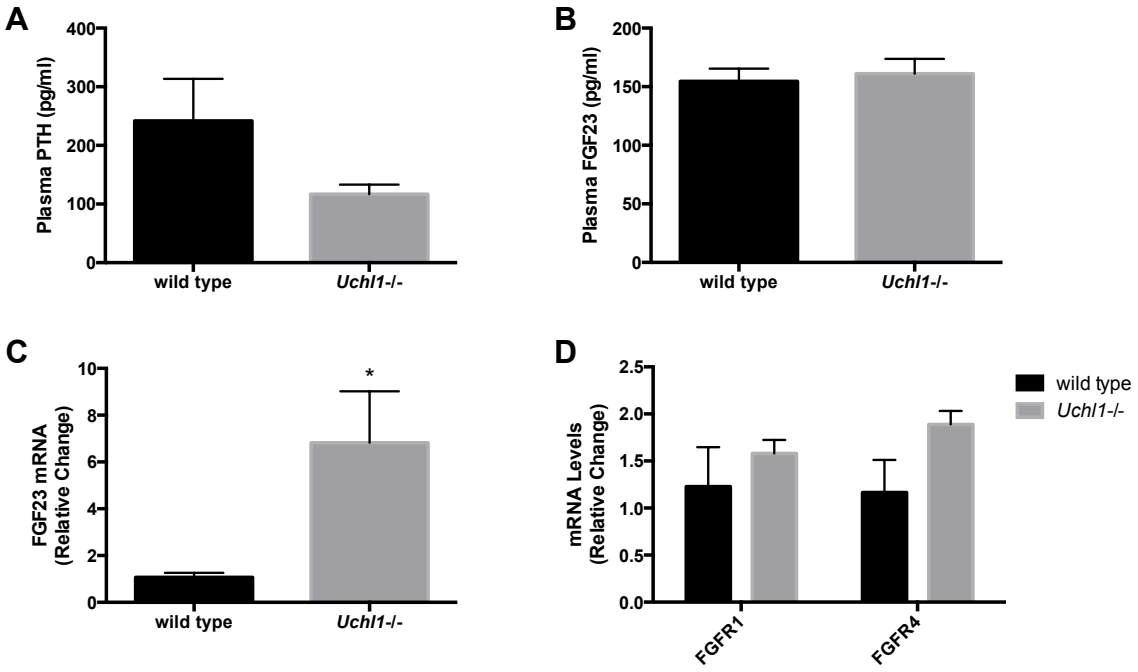

Figure 3. Phosphaturic hormones are unchanged in *Uchl1*-/- mice. A. Plasma PTH concentration trended lower in *Uchl1*-/- mice but this trend was not statistically significant (n=14-16). Data depicts mean ± SE, analyzed by unpaired t-test. **B.** Plasma FGF23 concentration was not different in *Uchl1*-/- mice (n=14-16). Data depicts mean ± SE, analyzed by unpaired t-test. **C.** FGF23 mRNA levels were significantly increased in femur lysates isolated from *Uchl1*-/- mice ($p<0.05$; n=5-6). Data depicts mean ± SE, analyzed by unpaired t-test. **D.** FGFR1 and FGFR4 mRNA levels were not significantly different in renal cortical lysates from *Uchl1*-/- mice (n=3-4). Data depicts mean ± SE, analyzed by 2-way ANOVA with Sidak's multiple comparisons test.

Finally, FGFR1 and FGFR4 mRNA levels were not significantly different in renal cortical lysates from *Uchl1*-/- mice (Figure 3D). Despite elevated femur FGF23 mRNA levels, these data suggest that FGF23 signaling is not different in *Uchl1*-/- mice.

Intestinal Phosphate Absorption may not Contribute to Hyperphosphatemia in *Uchl1*-/- Mice

Phosphaturic hormones, namely 1,25-$(OH)_2$-D_3, can alter intestinal calcium/phosphate transport (7). Moreover, *Uchl1*-/- mice show impaired gastric motility, which may promote increased intestinal phosphate absorption (5). Therefore, the contribution of the gut to hyperphosphatemia was assessed. TRPV6 and Npt2b mRNA levels were unchanged in ileum lysates from *Uchl1*-/- mice (Figure 4A-B). Similarly, Npt2b protein levels were comparable to wild type levels in ileum BBMVs isolated from *Uchl1*-/- mice (Figure 4C-D), and as determined by immunofluorescence of ileum sections (Figure 4E). Fecal phosphate levels trended higher in *Uchl1*-/- mice to 18.4±2.4mg/day, compared to 11.9±2.2mg/day for wild type mice (Figure 4F). Fecal calcium levels were elevated ($p<0.05$) to 60.5±5.8mg/day in *Uchl1*-/- mice compared to 41.8±1.9mg/day in wild type mice (Figure 4G). Together these data suggest that increased intestinal phosphate absorption does not account for hyperphosphatemia in *Uchl1*-/- mice.

Renal α-Klotho is Attenuated in *Uchl1*-/- Mice

As the coreceptor for the FGFRs, klotho is indispensible to FGF23 signaling and its ablation in the kidney promotes hyperphosphatemia (12, 18, 23). We therefore assessed renal α-klotho expression in *Uchl1*-/- mice. By immunohistochemistry, α-klotho

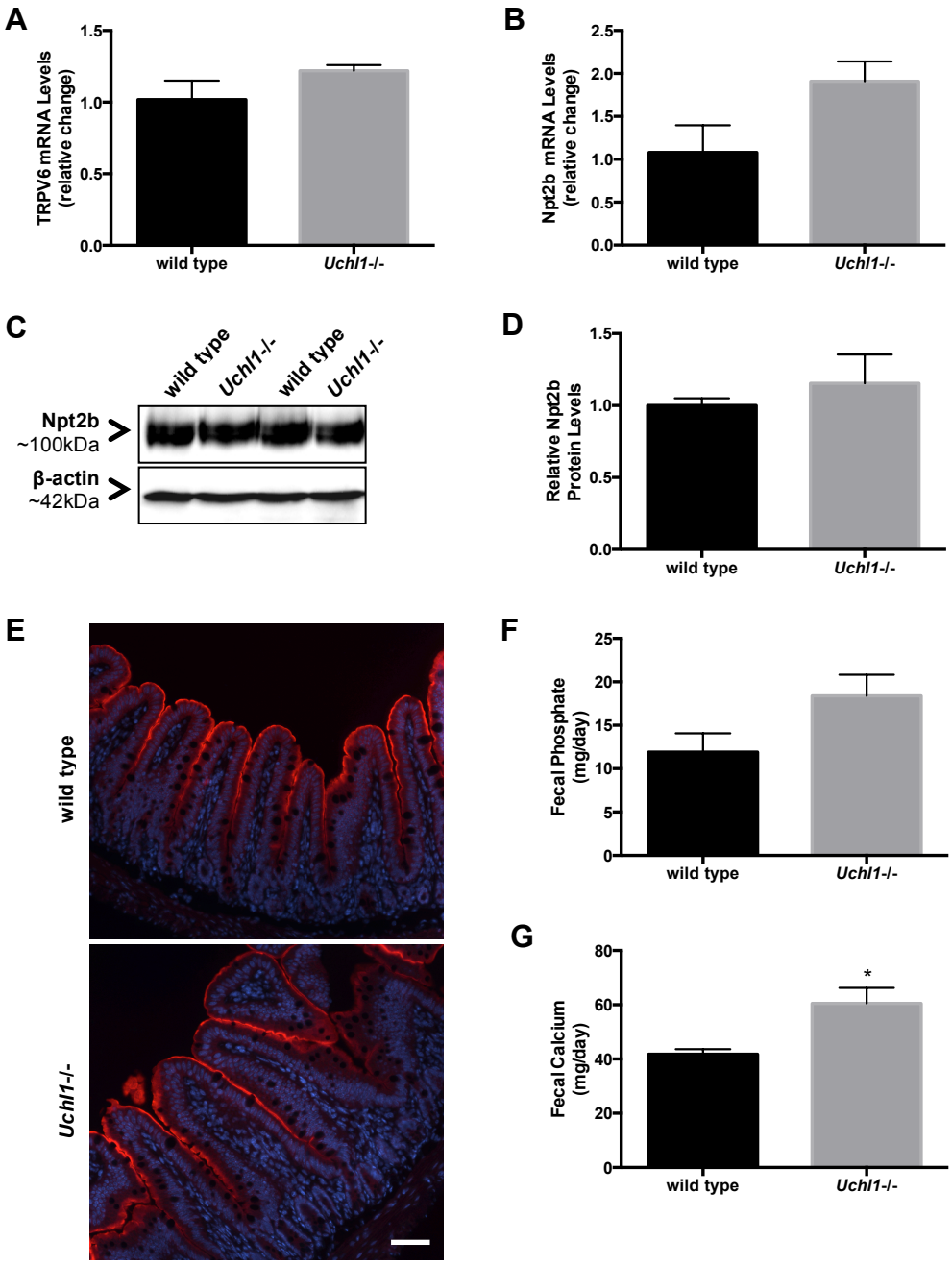

Figure 4. Ileum Npt2b expression is not different in *Uchl1*-/- mice. A. TRPV6 and **B.** Npt2b mRNA levels, determined by qPCR, were not different in ileum lysates collected from *Uchl1*-/- mice (n=3-4). **C.** Npt2b protein levels in ileum BBMVs were not significantly different in *Uchl1*-/- mice (n=6). **D.** Densitometry graph depicting Npt2b protein levels in ileum BBMVs isolated from *Uchl1*-/- mice (n=6). **E.** Immunofluorescence revealed wild type-comparable Npt2b expression in ileum BBMs of *Uchl1*-/- mice (n=4-5). Npt2b: red and nuclei: blue. Scale bar = 50µm. **F.** Fecal phosphate levels trended higher in *Uchl1*-/- mice but this was not statistically significant (n=6). **G.** Fecal calcium levels were significantly increased in *Uchl1*-/- mice ($p<0.05$; n=6). Data depicts mean ± SE, analyzed by unpaired t-test.

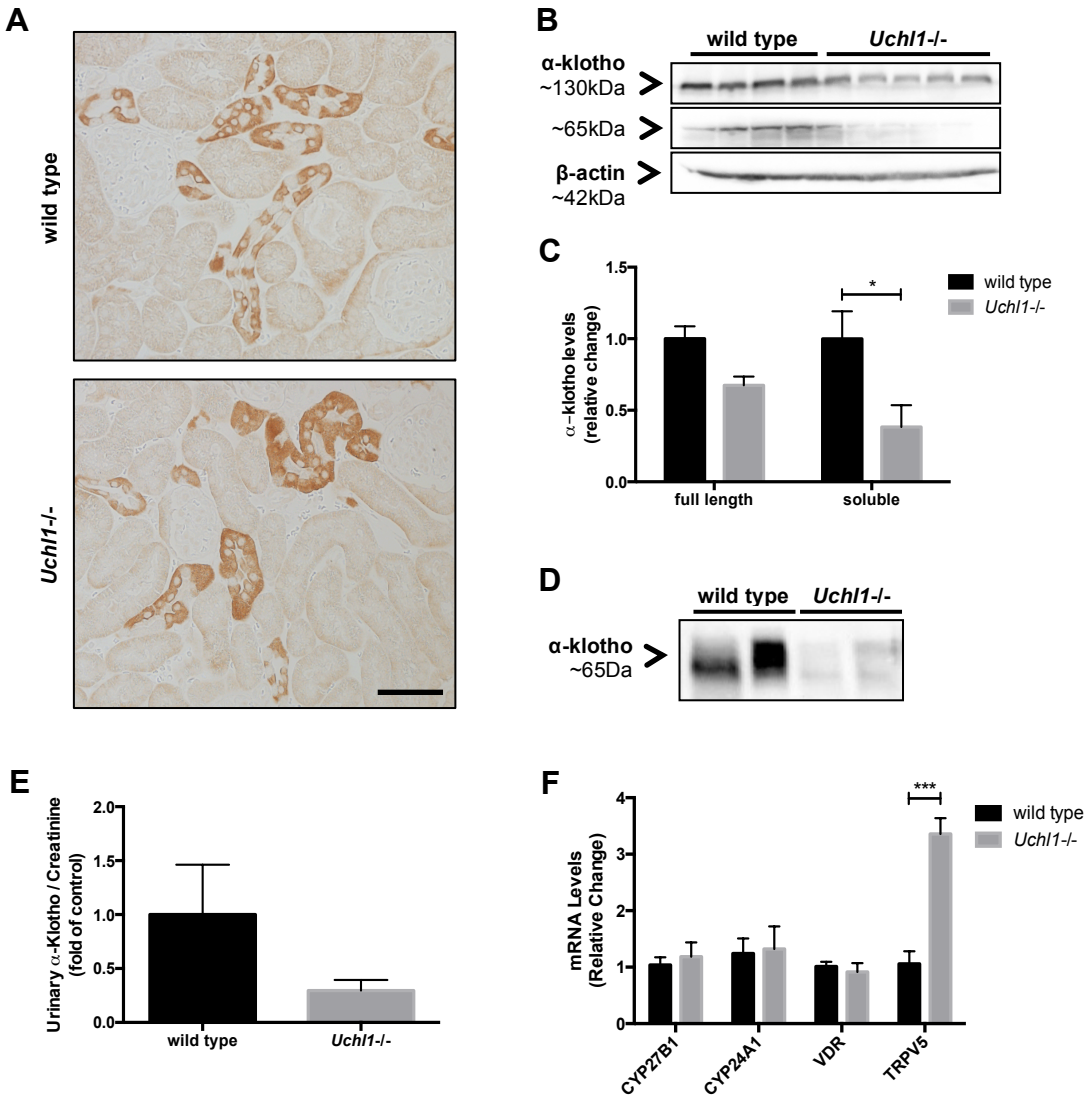

Figure 5. α-Klotho levels are attenuated in *Uchl1*-/- mice.
A. Immunohistochemistry revealed comparable α-klotho expression in distal tubules of wild type and *Uchl1*-/- mice (n=4-7). Scale bar = 50μm. **B.** Full length (130kDa) and soluble (65kDa) α-klotho protein levels were decreased in renal cortical lysates from *Uchl1*-/- mice, as determined by Western immunoblot (n=4-5). **C.** Densitometry graph depicting reduced full length and soluble α-klotho protein levels in renal cortical lysates from *Uchl1*-/- mice (n=4-5; $p<0.05$). Data depicts mean ± SE, analyzed by 2-way ANOVA with Sidak's multiple comparisons test. **D.** Western immunoblotting of urinary samples (25μl) using anti-α-klotho revealed a strong band between 50-75kDa (likely soluble α-klotho, ~65kDa) in wild type mice that was attenuated in *Uchl1*-/- mice (n=5). **E.** Densitometry graph depicting reduced soluble α-klotho expression levels (~65kDa) in spot urine samples from *Uchl1*-/- mice (n=5). Densitometry values were normalized to urinary creatinine. Data depicts mean ± SE, analyzed by unpaired t-test. **F.** TRPV5 mRNA, determined by qPCR, was significantly increased in renal cortical lysates of *Uchl1*-/- mice ($p<0.001$; n=5). Other elements involved in vitamin D biosynthesis and signaling were unaltered between groups (n=5). Data depicts mean ± SE, analyzed by 2-way ANOVA with Sidak's multiple comparisons test.

expression appeared comparable between groups (Figure 5A). However, Western immunoblotting revealed significantly attenuated α-klotho protein levels in renal cortical lysates from *Uchl1*-/- mice. Specifically, full length α-klotho protein levels were reduced by 1.5-fold, while soluble α-klotho protein levels were reduced by 2.6-fold ($p<0.05$) in *Uchl1*-/- mice (Figure 5B-C). Soluble α-klotho levels were also reduced by 1.7-fold in *Uchl1*-/- mice urine, although this was not statistically significant (Figure 5D-E). Since the expression of vitamin D regulatory enzymes and components of vitamin D signaling are altered in klotho-deficient kidneys, we assessed whether elements of 1,25-$(OH)_2$-D_3 metabolism were altered in *Uchl1*-/- mice.[13,22,25] CYP27B1, CYP24A1 and the vitamin D receptor (VDR) mRNA levels were unchanged, suggesting that 1,25-$(OH)_2$-D_3 levels may be unaltered in *Uchl1*-/- mice. Interestingly, we determined that TRPV5 mRNA levels were increased ($p<0.001$; by 3.1-fold) in *Uchl1*-/- mice (Figure 5F). Therefore, loss of α-klotho in *Uchl1*-/- mice likely results in impaired FGF23 signaling, sustained Npt2a and Npt2c expression, thereby promoting hyperphosphatemia.

A Phosphate-Deficient Diet Restores Phosphate Homeostasis in *Uchl1*-/- Mice

To determine whether phosphate homeostasis could be restored, *Uchl1*-/- mice were subjected to a low phosphate diet for 7 days. Body weights did not change over the course the study (data not shown). Plasma phosphate was significantly reduced to 0.9±0.1mM in *Uchl1*-/- mice subjected to a low phosphate diet, compared to 1.6±0.1mM in normal diet-fed *Uchl1*-/- controls ($p<0.0001$). These levels were comparable to wild type mice fed a low phosphate diet (0.6±0.1mM vs. 1.2±0.1mM for wild type + normal diet) (Figure 6A). While plasma calcium was significantly increased ($p<0.05$) to

2.3±0.1mM in *Uchl1*-/- mice fed a low phosphate diet (vs. 1.9±0.0mM for *Uchl1*-/- + normal diet), this increase was comparable to that of wild type mice fed a low phosphate diet (2.2±0.1mM; wild type + normal diet: 1.9±0.1mM) (Figure 6B). Urinary phosphate/creatinine ratios were decreased ($p<0.01$) to 0.1±0.0 in *Uchl1*-/- mice fed a low phosphate diet (vs. 9.1±2.6 for *Uchl1*-/- + normal diet) and this decrease was comparable to wild type mice fed a low phosphate diet (0.1±0.0; wild type + normal diet: 1.9±0.6) (Figure 6C). Urinary calcium/creatinine ratios were increased ($p<0.001$) in low phosphate diet-fed *Uchl1*-/- mice to 5.3±0.5 compared to 0.3±0.1 in normal diet-fed *Uchl1*-/- mice. This increase was similar to low phosphate diet-fed wild type mice (6.6±1.3; wild type + normal diet: 0.5±0.0) (Figure 6D). Similarly, fractional excretion of phosphate was significantly reduced ($p<0.05$) to 0.1±0.0% in *Uchl1*-/- mice subjected to a low phosphate diet (vs. 4.8±1.6% for *Uchl1*-/- + normal diet). This reduction was comparable to wild type mice fed a low phosphate diet (0.2±0.1%; wild type + normal diet: 1.6±0.5%) (Figure 6E). In contrast, fractional excretion of calcium was elevated ($p<0.01$) to 2.5±0.6% in low phosphate diet-fed *Uchl1*-/- mice (vs. 0.2±0.1% in *Uchl1*-/- + normal diet). These levels were relatively similar to wild type mice subjected to a low phosphate diet (4.8±0.7%; wild type + normal diet: 0.3±0.0) (Figure 6F). As such, these data suggest that phosphate homeostasis can be normalized in *Uchl1*-/- mice by lowering dietary phosphate intake.

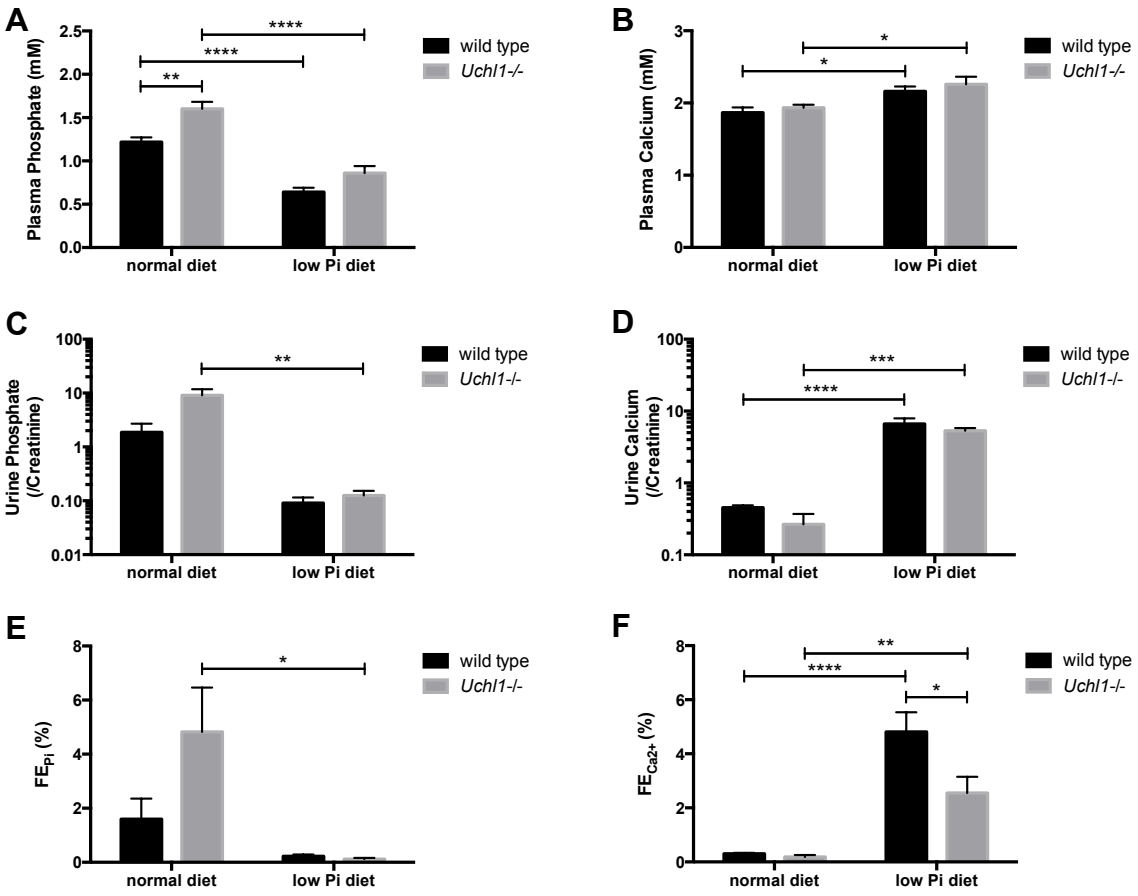

Figure 6. A low phosphate diet restores phosphate homeostasis in *Uchl1*-/- mice. **A.** Plasma phosphate levels were normalized in *Uchl1*-/- mice fed a low phosphate diet compared to their normal diet controls ($p<0.0001$; n=4-6). **B.** Plasma calcium was significantly increased in *Uchl1*-/- mice fed a low phosphate diet ($p<0.05$), but comparable to wild type mice fed a low phosphate diet (n=4-6). **C.** Urinary phosphate to creatinine ratios were significantly reduced in low phosphate diet-fed *Uchl1*-/- mice compared to normal diet controls ($p<0.01$; n=4-6). **D.** Urinary calcium to creatinine ratios were significantly increased in low phosphate diet-fed *Uchl1*-/- and wild type mice compared to their respective normal diet controls ($p<0.001$; n=4-6). **E.** Fractional excretion of phosphate (FE_{Pi}) was attenuated in *Uchl1*-/- mice fed a low phosphate diet ($p<0.05$; n=4-6). **F.** Fractional excretion of calcium (FE_{Ca2+}) was significantly increased in *Uchl1*-/- mice fed a low phosphate diet ($p<0.01$; n=4-6) but significantly lowered compared to wild type mice controls ($p<0.05$). Data depicts mean ± SE, analyzed by 2-way ANOVA with Sidak's multiple comparisons test.

Discussion

Uchl1-/- mice display disrupted phosphate homeostasis, namely hyperphosphatemia and phosphaturia, with unperturbed calcium homeostasis. No differences were identified in renal BBMVs Npt2a and Npt2c protein expression. Circulating PTH and FGF23 levels were unchanged in *Uchl1*-/- mice despite strong FGF23 mRNA induction in femur lysates. Components of the 1,25-$(OH)_2$-D_3 synthesis pathway were similarly unchanged. Intestinal phosphate absorption was ruled out as a contributor of hyperphosphatemia, however, lowering dietary phosphate intake restored phosphate homeostasis in *Uchl1*-/- mice. Finally, the expression of both the full length and soluble forms of α-klotho was attenuated in *Uchl1*-/- mice, suggesting that loss of α-klotho and loss of FGF23 signaling are likely culprits of perturbed phosphate homeostasis in *Uchl1*-/- mice.

Prolonged hyperphosphatemia can have a devastating impact on homeostasis as high phosphate levels promote cytotoxicity (6, 27, 35). Hyperphosphatemia is often associated with CKD and similarly, phosphate overloading can induce CKD in animals and humans (19, 24). In the present study, we identified a novel mouse model that exhibits phosphaturia associated with hyperphosphatemia. Unlike CKD models or other models that display severe hyperphosphatemia, *Uchl1*-/- mice maintain plasma phosphate levels near the upper range of normal (>1.45mM) or the lower range of what is considered mild hyperphosphatemia. As such, this may not render them susceptible the systemic cytotoxic effects associated with severe hyperphosphatemia (38).

Renal α-klotho deficiency in *Uchl1*-/- mice is indeed the major finding of this study and provides a likely explanation for phosphate homeostasis disruptions. The phenotypes observed in *Uchl1*-/- mice recapitulate in part the phenotypes observed in Ksp-KL$^{-/-}$ mice. Klotho deficiency leads to impaired FGF23 signaling and renal phosphate handling (23). Additionally, since klotho directly inhibits Npt2a, its absence promotes Npt2a stabilization (10). Other studies have also demonstrated that Npt2a expression is elevated in several mouse models lacking klotho in the proximal tubule (12, 23). Ksp-KL$^{-/-}$ mice are hyperphosphatemic, show increased circulating FGF23, lower circulating PTH, a mild increase in urinary calcium (likely stemming from reduced renal TRPV5 protein levels) and unchanged urinary phosphate (3, 23). In contrast to Ksp-KL$^{-/-}$ mice, *Uchl1*-/- mice demonstrate phosphaturia, unchanged plasma FGF23 (despite an increase in femur FGF23 mRNA levels) and unchanged calcium excretion, suggesting that *Uchl1*-/- mice harbour additional defects compared to Ksp-KL$^{-/-}$ mice. Similar to Ksp-KL$^{-/-}$ mice, *Uchl1*-/- mice display hyperphosphatemia and attenuated renal α-klotho levels. *Uchl1*-/- mice also display sustained Npt2a (and Npt2c) protein levels in renal BBMVs. By applying findings from klotho-deficient mouse models to our *Uchl1*-/- mice, we can conclude that loss of α-klotho impairs FGF23 signaling through the FGF23 receptors, leading to sustained Npt expression in renal BBMs.

Sustained Npt2a and Npt2c BBM expression/activity in the context of hyperphosphatemia likely further contribute to the phosphate imbalance determined in *Uchl1*-/- mice. The phosphaturia determined in *Uchl1*-/- mice is intriguing as neither Ksp-KL$^{-/-}$ mice or mice with proximal tubule-specific klotho deletion demonstrate this

phenotype (12, 23). Urinary phosphate trends lower in these models as a result of sustained Npt2a expression in renal BBMs. Additionally, strong Npt2a and Npt2c protein expression in *Uchl1*-deleted renal BBMs would suggest favourable phosphate reabsorption in the proximal tubule, which should offset the degree of phosphaturia. Since phosphaturia is observed, we can speculate that the phosphate load entering the renal proximal tubule may oversaturate the Npts leading to phosphaturia in *Uchl1*-/- mice. Moreover, our recent findings show that 12-week-old *Uchl1*-/- mice exhibit glomerular hyperfiltration, and as such, hyperfiltration may favour phosphate excretion (Boisvert *et al*, manuscript in preparation).

As previously mentioned, sustained Npt2a/Npt2c expression in renal BBMs likely further contributes to hyperphosphatemia in *Uchl1*-/- mice. But since these mice also demonstrate significant phosphaturia, unlike Ksp-KL$^{-/-}$ mice, we cannot exclude the possibility that hyperphosphatemia may arise from another (extra-renal) source. Indeed, hyperphosphatemia may result from progressive nerve and/or muscle damage as *Uchl1*-/- mice undergo neurodegeneration of the gracile tract between 6-12 weeks of age (4). Sensory ataxia predominates during this stage while motor ataxia manifests itself toward 16 weeks of age in *Uchl1*-/- mice (29). Phosphate resorption from the bone is possible, however, calcium homeostasis was intact at the chosen endpoint. Nonetheless, *Uchl1*-/- mice exhibit some bone alterations, namely scoliosis of the spine (22). We also observed trabecular bone hypotrophy in femur sections from *Uchl1*-/- mice (Figure 7), suggesting that bone resorption may contribute to hyperphosphatemia.

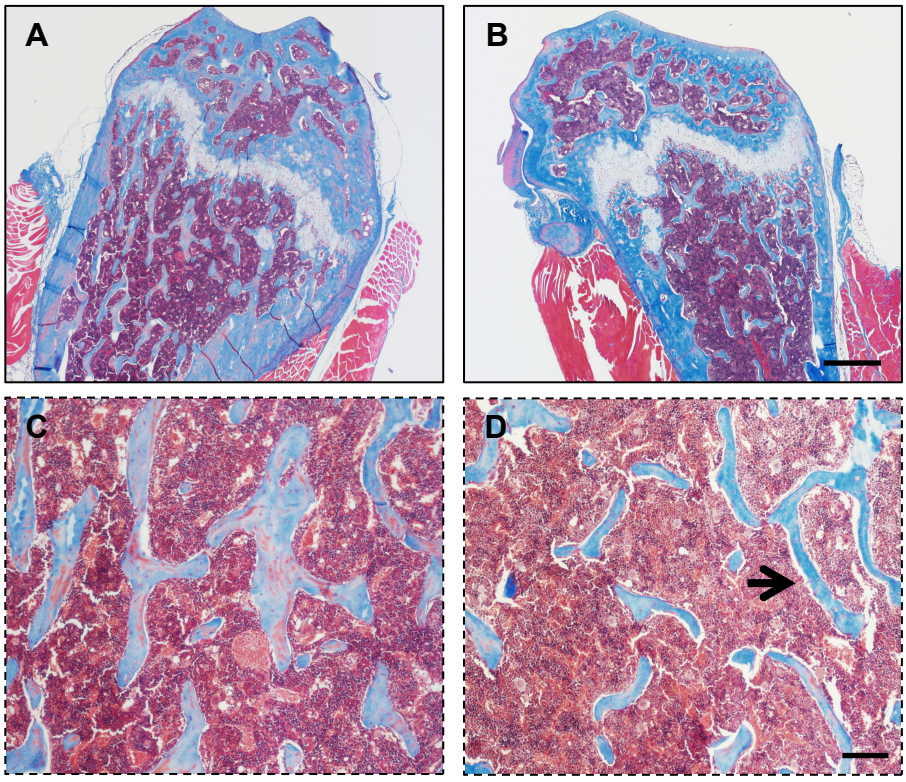

Figure 7. Trabecular bone density is reduced in *Uchl1*-/- mice. A-B. Masson's trichrome-stained femur sections revealed smaller and thinner trabecular bone structures in *Uchl1*-/- mice (**B**) compared to wild type mice (**A**) (n=6). Scale bar = 500µm. **C.** Inset from (**A**) and **D.** inset from (**B**) depicting reduced trabecular bone area (arrow) in *Uchl1*-/- mice compared to wild type mice (n=6). Scale bar = 100µm.

Under healthy conditions, a rise in plasma phosphate is accompanied by a concomitant increase in FGF23 that in turn normalizes phosphate homeostasis through its phosphaturic actions (15). Moreover, in the context of α-klotho deficiency, FGF23 levels are predicted to rise as a compensatory mechanism to disturbed FGF23 signaling and as observed in klotho-deficient models (12, 23). However, plasma FGF23 was unchanged in 12-week-old *Uchl1*-/- mice. Interestingly, FGF23 mRNA was significantly elevated in femur homogenates isolated from *Uchl1*-/- mice, suggesting that osteoblasts and osteocytes are responding to hyperphosphatemia by inducing FGF23 synthesis. It remains possible that FGF23 secretion from the bone is impaired in *Uchl1*-/- mice. Additionally,

since the degree of hyperphosphatemia is mild (1.6mM) in *Uchl1*-/- mice, a dramatic increase in circulating FGF23 levels may not be required. A modest rise in circulating FGF23 levels may therefore go undetected. Nonetheless, considering that α-klotho levels are attenuated in *Uchl1*-/- mice, renal FGF23 signaling is likely blunted.

Uchl1-/- mice display structural abnormalities in the enteric nervous system resulting in a gut motility deficit. Specifically, *Uchl1*-/- mice demonstrate increased gut transit time between 8-12 weeks of age, resembling that of 26-month old mice (5). Since the gut is the source of dietary phosphate absorption, primarily through Npt2b and paracellular diffusion, we postulated that reduced gastric motility in *Uchl1*-/- mice might contribute to increased phosphate absorption and hyperphosphatemia. Moreover, 1,25-$(OH)_2$-D_3 may also promote increased intestinal calcium/phosphate absorption (7). The contribution of the gut was however ruled out. While there was no evidence for increased intestinal phosphate absorption, we cannot exclude that increased gut transit time contributes to hyperphosphatemia in *Uchl1*-/- mice. And despite finding that a low phosphate diet normalized both urinary and plasma phosphate levels in *Uchl1*-/- mice, we can only conclude that phosphate homeostasis can be restored by lowering dietary phosphate.

The question remains, how does *Uchl1* deletion lead to α-klotho attenuation? α-Klotho attenuation can be achieved through angiotensin II signaling at the angiotensin type 1 receptor, however, in *Uchl1*-/- mice, we have previously determined that the renin angiotensin system is attenuated (Boisvert *et al*, manuscript in preparation) (20). Oxidative stress also reduces α-klotho and while oxidative stress has been demonstrated

in *Uchl1*-/- mice, this was not specifically investigated in the kidney (5, 21). Finally, we cannot ignore the function of *Uchl1*, a ubiquitin C-terminal hydrolase that may serve to stabilize α-klotho in renal tubules through its deubiquitination. Absence of UCHL1 disrupts the ubiquitin-proteasome system and may contribute to lowering α-klotho levels. It is also interesting to note that *Uchl1*-/- mice exhibit some similarities to kl/kl mice. Kl/kl mice exhibit an ageing-like phenotype, associated with osteoporosis, hypokinesis and gait disturbances comparable to humans with Parkinson's disease (16). Similarly, 12-week-old *Uchl1*-/- mice display scoliosis, sensory ataxia (followed by motor ataxia by 16 weeks of age) and gait paralysis consequent to neurodegeneration (22). *Uchl1*-/- mice also exhibit features typically observed in aged mice, including impaired gastric motility (5). Therefore, UCHL1 may be involved in α-klotho regulation.

Acknowledgements

The authors thank Dr. Yves Sabbagh for generously contributing the Npt2b antibody.

They are also grateful to Julie Zhu for her help with mice colony maintenance.

Grants

This work is supported by grants from the Kidney Foundation of Canada.

N.C.B. is a recipient of the Queen Elizabeth II Graduate Scholarship in Science and Technology (QEII-GSST).

Disclosures

Disclosures: None

References

1. **Beck L, Karaplis AC, Amizuka N, Hewson AS, Ozawa H, Tenenhouse HS**. Targeted inactivation of Npt2 in mice leads to severe renal phosphate wasting, hypercalciuria, and skeletal abnormalities. *Proc Natl Acad Sci U S A* 95: 5372-5377, 1998.
2. **Biber J, Stieger B, Stange G, Murer H**. Isolation of renal proximal tubular brush-border membranes. *Nat Protoc* 2: 1356-1359, 2007.
3. **Chang Q, Hoefs S, van der Kemp AW, Topala CN, Bindels RJ, Hoenderop JG**. The beta-glucuronidase klotho hydrolyzes and activates the TRPV5 channel. *Science* 310: 490-493, 2005.
4. **Chen F, Sugiura Y, Myers KG, Liu Y, Lin W**. Ubiquitin carboxyl-terminal hydrolase L1 is required for maintaining the structure and function of the neuromuscular junction. *Proc Natl Acad Sci U S A* 107: 1636-1641, 2010.
5. **Coulombe J, Gamage P, Gray MT, Zhang M, Tang MY, Woulfe J, Saffrey MJ, Gray DA**. Loss of UCHL1 promotes age-related degenerative changes in the enteric nervous system. *Front Aging Neurosci* 6: 129, 2014.
6. **Di Marco GS, Hausberg M, Hillebrand U, Rustemeyer P, Wittkowski W, Lang D, Pavenstadt H**. Increased inorganic phosphate induces human endothelial cell apoptosis in vitro. *Am J Physiol Renal Physiol* 294: F1381-1387, 2008.
7. **Fukumoto S**. Phosphate metabolism and vitamin D. *Bonekey Rep* 3: 497, 2014.
8. **Gattineni J, Alphonse P, Zhang Q, Mathews N, Bates CM, Baum M**. Regulation of renal phosphate transport by FGF23 is mediated by FGFR1 and FGFR4. *Am J Physiol Renal Physiol* 306: F351-358, 2014.
9. **Gutierrez OM, Mannstadt M, Isakova T, Rauh-Hain JA, Tamez H, Shah A, Smith K, Lee H, Thadhani R, Juppner H, Wolf M**. Fibroblast growth factor 23 and mortality among patients undergoing hemodialysis. *N Engl J Med* 359: 584-592, 2008.
10. **Hu MC, Shi M, Zhang J, Pastor J, Nakatani T, Lanske B, Razzaque MS, Rosenblatt KP, Baum MG, Kuro-o M, Moe OW**. Klotho: a novel phosphaturic substance acting as an autocrine enzyme in the renal proximal tubule. *FASEB J* 24: 3438-3450, 2010.
11. **Hu MC, Shi M, Zhang J, Quinones H, Griffith C, Kuro-o M, Moe OW**. Klotho deficiency causes vascular calcification in chronic kidney disease. *J Am Soc Nephrol* 22: 124-136, 2011.
12. **Ide N, Olauson H, Sato T, Densmore MJ, Wang H, Hanai J, Larsson TE, Lanske B**. In vivo evidence for a limited role of proximal tubular Klotho in renal phosphate handling. *Kidney Int* 90: 348-362, 2016.
13. **Isakova T, Xie H, Yang W, Xie D, Anderson AH, Scialla J, Wahl P, Gutierrez OM, Steigerwalt S, He J, Schwartz S, Lo J, Ojo A, Sondheimer J, Hsu CY, Lash J, Leonard M, Kusek JW, Feldman HI, Wolf M, Chronic Renal Insufficiency Cohort Study G**. Fibroblast growth factor 23 and risks of mortality and end-stage renal disease in patients with chronic kidney disease. *JAMA* 305: 2432-2439, 2011.
14. **Iwaki T, Sandoval-Cooper MJ, Tenenhouse HS, Castellino FJ**. A missense mutation in the sodium phosphate co-transporter Slc34a1 impairs phosphate homeostasis. *J Am Soc Nephrol* 19: 1753-1762, 2008.

15. **Kuro-o M**. Klotho, phosphate and FGF-23 in ageing and disturbed mineral metabolism. *Nat Rev Nephrol* 9: 650-660, 2013.
16. **Kuro-o M, Matsumura Y, Aizawa H, Kawaguchi H, Suga T, Utsugi T, Ohyama Y, Kurabayashi M, Kaname T, Kume E, Iwasaki H, Iida A, Shiraki-Iida T, Nishikawa S, Nagai R, Nabeshima YI**. Mutation of the mouse klotho gene leads to a syndrome resembling ageing. *Nature* 390: 45-51, 1997.
17. **Kurosu H, Ogawa Y, Miyoshi M, Yamamoto M, Nandi A, Rosenblatt KP, Baum MG, Schiavi S, Hu MC, Moe OW, Kuro-o M**. Regulation of fibroblast growth factor-23 signaling by klotho. *J Biol Chem* 281: 6120-6123, 2006.
18. **Lindberg K, Amin R, Moe OW, Hu MC, Erben RG, Ostman Wernerson A, Lanske B, Olauson H, Larsson TE**. The kidney is the principal organ mediating klotho effects. *J Am Soc Nephrol* 25: 2169-2175, 2014.
19. **Mackay EM, Oliver J**. Renal Damage Following the Ingestion of a Diet Containing an Excess of Inorganic Phosphate. *J Exp Med* 61: 319-334, 1935.
20. **Mitani H, Ishizaka N, Aizawa T, Ohno M, Usui S, Suzuki T, Amaki T, Mori I, Nakamura Y, Sato M, Nangaku M, Hirata Y, Nagai R**. In vivo klotho gene transfer ameliorates angiotensin II-induced renal damage. *Hypertension* 39: 838-843, 2002.
21. **Nagamine S, Kabuta T, Furuta A, Yamamoto K, Takahashi A, Wada K**. Deficiency of ubiquitin carboxy-terminal hydrolase-L1 (UCH-L1) leads to vulnerability to lipid peroxidation. *Neurochem Int* 57: 102-110, 2010.
22. **Oda K, Yamazaki K, Miura H, Shibasaki H, Kikuchi T**. Dying back type axonal degeneration of sensory nerve terminals in muscle spindles of the gracile axonal dystrophy (GAD) mutant mouse. *Neuropathol Appl Neurobiol* 18: 265-281, 1992.
23. **Olauson H, Lindberg K, Amin R, Jia T, Wernerson A, Andersson G, Larsson TE**. Targeted deletion of Klotho in kidney distal tubule disrupts mineral metabolism. *J Am Soc Nephrol* 23: 1641-1651, 2012.
24. **Ori Y, Herman M, Tobar A, Chernin G, Gafter U, Chagnac A, Izhak OB, Korzets A**. Acute phosphate nephropathy-an emerging threat. *Am J Med Sci* 336: 309-314, 2008.
25. **Osaka H, Wang YL, Takada K, Takizawa S, Setsuie R, Li H, Sato Y, Nishikawa K, Sun YJ, Sakurai M, Harada T, Hara Y, Kimura I, Chiba S, Namikawa K, Kiyama H, Noda M, Aoki S, Wada K**. Ubiquitin carboxy-terminal hydrolase L1 binds to and stabilizes monoubiquitin in neuron. *Hum Mol Genet* 12: 1945-1958, 2003.
26. **Perwad F, Azam N, Zhang MY, Yamashita T, Tenenhouse HS, Portale AA**. Dietary and serum phosphorus regulate fibroblast growth factor 23 expression and 1,25-dihydroxyvitamin D metabolism in mice. *Endocrinology* 146: 5358-5364, 2005.
27. **Reynolds JL, Joannides AJ, Skepper JN, McNair R, Schurgers LJ, Proudfoot D, Jahnen-Dechent W, Weissberg PL, Shanahan CM**. Human vascular smooth muscle cells undergo vesicle-mediated calcification in response to changes in extracellular calcium and phosphate concentrations: a potential mechanism for accelerated vascular calcification in ESRD. *J Am Soc Nephrol* 15: 2857-2867, 2004.
28. **Sabbagh Y, O'Brien SP, Song W, Boulanger JH, Stockmann A, Arbeeny C, Schiavi SC**. Intestinal npt2b plays a major role in phosphate absorption and homeostasis. *J Am Soc Nephrol* 20: 2348-2358, 2009.

29. **Saigoh K, Wang YL, Suh JG, Yamanishi T, Sakai Y, Kiyosawa H, Harada T, Ichihara N, Wakana S, Kikuchi T, Wada K**. Intragenic deletion in the gene encoding ubiquitin carboxy-terminal hydrolase in gad mice. *Nat Genet* 23: 47-51, 1999.
30. **Segawa H, Onitsuka A, Furutani J, Kaneko I, Aranami F, Matsumoto N, Tomoe Y, Kuwahata M, Ito M, Matsumoto M, Li M, Amizuka N, Miyamoto K**. Npt2a and Npt2c in mice play distinct and synergistic roles in inorganic phosphate metabolism and skeletal development. *Am J Physiol Renal Physiol* 297: F671-678, 2009.
31. **Shaman AM, Kowalski SR**. Hyperphosphatemia Management in Patients with Chronic Kidney Disease. *Saudi Pharm J* 24: 494-505, 2016.
32. **Shamseddin MK, Parfrey PS**. Sudden cardiac death in chronic kidney disease: epidemiology and prevention. *Nat Rev Nephrol* 7: 145-154, 2011.
33. **Shimada T, Hasegawa H, Yamazaki Y, Muto T, Hino R, Takeuchi Y, Fujita T, Nakahara K, Fukumoto S, Yamashita T**. FGF-23 is a potent regulator of vitamin D metabolism and phosphate homeostasis. *J Bone Miner Res* 19: 429-435, 2004.
34. **Shimada T, Kakitani M, Yamazaki Y, Hasegawa H, Takeuchi Y, Fujita T, Fukumoto S, Tomizuka K, Yamashita T**. Targeted ablation of Fgf23 demonstrates an essential physiological role of FGF23 in phosphate and vitamin D metabolism. *J Clin Invest* 113: 561-568, 2004.
35. **Shuto E, Taketani Y, Tanaka R, Harada N, Isshiki M, Sato M, Nashiki K, Amo K, Yamamoto H, Higashi Y, Nakaya Y, Takeda E**. Dietary phosphorus acutely impairs endothelial function. *J Am Soc Nephrol* 20: 1504-1512, 2009.
36. **Torres PU, Prie D, Molina-Bletry V, Beck L, Silve C, Friedlander G**. Klotho: an antiaging protein involved in mineral and vitamin D metabolism. *Kidney Int* 71: 730-737, 2007.
37. **Urakawa I, Yamazaki Y, Shimada T, Iijima K, Hasegawa H, Okawa K, Fujita T, Fukumoto S, Yamashita T**. Klotho converts canonical FGF receptor into a specific receptor for FGF23. *Nature* 444: 770-774, 2006.
38. **Vervloet MG, Sezer S, Massy ZA, Johansson L, Cozzolino M, Fouque D, Disease-Mineral E-EWGoCK, Bone D, the European Renal Nutrition Working G**. The role of phosphate in kidney disease. *Nat Rev Nephrol* 13: 27-38, 2017.
39. **Wilkinson KD, Lee KM, Deshpande S, Duerksen-Hughes P, Boss JM, Pohl J**. The neuron-specific protein PGP 9.5 is a ubiquitin carboxyl-terminal hydrolase. *Science* 246: 670-673, 1989.
40. **Yoshida T, Fujimori T, Nabeshima Y**. Mediation of unusually high concentrations of 1,25-dihydroxyvitamin D in homozygous klotho mutant mice by increased expression of renal 1alpha-hydroxylase gene. *Endocrinology* 143: 683-689, 2002.

GENERAL DISCUSSION

UCHL1 undoubtedly plays an important role in Ub maintenance and cellular function, and by extension, renal function and glomerular disease. The present studies demonstrate that global loss of *Uchl1* has differential effects on the kidney and these differences may largely be due to ablation of *Uchl1* in distinct cellular locales during specific challenges imposed upon the kidney. Global loss of *Uchl1* in a mouse model of *ACTN4*-associated FSGS ameliorated podocyte injury, albuminuria and glomerular lesions, suggesting that ablation of *Uchl1* in stressed podocytes is beneficial. However, global loss of *Uchl1* in mice also impacts renal hemodynamics, leading to glomerular hyperfiltration and increased RBF, a phenotype that may arise from loss of *Uchl1* in renal nerves. Finally, loss of *Uchl1* led to hyperphosphatemia and affected the kidney's ability to properly respond to hyperphosphatemia, as evidenced by sustained Npt2a/c expression and attenuated α-klotho levels. While it remains unclear how loss of *Uchl1* contributes to hyperphosphatemia in mice, there are no doubt alterations in *Uchl1*-deleted kidneys that impair their ability to respond to the perturbations in phosphate homeostasis. As such, it is fitting to conclude that *Uchl1* deletion in mice has direct and indirect effects on renal function and the benefits of UCHL1 ablation may differ according to the state of cellular distress (i.e. diseased vs. non-diseased kidneys).

Uchl1 Deletion Ameliorates Glomerular Injury in *ACTN4*-Associated FSGS

The notion that *Uchl1*-deleted K256E-*ACTN4*$^{pod+}$ mice demonstrate elevated albuminuria at 4 weeks of age that is significantly improved by 10 weeks of age is intriguing. The amelioration in albuminuria and other markers of podocyte injury is similar to findings of

Meyer-Schwesinger *et al* who demonstrated that UCHL1 inhibition in rats subjected to PHN led to improvements in albuminuria, associated with restoration of the Ub-proteasome (Meyer-Schwesinger et al., 2011). While the status of the Ub-proteasome is unclear in our model, we determined that K256E-α-actinin-4 expression levels were higher in *Uchl1*-deleted K256E-*ACTN4*$^{pod+}$ mice compared to K256E-*ACTN4*$^{pod+}$ mice, suggesting attenuated Ub-proteasome activity when *Uchl1* was deleted. We postulated that loss of UCHL1 and Ub levels in podocytes reduced poly-ubiquitination of K256E-α-actinin-4 (which can heterodimerize with wild type α-actinin-4), thereby stabilizing wild type/K256E-α-actinin-4 heterodimers and partially preserving podocyte architecture. However, this does not completely explain why albuminuria improvement is delayed.

While we proposed the latter mechanism to be the primary means responsible for the ameliorated phenotype in *Uchl1*-deleted K256E-*ACTN4*$^{pod+}$ mice, findings from our second study bring into question whether the alterations in renal hemodynamics characteristic of *Uchl1*-/- mice also contributed to the ameliorations observed. The onset of albuminuria in *Uchl1*-deleted K256E-*ACTN4*$^{pod+}$ mice at 4 weeks corresponds to a time point prior to sensory ataxia manifestation in *Uchl1* null mice. The improvement in albuminuria in 10-week-old *Uchl1*-deleted K256E-*ACTN4*$^{pod+}$ mice also corresponds a time point when neurodegeneration is well underway in *Uchl1*-/- mice and when these begin to display glomerular hyperfiltration (confirmed at 9 weeks of age). There is no doubt that the improvement in albuminuria in *Uchl1*-deleted K256E-*ACTN4*$^{pod+}$ mice correlates with the manifestation of glomerular hyperfiltration in *Uchl1*-/- mice. It is well documented that the onset of glomerular lesions in patients with FSGS is associated with

GFR decline, and this trend is likely in albuminuric K256E-*ACTN4*$^{pod+}$ mice. Loss of *Uchl1* may therefore prevent GFR decline in K256E-*ACTN4*$^{pod+}$ mice. Moreover, increased GFR and RBF associated with *Uchl1* deletion may promote adequate perfusion of the glomerulus further contributing to the improved podocyte phenotype.

Persistent elevations in GFR are associated with glomerular injury due to increased P_G. As a result, hyperfiltration in *Uchl1*-deleted K256E-*ACTN4*$^{pod+}$ mice may initially reverse the onset of injury, only to then delay it. When *Uchl1*-deleted mice were followed to 20 weeks of age these did not display significant changes in glomerular scarring or albuminuria. However, that is not to say that when superimposed with a model of glomerular injury such as our mouse model of *ACTN4*-associated FSGS, these would develop glomerular lesions resulting from sustained hyperfiltration at later time points. These implications need to be considered and further validated should UCHL1 be a target of future studies in glomerular injury, and more importantly, in therapies aimed at ameliorating chronic kidney disease.

Systolic blood pressure trends lower in *Uchl1*-/- mice compared to wild type mice at various time points between 6-12 weeks of age. *Uchl1*-deleted K256E-*ACTN4*$^{pod+}$ mice also displayed attenuated systolic blood pressure compared to K256E-*ACTN4*$^{pod+}$ mice controls. While components of the RAS (renin, ACE1) were upregulated in *Uchl1*-/- mice, we determined that the RAS may be attenuated in these mice as baseline plasma renin concentration trended lower and lisinopril treatment had no impact on systolic blood pressure or GFR. Accordingly, decreased RAS activity in K256E-*ACTN4*$^{pod+}$ mice

through *Uchl1* deletion may account for systolic blood pressure reductions in this group. Furthermore, reduced/dysregulated renal sympathetic tone may also account for the reduced systolic blood pressure when *Uchl1* is ablated. Renal denervation in patients with resistant hypertension (SYMPLICITY HTN-1/HTN-2 trials) significantly attenuated blood pressure (Krum et al., 2014, Symplicity et al., 2010). While it is unclear as to whether *Uchl1*-/- mice depict a true model of renal denervation, our second study provides evidence of renal nerve dysfunction as these displayed increased renal nerve arborization and decreased urinary NE. *Uchl1*-/- mice also demonstrated reduced Phe-induced vasoconstriction in mesenteric vessels, suggesting global impairment of sympathetic/vascular reactivity in this model. As such, it cannot be ruled out that nerve dysfunction and by extension ablated sympathetic activity (resulting from loss of UCHL1) may account for systolic blood pressure reductions in *Uchl1*-/- mice and in *Uchl1*-deleted K256E-*ACTN4*$^{pod+}$ mice.

Uchl1 Deletion Leads to Glomerular Hyperfiltration

As previously mentioned, glomerular hyperfiltration in *Uchl1*-/- mice is most likely a result of renal nerve dysfunction consequent to loss of UCHL1. In this study multiple sources that could contribute to glomerular hyperfiltration were ruled out, including increased nephron numbers, the RAS, hyperglycemia, COX-2-derived PGs and NOS-derived NO. Additionally, we provided evidence that attenuated renal sympathetic nerve activity is a strong candidate for glomerular hyperfiltration in *Uchl1*-/- mice. First, UCHL1 was extensively expressed in the renal nerves all throughout the kidney, including the finest axonal branches in the kidney. UCHL1 was also detectable in the

periglomerular region. Second, analyses of the renal nerves in *Uchl1*-deleted mice revealed increased renal nerve arborization compared to wild type mice. This may point to an early compensation to reduced neurotransmission. Third, DCE-MRI revealed increased cortical RBF in *Uchl1*-/- mice, suggesting that glomerular hyperfiltration stems from reduced resistance at the afferent arteriole, which is richly innervated. Fourth, mesenteric arteries isolated from *Uchl1*-/- mice display delayed vasoconstriction following adrenergic stimulation. Extrapolating these findings to renal vessels, specifically the afferent arteriole, would suggest loss of vascular resistance and increased P_G. Finally, urinary catecholamines, notably NE (and epinephrine, which trended lower), are reduced in *Uchl1*-/- mice suggesting that renal sympathetic tone is impaired. While these indirect assessments of renal sympathetic nerve activity provide considerable evidence for impaired neural input in the kidney, measuring renal sympathetic nerve activity would provide the most convincing evidence to this end. Although directly linking impaired renal sympathetic nerve activity to increased GFR is difficult to test. As such, it cannot be ruled out that dysregulated/reduced renal sympathetic nerve activity is a contributor to glomerular hyperfiltration in *Uchl1*-/- mice.

Renal denervation in animal models has yielded conflicting findings where many studies demonstrate a lack of effect on GFR. In contrast to these models, *Uchl1*-/- mice demonstrate glomerular hyperfiltration that we postulate is attributed to dyregulated/reduced renal sympathetic tone. In this model, renal sympathetic nerve activity may be progressively impaired as *Uchl1*-/- mice undergo progressive neurodegeneration. Renal denervation, on the other hand, results in a sudden

disconnection of the renal nerves through a surgical procedure. If our hypothesis stands correct and dyregulated/reduced renal sympathetic nerve activity is the source of glomerular hyperfiltration, then it remains to be determined which differences are present in our model that yield an increased GFR compared to other models of renal denervation. While renal denervation may result in the activation of compensatory mechanisms aimed at buffering afferent arteriole dilation (i.e. increased adenosine release), these mechanisms may otherwise be compromised in *Uchl1*-/- mice. Indeed, increases in arterial stretch due to increased RBF should lead to activation of the myogenic mechanism and TGF. This may in fact be the case in denervated kidneys. In *Uchl1*-/- mice however, autoregulation may be impaired, resulting in reduced afferent arteriole tone and glomerular hyperfiltration.

Uchl1 Deletion Leads to Altered Renal Phosphate Balance

Findings from the third study suggest that loss of *Uchl1* leads to perturbed phosphate homeostasis and renal handling of phosphate. The source of hyperphosphatemia in *Uchl1*-/- mice remains inconclusive as we cannot completely exclude the contribution of nerve degeneration, muscle wasting, bone resorption and finally, increased intestinal absorption. The onset of phosphaturia in *Uchl1*-/- mice in a hyperphosphatemic state would normally be an adaptive mechanism to couterbalance increases in circulating phosphate. However, phosphaturia in several models (i.e. Npt2a-/- mice, patients with hereditary hypophosphatemic rickets with hypercalciuria) generally results from the downregulation of sodium-phosphate cotransporters in the renal proximal tubule (Bergwitz et al., 2006, Segawa et al., 2009). In contrast, *Uchl1*-/- mice display wild type-

comparable Npt2a and Npt2c expression levels in renal BBMVs. In the kidney, the main phosphate transporters (Npt2a, Npt2c and Pit2) are expressed in the proximal tubule. As such, phosphate reabsorption is limited to a small number of phosphate transporters expressed exclusively in the proximal tubule. Considering that *Uchl1*-/- mice hyperfilter, phosphate entering the urinary filtrate is therefore subject to high flow rates as it travels through the proximal tubule, which may decrease its likelihood of being reabsorbed. Since there are no known mechanisms of phosphate fine-tuning downstream of the proximal tubule, phosphate meets its fate as it is excreted into the urine of *Uchl1*-/- mice. In this case, glomerular hyperfiltration is beneficial as it promotes phosphaturia, whereas sustained Npt2a and Npt2c expression is maladaptive, as it promotes a certain degree of phosphate reabsorption and contributes to hyperphosphatemia in *Uchl1*-/- mice.

In chronic kidney disease, patients suffer from hyperphosphatemia and display reduced klotho levels. *Uchl1*-/- mice similarly display these features, but hyperphosphatemia is milder. In contrast to patients with chronic kidney disease wherein hyperphosphatemia results from progressive renal damage and the inability to adequately clear phosphate, *Uchl1*-/- mice do not exhibit renal damage and these maintain the ability to excrete phosphate. Moreover, patients with chronic kidney disease display hyperphosphatemia that is associated with progressive GFR decline, whereas *Uchl1*-/- mice display hyperphosphatemia associated with glomerular hyperfiltration. Therefore the root of hyperphosphatemia and ability to excrete phosphate in *Uchl1*-/- mice is not comparable to patients with chronic kidney disease. Nevertheless, these mice may provide a useful tool to draw parallels to patients affected by this disease. Importantly, studying *Uchl1*

deletion in a model of glomerular disease may exacerbate hyperphosphatemia. Although plasma and urinary phosphate levels were not specifically examined in *Uchl1*-deleted K256E-*ACTN4*$^{pod+}$ mice, we predict that hyperphosphatemia may be further impaired (at least at 4 weeks of age, when albuminuria is elevated) and may promote other complications such as vascular calcification. In fact, since hyperphosphatemia is mild in *Uchl1*-/- mice, further work characterizing renal phosphate handling following a high phosphate challenge would help provide further insight as to the ability of these mice to handle phosphate.

Conclusions, Perspectives and Future Work

In summary, we have identified a role for UCHL1 in renal function, renal hemodynamics and glomerular disease. In diseased podocytes overexpressing K256E-α-actinin-4, we determined that UCHL1 plays a maladaptive role, likely by over-fueling the Ub-proteasome. Our findings corroborate those by others that have demonstrated that UCHL1 inhibition improved glomerular disease and Ub-proteasome function. While ablation of UCHL1 in glomerular disease has proven to be beneficial, future work investigating UCHL1 in glomerular disease will need to be informed by our findings that *Uchl1*-/- mice display altered glomerular hemodynamics and renal function, namely glomerular hyperfiltration and hyperphosphatemia. Both glomerular hyperfiltration and hyperphosphatemia are associated with negative outcomes in glomerular disease and chronic kidney disease. *Uchl1*-/- mice may provide a useful model to study glomerular hyperfiltration and perturbed phosphate homeostasis. However, these parameters will

need to be carefully considered when studying *Uchl1* ablation in glomerular disease models and other non-renal models of injury.

It remains to be determined whether UCHL1 inhibition in mice leads to comparable changes to renal hemodynamics and phosphate homeostasis as observed in *Uchl1*-deleted mice. A conditional *Uchl1* knockout mouse model would also help delineate whether *Uchl1* ablation alone promotes glomerular hyperfiltration and dysregulated phosphate homeostasis or whether these phenotypes result from *Uchl1* loss during mouse development. Perhaps the most informative experiment would be conditionally knocking out *Uchl1* exclusively in neurons, which would tease out the effects of *Uchl1* loss in other cellular locales and determine with greater certainty whether changes to renal hemodynamics are linked to neuronal UCHL1. These experiments would also delineate the effects of neuronal UCHL1 to perturbed phosphate homeostasis and renal phosphate handling.

Moreover, studying UCHL1 inhibition in *ACTN4*-associated FSGS or other mouse models of glomerular disease would strengthen the findings from the first study. These studies would help identify the developmental role of UCHL1 resulting in progressive neurodegeneration versus the effects of attenuating UCHL1 post-development. In this case a conditional knockout approach would also be informative. However, given the fact that global *Uchl1* deletion leads to other renal phenotypes that may confound the findings observed in animal models of glomerular disease, taking advantage of a cell-specific

knockout (such as a podocyte-specific *Uchl1* knockout) would be a more stringent method of evaluating the role of podocyte UCHL1 in glomerular disease.

REFERENCES

1. Abe, S. and K. Maruyama. 1973. Effect of alpha-actinin on F-actin. A dynamic viscoelastic study. Journal of Biochemistry. 73, 1205-1210.
2. Alberola, A.M., F.J. Salazar, T. Nakamura and J.P. Granger. 1994. Interaction between angiotensin II and nitric oxide in control of renal hemodynamics in conscious dogs. American Journal of Physiology. 267, R1472-1478.
3. Barajas, L., K. Powers and P. Wang. 1984. Innervation of the renal cortical tubules: a quantitative study. American Journal of Physiology. 247, F50-60.
4. Barajas, L., L. Liu and K. Powers. 1992. Anatomy of the renal innervation: intrarenal aspects and ganglia of origin. Canadian Journal of Physiology and Pharmacology. 70, 735-749.
5. Baumann, J.E., P.B. Persson, H. Ehmke, B. Nafz and H.R. Kirchheim. 1992. Role of endothelium-derived relaxing factor in renal autoregulation in conscious dogs. American Journal of Physiology. 263, F208-213.
6. Beggs, A.H., T.J. Byers, J.H. Knoll, F.M. Boyce, G.A. Bruns and L.M. Kunkel. 1992. Cloning and characterization of two human skeletal muscle alpha-actinin genes located on chromosomes 1 and 11. Journal of Biological Chemistry. 267, 9281-9288.
7. Bergwitz, C., N.M. Roslin, M. Tieder, J.C. Loredo-Osti, M. Bastepe, H. Abu-Zahra, D. Frappier, K. Burkett, T.O. Carpenter, D. Anderson, M. Garabedian, I. Sermet, T.M. Fujiwara, K. Morgan, H.S. Tenenhouse and H. Juppner. 2006. SLC34A3 mutations in patients with hereditary hypophosphatemic rickets with hypercalciuria predict a key role for the sodium-phosphate cotransporter NaPi-IIc in maintaining phosphate homeostasis. American Journal of Human Genetics. 78, 179-192.
8. Berthold, H., A. Just, H.R. Kirchheim and H. Ehmke. 1999. Interaction between nitric oxide and endogenous vasoconstrictors in control of renal blood flow. Hypertension. 34, 1254-1258.
9. Bishop, P., D. Rocca and J.M. Henley. 2016. Ubiquitin C-terminal hydrolase L1 (UCH-L1): structure, distribution and roles in brain function and dysfunction. Biochemical Journal. 473, 2453-2462.
10. Boute, N., O. Gribouval, S. Roselli, F. Benessy, H. Lee, A. Fuchshuber, K. Dahan, M.C. Gubler, P. Niaudet and C. Antignac. 2000. NPHS2, encoding the glomerular protein podocin, is mutated in autosomal recessive steroid-resistant nephrotic syndrome. Nature Genetics. 24, 349-354.
11. Bradbury, J.M. and R.J. Thompson. 1985. Immunoassay of the neuronal and neuroendocrine marker PGP 9.5 in human tissues. Journal of Neurochemistry. 44, 651-653.
12. Brown, E.J., J.S. Schlondorff, D.J. Becker, H. Tsukaguchi, S.J. Tonna, A.L. Uscinski, H.N. Higgs, J.M. Henderson and M.R. Pollak. 2010. Mutations in the formin gene INF2 cause focal segmental glomerulosclerosis. Nature Genetics. 42, 72-76.
13. Burgie, S.E., C.A. Bingman, A.B. Soni and G.N. Phillips, Jr. 2012. Structural characterization of human Uch37. Proteins. 80, 649-654.

14. Burke, M., M.R. Pabbidi, J. Farley and R.J. Roman. 2014. Molecular mechanisms of renal blood flow autoregulation. Current Vascular Pharmacology. 12, 845-858.
15. Carmines, P.K., T.K. Morrison and L.G. Navar. 1986. Angiotensin II effects on microvascular diameters of in vitro blood-perfused juxtamedullary nephrons. American Journal of Physiology. 251, F610-618.
16. Caverson, M.M. and J. Ciriello. 1987. Effect of stimulation of afferent renal nerves on plasma levels of vasopressin. American Journal of Physiology. 252, R801-807.
17. Chen, F., Y. Sugiura, K.G. Myers, Y. Liu and W. Lin. 2010. Ubiquitin carboxyl-terminal hydrolase L1 is required for maintaining the structure and function of the neuromuscular junction. Proceedings of the National Academy of Sciences of the United States of America. 107, 1636-1641.
18. Chen, W.T. and S.J. Singer. 1982. Immunoelectron microscopic studies of the sites of cell-substratum and cell-cell contacts in cultured fibroblasts. Journal of Cell Biology. 95, 205-222.
19. Cheng, H.F., J.L. Wang, M.Z. Zhang, Y. Miyazaki, I. Ichikawa, J.A. McKanna and R.C. Harris. 1999. Angiotensin II attenuates renal cortical cyclooxygenase-2 expression. Journal of Clinical Investigation. 103, 953-961.
20. Cheng, H.F., J.L. Wang, M.Z. Zhang, S.W. Wang, J.A. McKanna and R.C. Harris. 2001. Genetic deletion of COX-2 prevents increased renin expression in response to ACE inhibition. American Journal of Physiology: Renal Physiology. 280, F449-456.
21. Ciriello, J. and F.R. Calaresu. 1983. Central projections of afferent renal fibers in the rat: an anterograde transport study of horseradish peroxidase. Journal of the Autonomic Nervous System. 8, 273-285.
22. Ciriello, J., M.M. Caverson and C. Polosa. 1986. Function of the ventrolateral medulla in the control of the circulation. Brain Research. 396, 359-391.
23. Coleman, M. 2005. Axon degeneration mechanisms: commonality amid diversity. Nature Reviews: Neuroscience. 6, 889-898.
24. Cortes, P., M. Mendez, B.L. Riser, C.J. Guerin, A. Rodriguez-Barbero, C. Hassett and J. Yee. 2000. F-actin fiber distribution in glomerular cells: structural and functional implications. Kidney International. 58, 2452-2461.
25. Coulombe, J., P. Gamage, M.T. Gray, M. Zhang, M.Y. Tang, J. Woulfe, M.J. Saffrey and D.A. Gray. 2014. Loss of UCHL1 promotes age-related degenerative changes in the enteric nervous system. Frontiers in Aging Neuroscience. 6, 129.
26. Cybulsky, A.V., T. Takano, J. Papillon, K. Bijian, J. Guillemette and C.R. Kennedy. 2009. Glomerular epithelial cell injury associated with mutant alpha-actinin-4. American Journal of Physiology: Renal Physiology. 297, F987-995.
27. Dai, S., Z. Wang, X. Pan, X. Chen, W. Wang, H. Ren, Q. Feng, J.C. He, B. Han and N. Chen. 2009. ACTN4 gene mutations and single nucleotide polymorphisms in idiopathic focal segmental glomerulosclerosis. Nephron: Clinical Practice. 111, c87-94.
28. Dai, S., Z. Wang, X. Pan, W. Wang, X. Chen, H. Ren, C. Hao, B. Han and N. Chen. 2010. Functional analysis of promoter mutations in the ACTN4 and SYNPO genes in focal segmental glomerulosclerosis. Nephrology, Dialysis and Transplantation. 25, 824-835.

29. Dandapani, S.V., H. Sugimoto, B.D. Matthews, R.J. Kolb, S. Sinha, R.E. Gerszten, J. Zhou, D.E. Ingber, R. Kalluri and M.R. Pollak. 2007. Alpha-actinin-4 is required for normal podocyte adhesion. Journal of Biological Chemistry. 282, 467-477.
30. Day, I.N. and R.J. Thompson. 2010. UCHL1 (PGP 9.5): neuronal biomarker and ubiquitin system protein. Progress in Neurobiology. 90, 327-362.
31. Diomedi-Camassei, F., L. Rava, E. Lerut, F. Callea and B. Van Damme. 2005. Protein gene product 9.5 and ubiquitin are expressed in metabolically active epithelial cells of normal and pathologic human kidney. Nephrology, Dialysis and Transplantation. 20, 2714-2719.
32. Dixson, J.D., M.J. Forstner and D.M. Garcia. 2003. The alpha-actinin gene family: a revised classification. Journal of Molecular Evolution. 56, 1-10.
33. Djinovic-Carugo, K., P. Young, M. Gautel and M. Saraste. 1999. Structure of the alpha-actinin rod: molecular basis for cross-linking of actin filaments. Cell. 98, 537-546.
34. Drenckhahn, D. and R.P. Franke. 1988. Ultrastructural organization of contractile and cytoskeletal proteins in glomerular podocytes of chicken, rat, and man. Laboratory Investigation. 59, 673-682.
35. Ellederova, Z., P. Halada, P. Man, M. Kubelka, J. Motlik and H. Kovarova. 2004. Protein patterns of pig oocytes during in vitro maturation. Biology of Reproduction. 71, 1533-1539.
36. Endo, T. and T. Masaki. 1984. Differential expression and distribution of chicken skeletal- and smooth-muscle-type alpha-actinins during myogenesis in culture. Journal of Cell Biology. 99, 2322-2332.
37. Franco-Cereceda, A., H. Henke, J.M. Lundberg, J.B. Petermann, T. Hokfelt and J.A. Fischer. 1987. Calcitonin gene-related peptide (CGRP) in capsaicin-sensitive substance P-immunoreactive sensory neurons in animals and man: distribution and release by capsaicin. Peptides. 8, 399-410.
38. Fukuda, T., T. Tsuruga, T. Kuroda, H. Nishikawa and T. Ohta. 2016. Functional Link between BRCA1 and BAP1 through Histone H2A, Heterochromatin and DNA Damage Response. Current Cancer Drug Targets. 16, 101-109.
39. Fukumoto, S. 2014. Phosphate metabolism and vitamin D. Bonekey Rep. 3, 497.
40. Furukawa, T., S. Ohno, H. Oguchi, K. Hora, S. Tokunaga and S. Furuta. 1991. Morphometric study of glomerular slit diaphragms fixed by rapid-freezing and freeze-substitution. Kidney International. 40, 621-624.
41. Gattineni, J., P. Alphonse, Q. Zhang, N. Mathews, C.M. Bates and M. Baum. 2014. Regulation of renal phosphate transport by FGF23 is mediated by FGFR1 and FGFR4. American Journal of Physiology: Renal Physiology. 306, F351-358.
42. Greka, A. and P. Mundel. 2012. Cell biology and pathology of podocytes. Annual Review of Physiology. 74, 299-323.
43. Grou, C.P., M.P. Pinto, A.V. Mendes, P. Domingues and J.E. Azevedo. 2015. The de novo synthesis of ubiquitin: identification of deubiquitinases acting on ubiquitin precursors. Scientific Reports. 5, 12836.
44. Guyton, A.C. and J.E. Hall. 2007. Guyton and Hall, Textbook of Medical Physiology. 11th edition. (University of Michigan: Elsevier Saunders).

45. Handa, R.K. and E.J. Johns. 1985. Interaction of the renin-angiotensin system and the renal nerves in the regulation of rat kidney function. Journal of Physiology. 369, 311-321.
46. Hao, C.M. and M.D. Breyer. 2008. Physiological regulation of prostaglandins in the kidney. Annual Review of Physiology. 70, 357-377.
47. Hesse, I.F. and E.J. Johns. 1984. The effect of graded renal nerve stimulation on renal function in the anaesthetized rabbit. Comparative Biochemistry and Physiology. A: Comparative Physiology. 79, 409-414.
48. Honda, K., T. Yamada, R. Endo, Y. Ino, M. Gotoh, H. Tsuda, Y. Yamada, H. Chiba and S. Hirohashi. 1998. Actinin-4, a novel actin-bundling protein associated with cell motility and cancer invasion. Journal of Cell Biology. 140, 1383-1393.
49. Housley, G.D., R.L. Martin-Body, N.J. Dawson and J.D. Sinclair. 1987. Brain stem projections of the glossopharyngeal nerve and its carotid sinus branch in the rat. Neuroscience. 22, 237-250.
50. Hu, M.C., M. Shi, J. Zhang, J. Pastor, T. Nakatani, B. Lanske, M.S. Razzaque, K.P. Rosenblatt, M.G. Baum, M. Kuro-o and O.W. Moe. 2010. Klotho: a novel phosphaturic substance acting as an autocrine enzyme in the renal proximal tubule. FASEB Journal. 24, 3438-3450.
51. Ichihara, A., E.W. Inscho, J.D. Imig and L.G. Navar. 1998. Neuronal nitric oxide synthase modulates rat renal microvascular function. American Journal of Physiology. 274, F516-524.
52. Ichihara, N., J. Wu, D.H. Chui, K. Yamazaki, T. Wakabayashi and T. Kikuchi. 1995. Axonal degeneration promotes abnormal accumulation of amyloid beta-protein in ascending gracile tract of gracile axonal dystrophy (GAD) mouse. Brain Research. 695, 173-178.
53. Ide, N., H. Olauson, T. Sato, M.J. Densmore, H. Wang, J. Hanai, T.E. Larsson and B. Lanske. 2016. In vivo evidence for a limited role of proximal tubular Klotho in renal phosphate handling. Kidney International. 90, 348-362.
54. Jang, M.J., S.H. Baek and J.H. Kim. 2011. UCH-L1 promotes cancer metastasis in prostate cancer cells through EMT induction. Cancer Letters. 302, 128-135.
55. Jara, J.H., B. Genc, G.A. Cox, M.C. Bohn, R.P. Roos, J.D. Macklis, E. Ulupinar and P.H. Ozdinler. 2015. Corticospinal Motor Neurons Are Susceptible to Increased ER Stress and Display Profound Degeneration in the Absence of UCHL1 Function. Cerebral Cortex. 25, 4259-4272.
56. Johns, E.J., B.A. Lewis and B. Singer. 1976. The sodium-retaining effect of renal nerve activity in the cat: role of angiotensin formation. Clinical Science and Molecular Medicine. 51, 93-102.
57. Johns, E.J., U.C. Kopp and G.F. DiBona. 2011. Neural control of renal function. Compr Physiol. 1, 731-767.
58. Kaplan, J.M., S.H. Kim, K.N. North, H. Rennke, L.A. Correia, H.Q. Tong, B.J. Mathis, J.C. Rodriguez-Perez, P.G. Allen, A.H. Beggs and M.R. Pollak. 2000. Mutations in ACTN4, encoding alpha-actinin-4, cause familial focal segmental glomerulosclerosis. Nature Genetics. 24, 251-256.
59. Kestila, M., U. Lenkkeri, M. Mannikko, J. Lamerdin, P. McCready, H. Putaala, V. Ruotsalainen, T. Morita, M. Nissinen, R. Herva, C.E. Kashtan, L. Peltonen, C.

Holmberg, A. Olsen and K. Tryggvason. 1998. Positionally cloned gene for a novel glomerular protein--nephrin--is mutated in congenital nephrotic syndrome. Molecular Cell. 1, 575-582.
60. Kikuchi, T., M. Mukoyama, K. Yamazaki and H. Moriya. 1990. Axonal degeneration of ascending sensory neurons in gracile axonal dystrophy mutant mouse. Acta Neuropathologica. 80, 145-151.
61. Kim, H.J., Y.M. Kim, S. Lim, Y.K. Nam, J. Jeong, H.J. Kim and K.J. Lee. 2009. Ubiquitin C-terminal hydrolase-L1 is a key regulator of tumor cell invasion and metastasis. Oncogene. 28, 117-127.
62. Kim, J.M., H. Wu, G. Green, C.A. Winkler, J.B. Kopp, J.H. Miner, E.R. Unanue and A.S. Shaw. 2003. CD2-associated protein haploinsufficiency is linked to glomerular disease susceptibility. Science. 300, 1298-1300.
63. Kim, S.M., L. Chen, D. Mizel, Y.G. Huang, J.P. Briggs and J. Schnermann. 2007. Low plasma renin and reduced renin secretory responses to acute stimuli in conscious COX-2-deficient mice. American Journal of Physiology: Renal Physiology. 292, F415-422.
64. Kobayashi, N. and P. Mundel. 1998. A role of microtubules during the formation of cell processes in neuronal and non-neuronal cells. Cell and Tissue Research. 291, 163-174.
65. Kompanowska-Jezierska, E., A. Walkowska, E.J. Johns and J. Sadowski. 2001. Early effects of renal denervation in the anaesthetised rat: natriuresis and increased cortical blood flow. Journal of Physiology. 531, 527-534.
66. Kos, C.H., T.C. Le, S. Sinha, J.M. Henderson, S.H. Kim, H. Sugimoto, R. Kalluri, R.E. Gerszten and M.R. Pollak. 2003. Mice deficient in alpha-actinin-4 have severe glomerular disease. Journal of Clinical Investigation. 111, 1683-1690.
67. Krum, H., M. Schlaich, R. Whitbourn, P.A. Sobotka, J. Sadowski, K. Bartus, B. Kapelak, A. Walton, H. Sievert, S. Thambar, W.T. Abraham and M. Esler. 2009. Catheter-based renal sympathetic denervation for resistant hypertension: a multicentre safety and proof-of-principle cohort study. Lancet. 373, 1275-1281.
68. Krum, H., M.P. Schlaich, P.A. Sobotka, M. Bohm, F. Mahfoud, K. Rocha-Singh, R. Katholi and M.D. Esler. 2014. Percutaneous renal denervation in patients with treatment-resistant hypertension: final 3-year report of the Symplicity HTN-1 study. Lancet. 383, 622-629.
69. Kurts, C., U. Panzer, H.J. Anders and A.J. Rees. 2013. The immune system and kidney disease: basic concepts and clinical implications. Nature Reviews: Immunology. 13, 738-753.
70. Langanger, G., J. de Mey, M. Moeremans, G. Daneels, M. de Brabander and J.V. Small. 1984. Ultrastructural localization of alpha-actinin and filamin in cultured cells with the immunogold staining (IGS) method. Journal of Cell Biology. 99, 1324-1334.
71. Larsen, C.N., B.A. Krantz and K.D. Wilkinson. 1998. Substrate specificity of deubiquitinating enzymes: ubiquitin C-terminal hydrolases. Biochemistry. 37, 3358-3368.
72. Lazarides, E. and K. Burridge. 1975. Alpha-actinin: immunofluorescent localization of a muscle structural protein in nonmuscle cells. Cell. 6, 289-298.

73. Majid, D.S. and L.G. Navar. 2001. Nitric oxide in the control of renal hemodynamics and excretory function. American Journal of Hypertension. 14, 74S-82S.
74. Mann, B., A. Hartner, B.L. Jensen, M. Kammerl, B.K. Kramer and A. Kurtz. 2001. Furosemide stimulates macula densa cyclooxygenase-2 expression in rats. Kidney International. 59, 62-68.
75. Manning, R.D., Jr., L. Hu, H.L. Mizelle and J.P. Granger. 1993. Role of nitric oxide in long-term angiotensin II-induced renal vasoconstriction. Hypertension. 21, 949-955.
76. Mathis, B.J., S.H. Kim, K. Calabrese, M. Haas, J.G. Seidman, C.E. Seidman and M.R. Pollak. 1998. A locus for inherited focal segmental glomerulosclerosis maps to chromosome 19q13. Kidney International. 53, 282-286.
77. Meigs, J.B. and Y.L. Wang. 1986. Reorganization of alpha-actinin and vinculin induced by a phorbol ester in living cells. Journal of Cell Biology. 102, 1430-1438.
78. Meyer-Schwesinger, C., T.N. Meyer, S. Munster, P. Klug, M. Saleem, U. Helmchen and R.A. Stahl. 2009. A new role for the neuronal ubiquitin C-terminal hydrolase-L1 (UCH-L1) in podocyte process formation and podocyte injury in human glomerulopathies. Journal of Pathology. 217, 452-464.
79. Meyer-Schwesinger, C., T.N. Meyer, H. Sievert, E. Hoxha, M. Sachs, E.M. Klupp, S. Munster, S. Balabanov, L. Carrier, U. Helmchen, F. Thaiss and R.A. Stahl. 2011. Ubiquitin C-terminal hydrolase-l1 activity induces polyubiquitin accumulation in podocytes and increases proteinuria in rat membranous nephropathy. American Journal of Pathology. 178, 2044-2057.
80. Michaud, J.L., L.I. Lemieux, M. Dube, B.C. Vanderhyden, S.J. Robertson and C.R. Kennedy. 2003. Focal and segmental glomerulosclerosis in mice with podocyte-specific expression of mutant alpha-actinin-4. Journal of the American Society of Nephrology. 14, 1200-1211.
81. Michaud, J.L., K.M. Chaisson, R.J. Parks and C.R. Kennedy. 2006. FSGS-associated alpha-actinin-4 (K256E) impairs cytoskeletal dynamics in podocytes. Kidney International. 70, 1054-1061.
82. Miyoshi, Y., S. Nakayama, Y. Torikoshi, S. Tanaka, H. Ishihara, T. Taguchi, Y. Tamaki and S. Noguchi. 2006. High expression of ubiquitin carboxy-terminal hydrolase-L1 and -L3 mRNA predicts early recurrence in patients with invasive breast cancer. Cancer Science. 97, 523-529.
83. Mukoyama, M., K. Yamazaki, T. Kikuchi and T. Tomita. 1989. Neuropathology of gracile axonal dystrophy (GAD) mouse. An animal model of central distal axonopathy in primary sensory neurons. Acta Neuropathologica. 79, 294-299.
84. Oda, K., K. Yamazaki, H. Miura, H. Shibasaki and T. Kikuchi. 1992. Dying back type axonal degeneration of sensory nerve terminals in muscle spindles of the gracile axonal dystrophy (GAD) mutant mouse. Neuropathology and Applied Neurobiology. 18, 265-281.
85. Olauson, H., K. Lindberg, R. Amin, T. Jia, A. Wernerson, G. Andersson and T.E. Larsson. 2012. Targeted deletion of Klotho in kidney distal tubule disrupts mineral metabolism. Journal of the American Society of Nephrology. 23, 1641-1651.

86. Ollerstam, A., J. Pittner, A.E. Persson and C. Thorup. 1997. Increased blood pressure in rats after long-term inhibition of the neuronal isoform of nitric oxide synthase. Journal of Clinical Investigation. 99, 2212-2218.
87. Oppermann, M., D. Mizel, G. Huang, C. Li, C. Deng, F. Theilig, S. Bachmann, J. Briggs, J. Schnermann and H. Castrop. 2006. Macula densa control of renin secretion and preglomerular resistance in mice with selective deletion of the B isoform of the Na,K,2Cl co-transporter. Journal of the American Society of Nephrology. 17, 2143-2152.
88. Oppermann, M., P.B. Hansen, H. Castrop and J. Schnermann. 2007. Vasodilatation of afferent arterioles and paradoxical increase of renal vascular resistance by furosemide in mice. American Journal of Physiology: Renal Physiology. 293, F279-287.
89. Osaka, H., Y.L. Wang, K. Takada, S. Takizawa, R. Setsuie, H. Li, Y. Sato, K. Nishikawa, Y.J. Sun, M. Sakurai, T. Harada, Y. Hara, I. Kimura, S. Chiba, K. Namikawa, H. Kiyama, M. Noda, S. Aoki and K. Wada. 2003. Ubiquitin carboxy-terminal hydrolase L1 binds to and stabilizes monoubiquitin in neuron. Human Molecular Genetics. 12, 1945-1958.
90. Otey, C.A. and O. Carpen. 2004. Alpha-actinin revisited: a fresh look at an old player. Cell Motility and the Cytoskeleton. 58, 104-111.
91. Patzak, A., R. Mrowka, E. Storch, B. Hocher and P.B. Persson. 2001. Interaction of angiotensin II and nitric oxide in isolated perfused afferent arterioles of mice. Journal of the American Society of Nephrology. 12, 1122-1127.
92. Patzak, A., E. Lai, P.B. Persson and A.E. Persson. 2005. Angiotensin II-nitric oxide interaction in glomerular arterioles. Clinical and Experimental Pharmacology and Physiology. 32, 410-414.
93. Pavenstadt, H., W. Kriz and M. Kretzler. 2003. Cell biology of the glomerular podocyte. Physiological Reviews. 83, 253-307.
94. Pelletier, O., E. Pokidysheva, L.S. Hirst, N. Bouxsein, Y. Li and C.R. Safinya. 2003. Structure of actin cross-linked with alpha-actinin: a network of bundles. Physical Review Letters. 91, 148102.
95. Peti-Peterdi, J. and R.C. Harris. 2010. Macula densa sensing and signaling mechanisms of renin release. Journal of the American Society of Nephrology. 21, 1093-1096.
96. Rajfur, Z., P. Roy, C. Otey, L. Romer and K. Jacobson. 2002. Dissecting the link between stress fibres and focal adhesions by CALI with EGFP fusion proteins. Nature Cell Biology. 4, 286-293.
97. Reinalter, S.C., N. Jeck, C. Brochhausen, B. Watzer, R.M. Nusing, H.W. Seyberth and M. Komhoff. 2002. Role of cyclooxygenase-2 in hyperprostaglandin E syndrome/antenatal Bartter syndrome. Kidney International. 62, 253-260.
98. Ren, Y.L., J.L. Garvin, S. Ito and O.A. Carretero. 2001. Role of neuronal nitric oxide synthase in the macula densa. Kidney International. 60, 1676-1683.
99. Rodewald, R. and M.J. Karnovsky. 1974. Porous substructure of the glomerular slit diaphragm in the rat and mouse. Journal of Cell Biology. 60, 423-433.
100. Roman, R.J., A.W. Cowley, Jr., J. Garcia-Estan and J.H. Lombard. 1988. Pressure-diuresis in volume-expanded rats. Cortical and medullary hemodynamics. Hypertension. 12, 168-176.

101. Saigoh, K., Y.L. Wang, J.G. Suh, T. Yamanishi, Y. Sakai, H. Kiyosawa, T. Harada, N. Ichihara, S. Wakana, T. Kikuchi and K. Wada. 1999. Intragenic deletion in the gene encoding ubiquitin carboxy-terminal hydrolase in gad mice. Nature Genetics. 23, 47-51.
102. Salman, I.M., M.A. Sattar, N.A. Abdullah, O.Z. Ameer, F.B. Hussain, M.A. Hye Khan, M.F. Yam, K.R. Rathore, R.N. Kazi, H.M. Salman and E.J. Johns. 2010. Renal functional & haemodynamic changes following acute unilateral renal denervation in Sprague Dawley rats. Indian Journal of Medical Research. 131, 76-82.
103. Schlatter, E., M. Salomonsson, A.E. Persson and R. Greger. 1989. Macula densa cells sense luminal NaCl concentration via furosemide sensitive Na+2Cl-K+ cotransport. Pflügers Archiv. European Journal of Physiology. 414, 286-290.
104. Schweda, F., U. Friis, C. Wagner, O. Skott and A. Kurtz. 2007. Renin release. Physiology (Bethesda). 22, 310-319.
105. Segawa, H., A. Onitsuka, J. Furutani, I. Kaneko, F. Aranami, N. Matsumoto, Y. Tomoe, M. Kuwahata, M. Ito, M. Matsumoto, M. Li, N. Amizuka and K. Miyamoto. 2009. Npt2a and Npt2c in mice play distinct and synergistic roles in inorganic phosphate metabolism and skeletal development. American Journal of Physiology: Renal Physiology. 297, F671-678.
106. Sekiguchi, S., J. Kwon, E. Yoshida, H. Hamasaki, S. Ichinose, M. Hideshima, M. Kuraoka, A. Takahashi, Y. Ishii, S. Kyuwa, K. Wada and Y. Yoshikawa. 2006. Localization of ubiquitin C-terminal hydrolase L1 in mouse ova and its function in the plasma membrane to block polyspermy. American Journal of Pathology. 169, 1722-1729.
107. Shirato, I., K. Asanuma, Y. Takeda, K. Hayashi and Y. Tomino. 2000. Protein gene product 9.5 is selectively localized in parietal epithelial cells of Bowman's capsule in the rat kidney. Journal of the American Society of Nephrology. 11, 2381-2386.
108. Sigmon, D.H. and W.H. Beierwaltes. 2000. Influence of nitric oxide derived from neuronal nitric oxide synthase on glomerular filtration. General Pharmacology. 34, 95-100.
109. Simon, J.K., N.W. Kasting and J. Ciriello. 1989. Afferent renal nerve effects on plasma vasopressin and oxytocin in conscious rats. American Journal of Physiology. 256, R1240-1244.
110. Siragy, H.M. and R.M. Carey. 1997. The subtype 2 (AT2) angiotensin receptor mediates renal production of nitric oxide in conscious rats. Journal of Clinical Investigation. 100, 264-269.
111. Siragy, H.M. and R.M. Carey. 1999. Protective role of the angiotensin AT2 receptor in a renal wrap hypertension model. Hypertension. 33, 1237-1242.
112. Siragy, H.M., M. de Gasparo and R.M. Carey. 2000. Angiotensin type 2 receptor mediates valsartan-induced hypotension in conscious rats. Hypertension. 35, 1074-1077.
113. St John, P.L., R. Wang, Y. Yin, J.H. Miner, B. Robert and D.R. Abrahamson. 2001. Glomerular laminin isoform transitions: errors in metanephric culture are corrected by grafting. American Journal of Physiology: Renal Physiology. 280, F695-705.

114. Symplicity, H.T.N.I., M.D. Esler, H. Krum, P.A. Sobotka, M.P. Schlaich, R.E. Schmieder and M. Bohm. 2010. Renal sympathetic denervation in patients with treatment-resistant hypertension (The Symplicity HTN-2 Trial): a randomised controlled trial. Lancet. 376, 1903-1909.
115. Tezel, E., K. Hibi, T. Nagasaka and A. Nakao. 2000. PGP9.5 as a prognostic factor in pancreatic cancer. Clinical Cancer Research. 6, 4764-4767.
116. Walters, B.J., S.L. Campbell, P.C. Chen, A.P. Taylor, D.G. Schroeder, L.E. Dobrunz, K. Artavanis-Tsakonas, H.L. Ploegh, J.A. Wilson, G.A. Cox and S.M. Wilson. 2008. Differential effects of Usp14 and Uch-L1 on the ubiquitin proteasome system and synaptic activity. Molecular and Cellular Neuroscience. 39, 539-548.
117. Wang, J.L., H.F. Cheng and R.C. Harris. 1999. Cyclooxygenase-2 inhibition decreases renin content and lowers blood pressure in a model of renovascular hypertension. Hypertension. 34, 96-101.
118. Wang, W., S.A. Falk, S. Jittikanont, P.E. Gengaro, C.L. Edelstein and R.W. Schrier. 2002. Protective effect of renal denervation on normotensive endotoxemia-induced acute renal failure in mice. American Journal of Physiology: Renal Physiology. 283, F583-587.
119. Wang, Y.L., A. Takeda, H. Osaka, Y. Hara, A. Furuta, R. Setsuie, Y.J. Sun, J. Kwon, Y. Sato, M. Sakurai, M. Noda, Y. Yoshikawa and K. Wada. 2004. Accumulation of beta- and gamma-synucleins in the ubiquitin carboxyl-terminal hydrolase L1-deficient gad mouse. Brain Research. 1019, 1-9.
120. Weins, A., P. Kenlan, S. Herbert, T.C. Le, I. Villegas, B.S. Kaplan, G.B. Appel and M.R. Pollak. 2005. Mutational and Biological Analysis of alpha-actinin-4 in focal segmental glomerulosclerosis. Journal of the American Society of Nephrology. 16, 3694-3701.
121. Weins, A., J.S. Schlondorff, F. Nakamura, B.M. Denker, J.H. Hartwig, T.P. Stossel and M.R. Pollak. 2007. Disease-associated mutant alpha-actinin-4 reveals a mechanism for regulating its F-actin-binding affinity. Proceedings of the National Academy of Sciences of the United States of America. 104, 16080-16085.
122. Wilkinson, K.D., K.M. Lee, S. Deshpande, P. Duerksen-Hughes, J.M. Boss and J. Pohl. 1989. The neuron-specific protein PGP 9.5 is a ubiquitin carboxyl-terminal hydrolase. Science. 246, 670-673.
123. Wilkinson, K.D., S. Deshpande and C.N. Larsen. 1992. Comparisons of neuronal (PGP 9.5) and non-neuronal ubiquitin C-terminal hydrolases. Biochemical Society Transactions. 20, 631-637.
124. Williams, J.M., A. Sarkis, B. Lopez, R.P. Ryan, A.K. Flasch and R.J. Roman. 2007. Elevations in renal interstitial hydrostatic pressure and 20-hydroxyeicosatetraenoic acid contribute to pressure natriuresis. Hypertension. 49, 687-694.
125. Wilson, P.O., P.C. Barber, Q.A. Hamid, B.F. Power, A.P. Dhillon, J. Rode, I.N. Day, R.J. Thompson and J.M. Polak. 1988. The immunolocalization of protein gene product 9.5 using rabbit polyclonal and mouse monoclonal antibodies. British Journal of Experimental Pathology. 69, 91-104.

126. Winn, M.P., P.J. Conlon, K.L. Lynn, D.N. Howell, B.D. Slotterbeck, A.H. Smith, F.L. Graham, M. Bembe, L.D. Quarles, M.A. Pericak-Vance and J.M. Vance. 1999. Linkage of a gene causing familial focal segmental glomerulosclerosis to chromosome 11 and further evidence of genetic heterogeneity. Genomics. 58, 113-120.
127. Winn, M.P., P.J. Conlon, K.L. Lynn, M.K. Farrington, T. Creazzo, A.F. Hawkins, N. Daskalakis, S.Y. Kwan, S. Ebersviller, J.L. Burchette, M.A. Pericak-Vance, D.N. Howell, J.M. Vance and P.B. Rosenberg. 2005. A mutation in the TRPC6 cation channel causes familial focal segmental glomerulosclerosis. Science. 308, 1801-1804.
128. Yamazaki, K., N. Wakasugi, T. Tomita, T. Kikuchi, M. Mukoyama and K. Ando. 1988. Gracile axonal dystrophy (GAD), a new neurological mutant in the mouse. Proceedings of the Society for Experimental Biology and Medicine. 187, 209-215.
129. Yamazaki, T., K. Hibi, T. Takase, E. Tezel, H. Nakayama, Y. Kasai, K. Ito, S. Akiyama, T. Nagasaka and A. Nakao. 2002. PGP9.5 as a marker for invasive colorectal cancer. Clinical Cancer Research. 8, 192-195.
130. Yang, T., I. Singh, H. Pham, D. Sun, A. Smart, J.B. Schnermann and J.P. Briggs. 1998. Regulation of cyclooxygenase expression in the kidney by dietary salt intake. American Journal of Physiology. 274, F481-489.
131. Yao, B., J. Xu, Z. Qi, R.C. Harris and M.Z. Zhang. 2006. Role of renal cortical cyclooxygenase-2 expression in hyperfiltration in rats with high-protein intake. American Journal of Physiology: Renal Physiology. 291, F368-374.
132. Yao, J., T.C. Le, C.H. Kos, J.M. Henderson, P.G. Allen, B.M. Denker and M.R. Pollak. 2004. Alpha-actinin-4-mediated FSGS: an inherited kidney disease caused by an aggregated and rapidly degraded cytoskeletal protein. PLoS Biology. 2, e167.
133. Yao, T., L. Song, W. Xu, G.N. DeMartino, L. Florens, S.K. Swanson, M.P. Washburn, R.C. Conaway, J.W. Conaway and R.E. Cohen. 2006. Proteasome recruitment and activation of the Uch37 deubiquitinating enzyme by Adrm1. Nature Cell Biology. 8, 994-1002.
134. Yoshimoto, M., T. Sakagami, S. Nagura and K. Miki. 2004. Relationship between renal sympathetic nerve activity and renal blood flow during natural behavior in rats. American Journal of Physiology: Regulatory, Integrative and Comparative Physiology. 286, R881-887.
135. Yu, H., N. Mashtalir, S. Daou, I. Hammond-Martel, J. Ross, G. Sui, G.W. Hart, F.J. Rauscher, 3rd, E. Drobetsky, E. Milot, Y. Shi and B. Affar el. 2010. The ubiquitin carboxyl hydrolase BAP1 forms a ternary complex with YY1 and HCF-1 and is a critical regulator of gene expression. Molecular and Cellular Biology. 30, 5071-5085.
136. Zhang, M.Z., B. Yao, H.F. Cheng, S.W. Wang, T. Inagami and R.C. Harris. 2006. Renal cortical cyclooxygenase 2 expression is differentially regulated by angiotensin II AT(1) and AT(2) receptors. Proceedings of the National Academy of Sciences of the United States of America. 103, 16045-16050.

137. Zhou, Z.R., Y.H. Zhang, S. Liu, A.X. Song and H.Y. Hu. 2012. Length of the active-site crossover loop defines the substrate specificity of ubiquitin C-terminal hydrolases for ubiquitin chains. Biochemical Journal. 441, 143-149.